UNIVERSITÀ DEGLI STUDI DI MILANO

Scuola di Dottorato in Fisica, Astrofisica e Fisica Applicata

Dipartimento di Fisica

Corso di Dottorato in Fisica, Astrofisica e Fisica Applicata

Ciclo XXVII

Emergent collective phenomena in quantum many-body systems

Settore Scientifico Disciplinare FIS/02

Supervisore: Professor Sergio Caracciolo

Coordinatore: Professor Marco Bersanelli

Tesi di Dottorato di:

Pietro Rotondo

Anno Accademico 2015/2016

Commission of the final examination:

External Referee:
Professor Rosario Fazio

External Member:
Professor Luca Tagliacozzo

Internal Member:
Professor Sergio Caracciolo

Final examination:

Date: January 15, 2016

Università degli Studi di Milano, Dipartimento di Fisica, Milano, Italy

Cover illustration:

pictorial representation of a Dicke simulator

MIUR subjects:

FIS/02

PACS:

42.50.Pq, 75.10.Nr, 05.70.Fh, 73.43.Nq

Contents

Motivation

Quoting a recent review [1], *many fundamental phenomena of strongly-correlated quantum systems such as high-T_c superconductivity, the fractional quantum Hall effect and quark confinement are still awaiting a universally accepted explanation. The main obstacle is the computational complexity of solving even the most simplified theoretical models that are designed to capture the relevant quantum correlations of the many-body system of interest. In his seminal 1982 paper [2], Richard Feynman suggested that such models might be solved by "simulation" with a new type of computer, whose constituent parts are effectively governed by a desired quantum many-body dynamics. Measurements on this engineered machine, now known as a "quantum simulator", would reveal some unknown or difficult to compute properties of a model of interest.*

In this spirit and motivated by a recent proposal by Lev and coworkers [3, 4], in the first part of this thesis, we will perform a theoretical investigation of a new class of quantum simulators: the so called *multimode disordered Dicke simulators*.

Our approach is mostly inspired from Statistical Mechanics: indeed we will merge together exact results obtained in the context of the Dicke model by Hepp and Lieb [5, 6, 7], with known results on disordered systems and neural networks [8, 9]. In this way we will be able to generalize the standard approach to the superradiant phase transition to the disordered case. As a byproduct of this analysis we will argue that this new class of quantum simulators (properly engineered) may be an alternative (or complementary) route toward quantum computation [10].

Also the second part of the thesis has a "quantum simulators motivation". Recently Bloch's group [11] implemented an Ising quantum magnet with long-range antiferromagnetic interactions, which exhibits a peculiar *devil's staircase* phase diagram, predicted long ago by Bak and Bruinsma [12].

This result, joined with recent theoretical investigations by Lesanowsky and coworkers [13] suggested to us to reconsider these spin models in the context of the fractional quantum Hall effect (FQHE) [14].

In the second part of this thesis we will show that the quantum Hall Hamitonian projected on the lowest Landau level can be mapped, in the so called *thin torus limit* [15], on the lattice gas studied by Bak and Bruinsma. This observation will lead us to predict a devil's staircase scenario for the Hall conductance as a function of the magnetic

field. This work stimulated us to investigate the connection between Laughlin wavefunction [16] and Tao-Thouless states [17], that we will explore in the last section of the second part.

Main results

In this thesis we are going to present the following results, based on four works, the first two published, the third under review and last one in preparation:

- We consider a system composed of trapped atoms within a multimode cavity, whose theoretical description is captured by a disordered multimode Dicke model. We show that in the resonant, zero-field limit the system exactly realizes a paradigm of spin glasses, the Sherrington- Kirkpatrick (SK) model. Upon a redefinition of the temperature, the same dynamics is realized in the dispersive, strong-field limit. This regime also gives access to spin-glass observables which can be used to detect replica symmetry breaking. (P. R., E. Tesio, S. Caracciolo, (2015). *Replica symmetry breaking in cold atoms and spin glasses*. Physical Review B, 91(1), 014415).

- Using an approach inspired from spin glasses, we show that the multimode disordered Dicke model is equivalent to a quantum Hopfield network. We propose variational ground states for the system at zero temperature, which we conjecture to be exact in the thermodynamic limit. These ground states contain the information on the disordered qubit-photon couplings. These results lead to two intriguing physical implications. First, once the qubit-photon couplings can be engineered, it should be possible to build scalable pattern-storing systems whose dynamics is governed by quantum laws. Second, we argue with an example of how such Dicke quantum simulators might be used as a solver of "hard" combinatorial optimization problems. (P. R., M. Cosentino Lagomarsino, G. Viola, (2015). *Dicke simulators with emergent collective quantum computational abilities*. Physical Review Letters, 114(14), 143601.)

- We consider the so-called thin-torus limit of the Hamiltonian describing interacting electrons in a strong magnetic field, restricted to the lowest Landau level, and we show that it can be mapped onto a one-dimensional lattice gas with repulsive interactions, with the magnetic field playing the role of a chemical potential. The statistical mechanics of such models leads to interpret the sequence of Hall plateaux as a fractal phase diagram, whose landscape shows a qualitative accordance with experiments. (P. R., L. G. Molinari, P. Ratti, M. Gherardi, *Devil's staircase phase diagram of the fractional quantum Hall effect in the thin torus limit*. This work is currently under review on Physical Review Letters.)

- We provide an explicit second quantization picture for fractional quantum Hall wavefunctions (Jack polynomials or Jacks times a Vandermonde determinant), introducing a four fermions generalized squeezing operator, which allows to representing these states as a Jastrow operator applied to a reference state, which is in general a simple periodic one dimensional pattern. Interestingly, Laughlin states

are squeezed Tao-Thouless states. (P. R., A. Di Gioacchino, M. Gherardi, L. G. Molinari, *Second quantization picture of fractional quantum Hall states*. This work is in preparation).

Organizational note

The present thesis consists of two parts, for a total of six Chapters plus an introduction on collective phenomena in Physics (**Chapter 1**). The first part is devoted to the presentation of our results [18, 19] on multimode disordered Dicke quantum simulators, which are the focus of **Chapter 4**. To make this part self contained and accessible to the non-expert reader, we present the fundamental background in the first two chapters. In **Chapter 2** we describe basic notions of spin glass physics, associative neural networks and their connection with non-deterministic polynomial (NP) hard problems (we remark that this chapter is not intended to be a self contained monograph on these topics). In **Chapter 3** our goal is to present the statistical mechanics approach to the Dicke model due to Hepp and Lieb [5]. We briefly review the experimental *state of the art*, with particular emphasis on the recently proposed multimode disordered Dicke simulators with ultracold atoms.

In the second part we present our results on the FQHE in the thin torus limit. The goal of **Chapter 5** is to review lattice gas models in one dimension with repulsive long-range interactions. In **Chapter 6** we obtain the Quantum Hall Hamiltonian projected on the lowest Landau level in second quantization and we present the modern approach to fractional quantum Hall states as Jack polynomials. This background is essential to presenting our original work in **Chapter 7**. In the following we add a brief description of the content of each chapter:

Chapter 2: we give an introduction to spin glass physics [8]. The SK model is presented as a benchmark to define fundamental keywords of disordered systems, such as *frustration*, *quenched disorder*, *self-averaging* and *replicas*. The Hopfield model is introduced as a paradigm for associative neural networks. Particular emphasys is given to the statistical mechanics approach due to Amit, Gutfreund and Sompolinsky [9, 20]. In the last section we explain the connection between disordered systems and NP-hard problems and we define the *number partitioning* problem [21].

Chapter 3: we review the statistical mechanics approach to the Dicke model [5, 6, 7]. From this viewpoint, *superradiance* is understood as a quantum phase transition. In the end we try to review, at the best of our knowledge, the current experimental state of the art of *Dicke simulators*. We describe the experiment by Esslinger group [22] and the proposal by Lev and coworkers [3] to obtain a *multimode disordered* Dicke simulator, which is the main motivation of our work.

Chapter 4: here we present our original contributions. In a preliminary paper [18] we put on rigorous grounds the qualitative connection between multimode disordered Dicke simulators and the Sherrington-Kirkpatrick model in two physical limits. In a second work [19] we recognized that these class of Dicke simulators are exactly the quantum counterpart of Hopfield networks. In the end we argue with an example (number partitioning) of how such Dicke quantum simulators might

be used as a solver of "hard" combinatorial optimization problems. Most of this chapter is a reproduction of our published results.

Chapter 5: we introduce the lattice gas model with repulsive long-range interactions and we prove the main steps to build up the devil's staircase phase diagram of the model [12]. We explicitly construct Hubbard ground states [23] and we prove the Burkov-Sinai formula [24].

Chapter 6: we review the fundamental facts about electrons systems in two dimensions. We introduce Landau levels and the basic facts about quantum Hall effect. The goals of this chapter are two: i) the first is to obtain the Quantum Hall Hamiltonian projected on the lowest Landau level in second quantization. Remarkably this step produces a sort of *dimensional reduction* of the problem. ii) the second is to introduce an approach to fractional quantum Hall states recently pointed out by Haldane and Bernevig [25].

Chapter 7: by restricting the analysis to the so-called thin torus limit (thus neglecting quantum correlations!), we show that the quantum Hall problem can be mapped on a classical lattice gas with repulsive interactions with the magnetic field acting as a chemical potential. The statistical mechanics of such models leads to interpret the sequence of Hall plateaux as a fractal phase diagram, whose landscape shows a qualitative accordance with experiments. This work is currently under review. In the last section we propose a second quantization picture of fractional quantum Hall states. This work is in preparation.

Emergent collective phenomena in classical and quantum many-body systems

1.1 Emergent collective phenomena in classical physics

We begin with a trivial observation: the most part of the physical phenomena that we observe in our everyday life *emerge* from the interaction of a huge number of single constituents of the physical system under consideration. In this sense they are *collective* phenomena. For instance, if we look up to the sky, we may observe flocking birds and recognize that they realize some sort of *order* (see Figure 1.1). In this case microscopic constituents are single birds interacting (socially) with the other birds of the flock. If regarded as a physical system (instead of a biological one), using more technical terms, birds are *self-organized* active matter, and thus they are by definition out of equilibrium. This terminology is borrowed from Statistical Mechanics. Actually both terminology and techniques firstly developed in the context of Statistical Mechanics are useful in order to investigate this physical system.

This statement is much more general: nowadays Statistical Mechanics techniques are widely used in order to characterize quantitatively systems that were considered typically (until a few years ago) outside the standard physics realm. In Fig. 1.2, 1.3 we show two examples, that are representative of entire research fields: economics (and finance) and biological neural networks.

In econophysics one of the goals of researchers is to predict *tipping points* (such as the 2001 and 2008 financial crisis), or, more feasible, to build up quantitative indicators in order to estabilish the health of a given market. Also here statistical mechanics is useful. For instance the phenomenon of *wealth condensation* can be understood as a classical phase transition. Usually single constituents are the agents operating on a given market.

In a biological neural network neurons interact with each other through synapses, which mediate both electric and chemical signals (obviously this description is a tremendous oversimplification of a real neural network). It is widely believed that the plasticity of the synapse is involved in the capability of human brain to store and process information. Memory can be understood as a collective phenomenon emerging from the interaction of single constituents (neurons and synapsis). Simplified toy models of artificial neural networks (often proposed by physicists) shed light on this statement. Artificial neural networks will play a major role in the first part of this thesis.
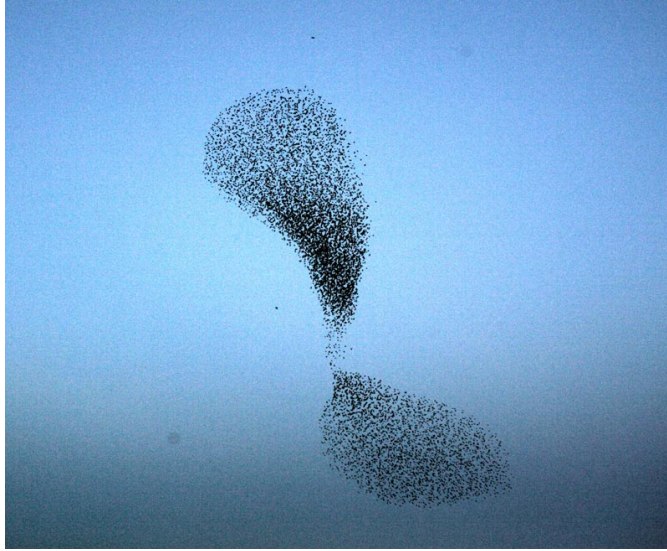
Figure 1.1: Flocking birds are a remarkable example of self organization in active matter. Both terminology and techniques borrowed from Statistical Mechanics are useful to investigate these biological systems, when regarded as physical systems.

The trivial observation at the beginning of this introductory chapter still works in the case of many-body quantum systems.

Figure 1.2: Speculative bubbles in a financial market: the time series of the SP 500 index is shown. Time period goes from 1985 to date. The two main financial crashes of the last twenty years are clearly visible (2001 and 2008).

1.2   Emergent collective phenomena in quantum many-body systems

Quantum systems with many degrees of freedom often exhibit (in extreme conditions) exotic states of matter characterized by non-trivial quantum correlations. One of the goals of condensed matter physics is to understand how these correlations emerge from

Figure 1.3: Pictorial representation of a neural network in human brain. Schematically neurons interact with each other through synapses, which mediate both electric and chemical signals (Obviously this description is a tremendous oversimplification of a real neural network).

the interaction of microscopic constituents. In order to do so theorists propose simplified models encoding the fundamental ingredients in order to capture a given phenomenon. These toy models can be studied both with analytical and numerical techniques.

In this thesis we are mainly interested in two different many-body quantum systems which display emergent collective phenomena in extreme conditions:

- atoms-light interacting systems that undergo a *superradiant* phase transition in the strong coupling regime;

- two dimensional interacting electrons at low temperature in a strong magnetic magnetic field, where the so called fractional quantum Hall effect is observed (see Fig. 7.2).

In the first part of this thesis, in particular, we will consider multimode disordered Dicke simulators and we will suggest that the collective phenomena emerging in this new class of quantum simulators are closely related to quantum computation. Interest in this topic is remarkable due to the D-Wave system, the first commercially available quantum annealer (see Fig. 1.5). For an introduction on the reason why quantum annealing protocols should outperform classical simulated annealing strategies, we suggest a beautiful talk by Hidetoshi Nishimori at Google Quantum Labs.

More in general quantum simulators represent the new frontier in order to investigate and understand strongly-correlated quantum systems. Most of them rely on the technological progress achieved with ultracold atoms in the last twenty years. The realization of a Bose-Einstein condensate in 1995 (see Fig. 1.6) is surely a cornerstone in this field.
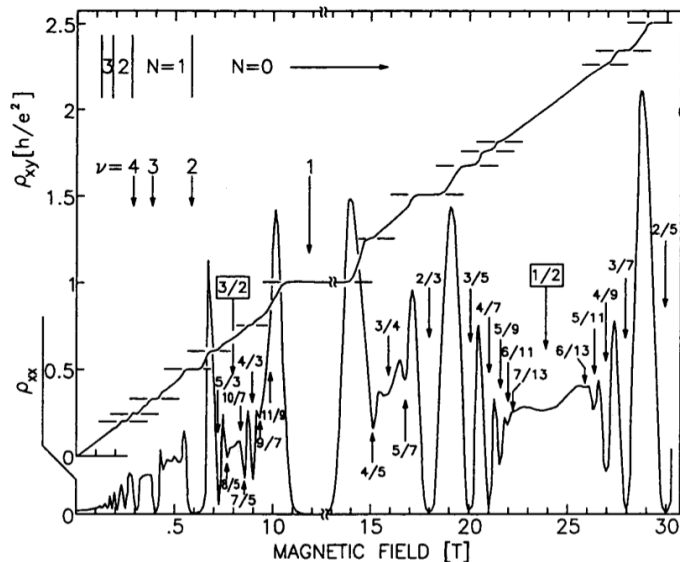
Figure 1.4: Fractional quantum Hall landscape: the Hall resistivity exhibits plateaux at integer and fractional values of the von Klitzing constant $\hbar/e^2$. In particular only odd denominators plateaux are observed at fractional fillings in the two lowest Landau levels. Nowadays more than fifty plateaux are observed only in the lowest Landau level.

Figure 1.5: The D-Wave architecture is based on superconducting qubits. The first version was a 128-qubit processor, superseded in 2013 by a 512-qbit processor. Whether this quantum annealer outperforms classical computers is source of debate.

Ultracold atoms are used, since this discovery, to "simulate" toy models which are supposed to describe interesting strongly-correlated systems: the Bose-Hubbard model and its superfluid-to-Mott insulator quantum phase transition is a paradigm in this field. We stress that ultracold atoms are not the only quantum platform to "simulate" strongly correlated systems. Atom-light interaction, for instance, can be engineered in photonic crystals or in circuit quantum electrodynamics (QED).
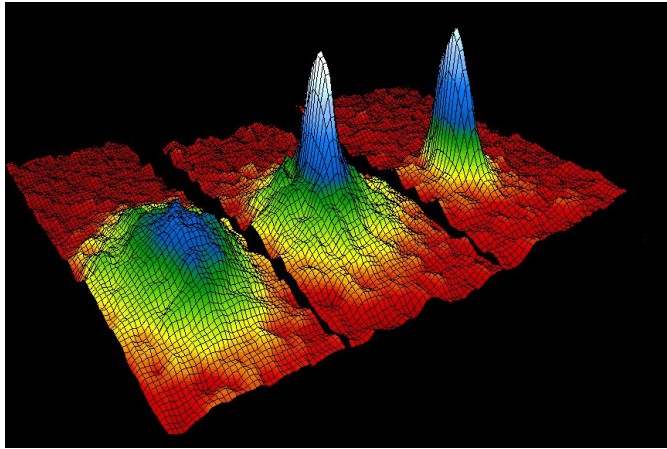
Figure 1.6: Bose-Einstein condensation in a gas of rubidium atoms. The momentum distribution is showed at three different stages: just before the appearance of the condensate (left), just after (centre) and after a further evaporation (right).

Part I

Dicke simulators with emergent collective quantum computational abilities

A short introduction to spin glasses, associative neural networks and NP-hard problems

The study of spin glasses has a long tradition in physics, dating back to the seventies [8]. The concept of spin glass was originally introduced to describe magnetic alloys that exhibit a non-periodic freezing of the orientations of the magnetic moments together with slow response and linear low- temperature heat capacity characteristic of conventional glasses [26].

It is worth remarking that nowadays spin glass techniques are heavily employed out of the condensed matter community: indeed many important devolpments in a plethora of different fields of science, such as biophysics [27, 28, 29], econophysics [30], computational complexity [31] and neural networks (and more recently machine learning), came out as a byproduct of smart applications of spin glass methods.

In the following our strategy will be to introduce the main ideas and definitions of spin glass physics directly considering *null* models containing the fundamental ingredients for this thesis. We think that this approach is the easiest one to present the essential background.

A possible route to modelling a spin glass is to consider an Ising model with *non-translational invariant* couplings between different spins. The simplest way to accomplish this requirement is to take *random* interactions: each pair of spins has a given *a priori* probability to be ferromagnetic or antiferromagnetic. This ingredient has a huge impact on the physical properties of the system, that we will try to examine in the following sections, introducing two celebrated paradigms of spin glass physics: the Sherrington-Kirkpatrick model [32] and the Hopfield neural network [33]. The thermodynamics of the two models is very similar: we will investigate in full detail only the second one.

2.1 A benchmark for spin glass physics: the Sherrington-Kirkpatrick model

Usually fully connected models of statistical mechanics are exactly solvable through *mean field* methods. When dealing with spin glasses, however, these standard techniques fail also in the simplest cases. In this sense, the Sherrington-Kirkpatrick model [32] is a paradigm because it brutally exhibits all the technical issues typical of a spin glass problem.

The SK model is a fully connected Ising model with disordered interactions. It consists of N boolean spins $\sigma_i \in \{+1, -1\}$, $i = 1, .., N$ that (in condensed matter language) represent the interacting magnetic dipole moments of atomic spins. The interaction between the spins can be ferromagnetic ($J_{ij} > 0$) or anti-ferromagnetic ($J_{ij} < 0$). The sign and the strength of the couplings are supposed to be chosen with a given probability distribution $P(J_{ij})$. The model is defined through its Hamiltonian function:

$$H_J[\sigma] = -\frac{1}{\sqrt{N}} \sum_{1 \leq j < i \leq N} J_{ij} \sigma_i \sigma_j , \qquad (2.1)$$

and by specifying the probability distribution $P(J_{ij})$ for the spin-spin interactions. The scaling factor in front of the Hamiltonian guarantees that the free energy is an extensive observable. The simplest choice for $P(J_{ij})$ (in order to perform analytical calculations) is to choose the couplings as independent normal random variables:

$$P(J_{ij}) = \frac{1}{\sqrt{2\pi J^2}} e^{-\frac{(J_{ij} - J_0)^2}{2J^2}} .$$

Both the spins $\{\sigma_i\}$ and the disordered couplings $\{J_{ij}\}$ should be considered as dynamical variables. However disorder is usually assumed to be *quenched*: this means that on the typical timescales of the spin dynamics, the couplings do not fluctuate: technically *all the averages over the disorder distribution have to be taken on the free energy*.This assumption has important consequences on the thermodynamics of the model, that we will discuss in the following.

Spin Glasses are typically systems where quenched disorder and *frustration* coexist. Formally a system is frustrated if there exists a loop on which the product of the couplings is negative. In order to analyze the concept of frustration Parisi, in the introduction of [8], suggests as an example the social behavior of three people. If each person has to choose between two sides and they like each other, they will choose the same side. Then there are two equivalent scenarios and the problem exhibits a trivial symmetry. This case is closely related to the ferromagnetic Ising model, where the two possible ground states are characterized by all spins aligned. Otherwise,when the three persons hate each other the situation is no more naive. There are three scenarios where two enemies have to be on the same side and consequently they are frustrated. This case is equivalent to the antiferromagnetic triangular Ising model, where the spins on a triangular lattice want to stay anti-aligned.

The triangular antiferromagnet displays a large number of ground states but the free energy barriers that separate these configuration are quite low. At non zero temperature, the system can move easily from one free energy valley to another and the energy landscape displays a network of many ground states connected by small energy barriers [34].

On the other hand, spin glasses display a more complex behavior: the Hamiltonian (2.1) exhibits again frustration, indeed it is impossible for the system to find an optimal configuration such that all the unfavorable interactions are excluded, even in the ground state. A spin glass has an exponential number of low energy states which do not correspond to the ground states. They are separated by high energy barriers and in the thermodynamic limit these barriers diverge. At low temperature, if the system falls in one of these valleys, it is not able to escape and, as a consequence, ergodicity is broken.
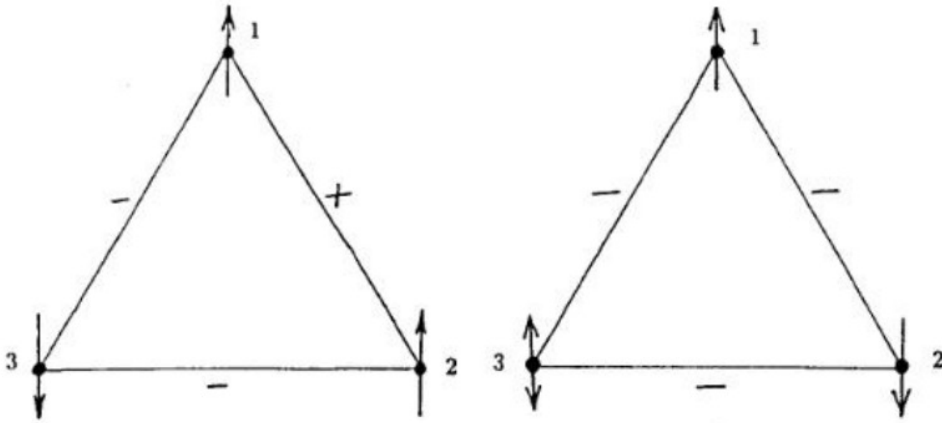
Figure 2.1: Frustration in a system of three spins: spin glasses are typically systems where quenched disorder and frustration coexist. In the first image there is no frustration: spins can find an optimal configuration and the product of the interactions along the triangle is positive. In the second image the product of the interactions along the triangle is negative: the system is frustrated, there is no configurations that can exclude all the unfavorable interactions. This image is reproduced from [34].

2.1.1   Self-averaging observables and the replica trick

As anticipated above, spin glasses are typically systems with quenched disorder in the Hamiltonian. In principle, we could expect that all the observables depend on the particular realization of the couplings J_{ij}, including the free energy density of the system

$$f_J^{(N)} = -\frac{1}{\beta N} \log Z_J = -\frac{1}{\beta N} \log \mathrm{Tr}_{\{\sigma_i\}} e^{-\beta H_J[\sigma]} .$$

This does not sound really physical, because it would imply that the macroscopic properties of the system are highly sample dependent. In fact, both common sense and experience suggest that if the system is large enough, thermodynamic properties do not depend on the disorder anymore. The observables that satisfy this property are called *self-averaging*. Free energy density is one of them. In formulas:

$$\lim_{N \to \infty} f_J^{(N)} = \int dJ P(J) f_J^{(\infty)} \equiv \left\langle\!\!\left\langle f_J^{(\infty)} \right\rangle\!\!\right\rangle . \tag{2.2}$$

Above we introduced the notation $\langle\!\langle \cdots \rangle\!\rangle$ to indicate the average over the distribution $P(J)$. This notation will be extensively used in the following.

Quenched averages always demand the calculation of a difficult integral involving the logarithm of the partition function. In order to overcome this problem we introduce the so called *replica trick*. The method consists in computing the average free energy as the analytic continuation of the average of the partition function of n uncoupled replicas of the initial system. If n is a real number, we have the following trivial identity:

$$\log Z = \lim_{n \to 0} \frac{Z^n - 1}{n} .$$

If n is an integer, the partition function of n uncoupled replicas of the initial system is:

$$Z_J^n = \left[\sum_{\{\sigma_i^a\}_{1\le i\le N}} e^{-\beta H[\{\sigma_i\}]} \right]^n = \sum_{\{\sigma_i^a\}_{1\le i\le N}^{1\le a\le n}} e^{-\beta \sum_{a=1}^n H[\{\sigma_i^a\}]},$$

i.e. it is possible to rewrite the sum over the configurations of one system to the power n as a sum over the configurations of n replicas of the same system with the same couplings J_{ij}. The average free energy per spin of a system made by n uncoupled replicas is:

$$f_n = -\frac{1}{\beta N n} \log \langle\!\langle Z_J^n \rangle\!\rangle .$$

It turns out that the free energy per spin is:

$$\lim_{n\to 0} f_n = \langle\!\langle f_J \rangle\!\rangle . \tag{2.3}$$

The proof is straightforward:

$$\lim_{n\to 0} f_n = -\frac{1}{\beta N} \lim_{n\to 0} \frac{1}{n} \log \langle\!\langle Z_J^n \rangle\!\rangle = -\frac{1}{\beta N} \lim_{n\to 0} \frac{1}{n} \log \left[\sum_J P(J) Z_J^n \right] =$$

$$= -\frac{1}{\beta N} \lim_{n\to 0} \frac{1}{n} \log \left[\sum_J P(J) (1 + n \log Z_J) \right] = -\frac{1}{\beta N} \sum_J P(J) \log Z_J =$$

$$= -\frac{1}{\beta N} \langle\!\langle \log Z_J \rangle\!\rangle = \langle\!\langle f_J \rangle\!\rangle .$$

The replica approach is extremely useful for spin glass systems. In particular, the SK model was solved for the first time using the replica method by Parisi [35]). Here we do not explore in full detail his solution. However we will see replicas at work when we will deal with the statistical mechanics of Hopfield networks.

2.2   Associative neural networks: the Hopfield model

The Hopfield model was originally proposed in 1982 by John Hopfield [33] as a simple toy model of neural network in order to understand, at least qualitatively, how memory works in the human brain.

The first problem to deal with was to give a good definition of memory. Hopfield overcame this issue proposing the following very general definition, that we quote litterally: "*Any physical system whose dynamics is dominated by a substantial number of locally stable states... The physical system will be a potentially useful memory if, in addition, any pre-scribed set of states can readily be made the stable state of the system*". This definition is a useful starting point, because it can be implemented in a simple mathematical model of neural network.

Let us consider a set of N binary neurons. Each neuron is an Ising spin with two possible states, $\sigma_i = +1$ (neuron is firing) or $\sigma_i = -1$ (neuron is silent). The phase space of the possible configurations of N binary spins is $S_N = \{-1, +1\}^N$ for a total of 2^N possible configurations. In the human brain, neurons are interconnected through synapses that
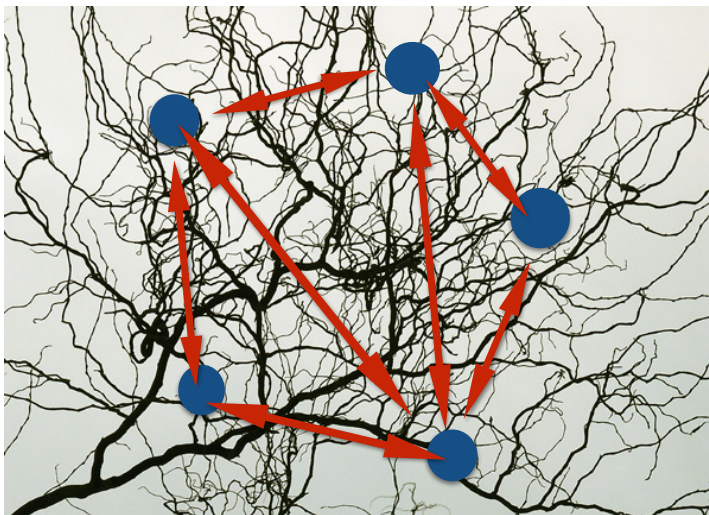
Figure 2.2: The Hopfield network is a rude modellization of a neural networks (in background). Synapses are the interconnections (red lines) between different neurons (blue dots) and are tuned properly in order to store information (see text).

make it possible to send both electrical and chemical signals from a neuron i to a neuron j. As a first rude approximation we can think that synapses are the main responsible for the tendency of two given neurons to fire or to be silent together. In the Hopfield net synapses are represented by a set of real numbers J_{ij}: If $J_{ij} > 0$, the corresponding pair of neurons is positively correlated and the two neurons tend to fire at the same time.

In order to define a neural network model, the discrete phase space built from neurons and synapses must be endowed with a dynamics. Hopfield considered the following *asyncronous* discrete-time updating rule for neuronal states:

$$\sigma_i\left(t+1\right) = \text{sign}\left(\sum_j^N J_{ij}\sigma_j\left(t\right)\right).$$ (2.4)

At time step t, a neuron is randomly chosen and its internal state is modified according to the above equation. This dynamics always ends up on a *fixed point*, which is defined through the stability equation:

$$\sigma_i\left(\sum_j^N J_{ij}\sigma_j\right) \geq 0, \qquad \forall i = 1, ..., N.$$ (2.5)

The previous equations define the first step of Hopfield's definition of a memory. At this stage, we would like to find a prescription to choose as fixed point *any* possible state of the neuronal phase space. This goal can be obtained by a suitable tuning of the synapses.

Let us fix the set of memory patterns that we want to store in the neural network:

$$\xi_i^\mu \qquad 1 \leq i \leq N, \quad 1 \leq \mu \leq p.$$ (2.6)

These patterns are simply a set of p *special* neuronal configurations of the phase space. If we want to promote them to be the stable states of the system, we must use the following prescription for the synapses:

$$J_{ij} = \begin{cases} \frac{1}{N} \sum_{\mu=1}^{p} \xi_i^\mu \xi_j^\mu & \forall i \neq j\,, \\ 0 & \forall i = j\,. \end{cases} \tag{2.7}$$

According to this definition, the J_{ij}'s are symmetric ($J_{ij} = J_{ji}$). Using equation (2.5), it is possible to show that the p memory patterns ξ^μ are stable states of the system, as long as they are not too much correlated.

Interestingly, the dynamical rules defined in equation (2.4) minimize the following energy function:

$$H[\sigma] = -\frac{1}{2} \sum_{i,j}^{N} J_{ij} \sigma_i \sigma_j\,. \tag{2.8}$$

This can be used to prove that the memory patterns are not only the stable states of the systems, but they are also the degenerate global minima of (2.8). Remarkably the Hamiltonian has the same functional form of an Ising model, with couplings given by (2.7).

To summarize, we introduced a deterministic dynamical rule on a discrete neuronal phase space in order to define a neural network with a given set of stable states. By a suitable choice of the synapses, any possible state of the system can be promoted to be a stable state. In this sense the network is able to *store* information. Moreover, it is possible to show that if we start the dynamics close enough to a memory (close in the sense of the Hamming distance), the neural network is able to *retrieve* the stored information.

In his original paper, Hopfield defined an asynchronous dynamics as in equation (2.4). This is nothing but a Monte Carlo dynamics at $T = 0$ and thus it can be generalized in the following way:

$$\sigma_i(t+1) = \begin{cases} \sigma_i(t) & \text{with probability } p_+ = \frac{e^{\beta \sigma_i \left(\sum_j^N J_{ij} \sigma_j \right)}}{e^{\beta \sigma_i \left(\sum_j^N J_{ij} \sigma_j \right)} + e^{-\beta \sigma_i \left(\sum_j^N J_{ij} \sigma_j \right)}}\,, \\ -\sigma_i(t) & \text{with probability } p_- = 1 - p_+\,, \end{cases}$$

where the parameter $\beta = 1/T$ has a straightforward interpretation as the temperature of the system. Ideally this generalized noisy dynamics defines a Fokker-Planck equation, whose stationary solution is given by a Gibbs distribution $e^{-\beta H}$ [9]. Within this standard mapping, all the properties of Hopfield networks presented here (and not proved) can be derived through statistical mechanics techniques. This was done for the first time in a series of remarkable papers by Amit, Gutfreund and Sompolinsky [9, 20]. This approach naturally defines a dictionary for translating to spin glass language claims formulated in the one of neural networks.

From the statistical mechanics viewpoint, the Hopfield model is an infinite range Ising model with couplings given by (2.7). The probability measure of a given neuronal configuration $\{\sigma_i\}_{1 \leq i \leq N}$ is given by its Gibbs measure:

$$\mathcal{G}_{N,\beta}[\sigma] \equiv \frac{1}{Z_{N,\beta}} e^{-\beta H_N[\sigma]}$$

where $Z_{N,\beta}$ is the partition function. A useful parameter to characterize the state of the neural network is the overlap of a generic state with the νth pattern:

$$m_\nu = \frac{1}{N} \sum_{i=1}^{N} \langle \sigma_i \rangle \, \xi_i^\nu \,, \tag{2.9}$$

where $\langle \cdots \rangle$ is the thermal average. In statistical mechanical language this overlap will be the *order parameter* of the system in the ferromagnetic phase.

The Hopfield model exhibits two different regimes in the low temperature phase:

- the retrieval phase (ferromagnetic phase), $\frac{p}{N} \to 0$ as $N \to \infty$.

  In this case p is finite whereas the size of system grows to infinity. At the critical temperature $T = T_C = 1$ the system exhibits a second order phase transition, from a disordered phase to an ordered phase. Below T_C, there are $2p$ equilibrium states, which are the degenerate minima of the free energy. Each one of these states is correlated to one of the learned patterns $\{\xi_i^\mu\}_{1 \leq i \leq N}$ and the overlap (2.9) is non zero and thus, in neural networks language, retrieval is possible. This regime can be studied without replicas [9].

- the confused phase (spin glass phase), $\frac{p}{N} \to \alpha$ finite, as long as $N \to \infty$.

  For $\alpha \geq \alpha_2 \approx 0.15$, the network is in the spin glass phase (retrieval is not possible) at low temperature. The equilibrium state of the system is uncorrelated with any of the learnt patterns. This phase is a manifestation of the clear physical intuition that we can not store in the network an arbitrary number of memories.

  For $\alpha \leq \alpha_1 \approx 0.05$, retrieval is possible and the system is still in its ferromagnetic phase. For $\alpha_1 \leq \alpha \leq \alpha_2$ the spin glass state is the ground state but the retrieval is still efficient. In the finite α regime we need replicas to investigate the thermodynamics of the system [20].

In the next sections we will present this statistical mechanics analysis in full detail.

2.3   Retrieval phase: the limit of finite p

The free energy density is given by

$$f_\beta = -\frac{1}{\beta} \lim_{N \to \infty} \left[\frac{1}{N} \left\langle\!\!\left\langle \log \operatorname{Tr}_\sigma e^{-\beta H[\sigma]} \right\rangle\!\!\right\rangle \right],$$

where $\langle\!\langle \cdots \rangle\!\rangle$ is the average over the probability distribution of the memories $\{\xi_i^\nu\}_{1 \leq i \leq N}^{1 \leq \nu \leq p}$. For a given realization of the ξ's, the partition function can be written as

$$Z = \operatorname{Tr}_\sigma e^{-\beta H} = e^{-\frac{\beta p}{2}} \operatorname{Tr}_\sigma \exp\left[\frac{\beta}{2N} \sum_{\mu=1}^{p} \left(\sum_{i=1}^{N} \sigma_i \xi_i^\mu \right)^2 \right] =$$

$$= (N\beta)^{\frac{p}{2}} e^{-\frac{\beta p}{2}} \int \prod_{\mu=1}^{p} \frac{dm_\mu}{2\pi} \exp\left[-\frac{N\beta \boldsymbol{m}^2}{2} + \sum_{i=1}^{N} \log\left[2\cosh\left(\beta \boldsymbol{m} \cdot \boldsymbol{\xi}_i \right) \right] \right],$$

where we introduced the notation $\boldsymbol{m}$ and $\boldsymbol{\xi}$ for indicating compactly the p-component vectors m_μ and ξ_i^μ. The last line is obtained using a property of Gaussian integral and performing explicitly the summation over the spins σ_i. For finite p, the integral over m can be evaluated with the saddle point approximation:

$$-\frac{1}{N\beta}\log Z = \frac{1}{2}\boldsymbol{m}^2 - \frac{1}{N\beta}\sum_{i=1}^N \log\left[2\cosh\left(\beta\boldsymbol{m}\cdot\boldsymbol{\xi}_i\right)\right].$$

The equilibrium state of the system is the lowest free energy solution of

$$\frac{\partial\log Z}{\partial m_\mu} = 0 = \boldsymbol{m} - \frac{1}{N}\sum_{i=1}^N \boldsymbol{\xi}_i\tanh\left(\beta\boldsymbol{m}\cdot\boldsymbol{\xi}_i\right).$$

This result is sample dependent as long as N is finite. In the thermodynamic limit summation can be replaced by an average over the distribution of patterns for the law of large numbers (this is true only if the memories are uncorrelated). In conclusion we obtain the following mean-field equations (exact in the thermodynamic limit):

$$f_\beta = \frac{1}{2}\boldsymbol{m}^2 - \frac{1}{\beta}\langle\!\langle\log\left[2\cosh\left(\beta\boldsymbol{m}\cdot\boldsymbol{\xi}\right)\right]\rangle\!\rangle, \tag{2.10}$$

$$\boldsymbol{m} = \langle\!\langle\boldsymbol{\xi}\tanh\left(\beta\boldsymbol{m}\cdot\boldsymbol{\xi}\right)\rangle\!\rangle. \tag{2.11}$$

It is possible to prove that $\boldsymbol{m}$ is the average overlap between the local magnetization and the ξ's:

$$m_\mu = \langle\!\langle\langle\sigma_i\rangle\,\xi_i^\mu\rangle\!\rangle,$$

where

$$\langle\sigma_i\rangle = \tanh\left(\beta\boldsymbol{m}\cdot\xi_i\right)$$

is the thermal average of the i-th spin. Among the solutions of equation (2.11) there is the paramagnetic one $\boldsymbol{m} = \boldsymbol{0}$. This solution is stable in the high temperature phase. In the low temperature regime new solutions appear that can be completely classified. This is the goal of the next section.

2.3.1   Classification of the low-temperature solutions in the ferromagnetic phase

In order to perform explicit calculations, we must specifying the probability distribution for the memory patterns. Let us consider

$$P\left(\{\xi_i^\mu\}\right) = \prod_{\mu,i} p\left(\xi_i^\mu\right), \tag{2.12}$$

with

$$p\left(\xi_i^\mu\right) = \frac{1}{2}\delta\left(\xi_i^\mu - 1\right) + \frac{1}{2}\delta\left(\xi_i^\mu + 1\right). \tag{2.13}$$

We can expand the saddle point equations (2.10), (2.11) in powers of $\boldsymbol{m}$ in order to obtain:

$$f = -T\log 2 + \frac{1}{2}\left(1 - \beta\right)\boldsymbol{m}^2 + O\left(m_\mu^4\right),$$

$$m_\mu = \beta m_\mu + \frac{2}{3}\beta^3\left(m_\mu\right)^3 - \beta^3 m_\mu\boldsymbol{m}^2 + O\left(m_\mu^4\right).$$

Above $T = T_c = 1$, these equations have only one solution, the paramagnetic state characterized by $\boldsymbol{m} = 0$ and $f = -T\log 2$. This solution is unstable below T_C, where new non-paramagnetic solutions appear.

Let us denote the number of nonzero components of $\boldsymbol{m}$ as n. From the previous equation, solutions are symmetric under permutation of m_μ or under exchange of the sign of each component of $\boldsymbol{m}$. For this reason we can consider only solutions such that the first n components are positive and the others are zero, without loss of generality.

For $n = 1$, we obtain the following simple equations:

$$f = \frac{1}{2}(m_1)^2 - \frac{1}{2}\log\left[2\cosh\left(\beta m_1\right)\right],$$
$$m_1 = \tanh\left(\beta m_1\right).$$

Interestingly, these are the mean field equations for the fully connected ferromagnetic Ising model. The local magnetization is given by

$$\langle\sigma_i\rangle = \xi_i^1\tanh\left(\beta m_1\right).$$

This state is a ferromagnetic state up to a gauge transformation of the spins. By symmetry, there are $2p$ equivalent states related to the different memories. We can prove that these states are the global minima of free energy in a neighborhood of $T = 0$. In this limit we have, for $n = 1$:

$$E\left(T = 0\right) = -\frac{1}{2},$$
$$\boldsymbol{m}\left(T = 0\right) = (1, 0, 0, ..., 0),$$

and in general, for all values of n:

$$E = -\frac{1}{2}\boldsymbol{m}^2,$$
$$\boldsymbol{m} = \langle\!\langle\boldsymbol{\xi}\,\mathrm{sign}\left(\boldsymbol{m}\cdot\boldsymbol{\xi}\right)\rangle\!\rangle,$$

but $\boldsymbol{m}^2 \leq 1$ and thus the $n = 1$ solutions are the global minima. This can be proved numerically at every temperatures. In addition to these global minima there are solutions with $n > 1$, which correspond to metastable states of the network. Physically they are spurious states with non-zero overlap with more than one memory at the same time.

Let us consider solutions of equations (2.10) and (2.11) such that all n non-zero components have the same module:

$$\boldsymbol{m} = m_n\left(1, 1, ..., 1, 0, 0, ..., 0\right),$$

where the first n components have unitary values and the others $p - n$ components are zeros. By symmetry there are $2^n\binom{p}{n}$ of such solutions. These states exist for every temperature $T < 1$. The mean field equations for the symmetric states are

$$f_n = \frac{n}{2}m_n^2 - \frac{1}{\beta}\langle\!\langle\log\left[2\cosh\left(\beta m_n z_n\right)\right]\rangle\!\rangle,$$
$$m_n = \frac{1}{n}\langle\!\langle z_n\tanh\left(\beta m_n z_n\right)\rangle\!\rangle,$$

where

$$z_n^i = \sum_{\mu=1}^{n} \xi_i^\mu \,.$$

It is possible to evaluate the behavior of such solutions by expanding these equations at $T = 1$ and $T = 0$. At $T = 1$ the averages give:

$$f_n \simeq -\frac{3n\,(T-1)^2}{4\,(3n-2)} \,,$$

$$m_n^2 \simeq \frac{3\,(1-T)}{3n-2} \,,$$

and thus $T = 1$ is the critical temperature for the appearance of all the symmetric solutions. The free energy is monotonically increasing with n. Therefore the $n = 1$ solutions are the global minima of the free energy also in this limit. At $T = 0$ the expansion gives two different results which differ if n is even or odd. For odd n:

$$f_{2k+1}\,(T=0) = -\frac{2k+1}{2^{4k+1}}\binom{2k}{2}^2 \,,$$

$$m_{2k+1}^2\,(T=0) = \frac{1}{2^{2k}}\binom{2k}{2} \,,$$

whereas for even n:

$$f_{2k}\,(T=0) = -\frac{2k}{2^{4k+1}}\binom{2k}{2}^2 \,,$$

$$m_{2k}^2\,(T=0) = \frac{1}{2^{2k}}\binom{2k}{2} \,.$$

All the functions of the sequence f_n are bounded from below by $f_1 = -\frac{1}{2}$ and from above by $f_2 = -\frac{1}{4}$. Moreover the sequence for even n is monotonically decreasing with k while the sequence with odd n is monotonically increasing, both with common limit $-\frac{1}{\pi}$ for $k \to \infty$.

The local stability of these solutions can be studied by analyzing the eigenvalues of the Hessian matrix of the free energy:

$$H^{\mu\nu} = \frac{\partial^2 f}{\partial m^\mu \partial m^\nu} \,.$$

A detailed analysis of the Hessian matrix shows that the states overlapping with a single memory are the only stable solutions near $T = 1$. At lower temperature also other odd-n solutions become stable. Even-n solutions are unstable for all T. At $T = 0$ all the odd-n solutions are stable, thus forming a hierarchy of metastable states.

2.4   Limit of finite α: from the retrieval to the spin glass phase

Let us now proceed with the analysis of thermodynamic properties of the Hamiltonian (2.8) in the limit of finite α [20]. In this case, in the low temperature phase, the random overlaps with most of the patterns will be weak, typically of order $1/\sqrt{N}$. However, one

or a finite number of overlaps could condense macroscopically. In other words, they may assume fixed and finite values as $N \to \infty$. In order to consider this possibility, it is useful to introduce external fields, aligned to a finite number of patterns $\{\xi_i^\nu\}_{1 \le i \le N}^{1 \le \nu \le s}$ (with $s \ll p$). Then the Hamiltonian will have a new term due to the presence of such external fields:

$$H_h[\sigma] = -\frac{1}{2} \sum_{i,j} J_{ij}\sigma_i\sigma_j - \sum_{\nu=1}^{s} h^\nu \sum_{i=1}^{N} \xi_i^\nu \sigma_i. \tag{2.14}$$

For finite α we need the replica trick to get some insight into the physical properties of the system. As a first step we consider the averaged replicated partition function:

$$\langle\!\langle Z^n \rangle\!\rangle = \left\langle\!\!\left\langle \sum_{\{\sigma_i^a\}_{1 \le i \le N}^{1 \le a \le n}} \exp\left[\frac{\beta N}{2} \sum_{a=1}^{n} \sum_{\mu=1}^{p} \left(\frac{1}{N} \sum_{j=1}^{N} \xi_j^\mu \sigma_j^a \right)^2 + \beta \sum_{\nu=1}^{s} h^\nu \sum_{i=1}^{N} \sum_{a=1}^{n} \xi_i^\nu \sigma_i^a \right] \right\rangle\!\!\right\rangle \tag{2.15}$$

where a is the replica index and h^ν are the external fields coupled to the projections of the configurations on the first s patterns.

With a few pages of algebra and a little bit of massage, we obtain the following functional form for the averaged free energy:

$$f_n = \frac{\alpha}{2} + \frac{1}{2n} \sum_{\nu=1}^{s} \sum_{a=1}^{n} (m_\nu^a)^2 + \frac{\alpha}{2\beta n} \operatorname{Tr} \log\left[(1-\beta)\mathbb{1} - \beta\mathbb{Q}\right] + \tag{2.16}$$

$$+ \frac{\alpha\beta}{2n} \sum_{a \ne b}^{n} r_{ab} q_{ab} - \frac{1}{n\beta} \langle\!\langle \log Z_0 \rangle\!\rangle \,,$$

where $\mathbb{Q}_{ab} = q_{ab}$ and

$$Z_0 = \operatorname{Tr}_{\{\sigma_i^a\}_{1 \le i \le N}^{1 \le a \le n}} \exp\left(\frac{\alpha\beta^2}{2} \sum_{a \ne b}^{n} r_{ab}\sigma_i^a\sigma_i^b + \beta \sum_a \sum_\nu (m_\nu^a + h^\nu)\xi_i^\nu\sigma_i^a \right).$$

All the parameters involved in the equation above have a straightforward interpretation in replica language:

$$m_\mu^a = \frac{1}{N} \left\langle\!\!\left\langle \sum_{i=0}^{N} \xi_i^\mu \langle \sigma_i^a \rangle \right\rangle\!\!\right\rangle, \tag{2.17}$$

$$q_{ab} = \frac{1}{N} \left\langle\!\!\left\langle \sum_{i=1}^{N} \langle \sigma_i^a \rangle \langle \sigma_i^b \rangle \right\rangle\!\!\right\rangle, \tag{2.18}$$

$$r_{ab} = \frac{1}{\alpha} \sum_{\mu > s}^{p} \left\langle\!\!\left\langle \left[\frac{1}{N} \sum_{i=1}^{N} \xi_i^\mu \langle \sigma_i^a \rangle \right] \cdot \left[\frac{1}{N} \sum_{i=1}^{N} \xi_i^\mu \langle \sigma_i^b \rangle \right] \right\rangle\!\!\right\rangle = \frac{1}{\alpha} \sum_{\mu=s+1}^{\alpha N} \langle\!\langle m_\mu^a m_\mu^b \rangle\!\rangle. \tag{2.19}$$

Now the goal is to minimize the free energy as a function of these parameters. In principle we do not have a good reason to believe that the parameters introduced above have some non-trivial dependence from the replica indices: all the fictitious replicas were introduced on the same footing at the beginning of the calculation. This observation naturally leads to the *replica symmetric ansatz* (RS) that we will discuss in the next section. In fact, this ansatz is only a first rude approximation, because the replica symmetric solution turns out to have negative entropy at zero temperature. In order to deal with this

unphysical result, replica symmetry must be broken in some way. Parisi was the first to propose a consistent scheme to break replica symmetry in the SK model [35, 36]. In the context of Hopfield networks this scheme is unnecessary: the RS solution is already a good approximation and replica symmetry breaking only slightly modifies this analysis.

2.4.1 Replica symmetric solutions

Inspired by the previous discussion, we consider the following replica symmetric ansatz:

$$m_\mu^a = m_\mu^b \qquad \forall \mu \,, \tag{2.20}$$

$$q_{ab} = q \qquad a \neq b \,, \tag{2.21}$$

$$r_{ab} = r \qquad a \neq b \,. \tag{2.22}$$

The free energy evaluated on this three dimensional subspace is given by:

$$f(m, q, r) = \frac{\alpha}{2} + \frac{1}{2} \sum_{\nu=1}^{s} (m_\nu)^2 + \frac{\alpha}{2\beta n} \left[\log \left(1 - \beta + q\beta \right) - \frac{q\beta}{(1 - \beta + q\beta)} \right] +$$

$$+ \frac{\alpha\beta}{2} r \left(1 - q \right) - \frac{1}{\beta} \int \frac{dz}{\sqrt{2\pi}} e^{-\frac{z^2}{2}} \left\langle\!\left\langle \log 2 \cosh \left[\beta\sqrt{\alpha r} z + \beta \left(\boldsymbol{m} + \boldsymbol{h} \right) \cdot \boldsymbol{\xi} \right] \right\rangle\!\right\rangle \,, \quad (2.23)$$

and by differentiation we obtain the saddle point equations:

$$m_\nu = \left\langle\!\left\langle \xi_\nu \tanh \left[\sqrt{\alpha r} z + \left(\boldsymbol{m} + \boldsymbol{h} \right) \cdot \boldsymbol{\xi} \right] \right\rangle\!\right\rangle_z \,, \tag{2.24}$$

$$q = \left\langle\!\left\langle \tanh^2 \left[\beta\sqrt{\alpha r} z + \beta \left(\boldsymbol{m} + \boldsymbol{h} \right) \cdot \boldsymbol{\xi} \right] \right\rangle\!\right\rangle_z \,, \tag{2.25}$$

$$r = \frac{q}{(1 - \beta + q\beta)^2} \,, \tag{2.26}$$

where the average $\langle\!\langle ... \rangle\!\rangle_z$ is the combined average over the discrete distribution of the ξ^ν's ($\nu = 1, \ldots, s$) and over a Gaussian noise z of zero mean and unitary variance.

For $\boldsymbol{h} = \boldsymbol{0}$ equation (2.24) can be compared with the one obtained in the finite p limit (2.11). The ferromagnetic contribution of the s condensed overlaps is supplemented by a spin glass contribution generated by the gaussian noise z, physically produced by the sum of the overlaps with the rest of the patterns.

Equations (2.24), (2.25) and (2.26) have two kinds of stable solutions: (1) a solution with $\boldsymbol{m} = 0$, $q, r \neq 0$, which is a Spin Glass state characterized by no macroscopic overlap with a finite number of patterns. (2) A ferromagnetic solution with non zero $\boldsymbol{m}$. It is instructive to consider the zero temperature limit, where the mean field equations can be solved exactly. In particular we have:

$$m_\nu = \left\langle\!\left\langle \xi_\nu \mathrm{erf} \left[\frac{1}{\sqrt{2\alpha r}} \left(\boldsymbol{m} + \boldsymbol{h} \right) \cdot \boldsymbol{\xi} \right] \right\rangle\!\right\rangle \,, \tag{2.27}$$

$$q = 1 - CT \,, \tag{2.28}$$

$$r = \frac{1}{(1 - C)^2} \,, \tag{2.29}$$

with

$$C = \left(\frac{2}{\pi r \alpha} \right)^{\frac{1}{2}} e^{-\frac{m^2}{2r\alpha}} \,.$$

These equations have always a spin glass solution with $m_\nu = 0$. For $\alpha > \alpha_C = 0.138$ this is the only solution. For $\alpha < \alpha_C$, there are also the ferromagnetic solutions with $m \neq 0$. They appear at $\alpha = \alpha_C$ with an overlap $m = 0.967$ (very close to unity) with the single memory patterns.

The average energy per spin when the system exhibits a macroscopic overlap m with one of the learned patterns is:

$$E = \left\langle\!\!\left\langle -\frac{1}{2N^2} \sum_{\mu=1}^{p} \sum_{ij}^{N} \xi_i^\mu \xi_j^\mu \sigma_i \sigma_j \right\rangle\!\!\right\rangle + \frac{\alpha}{2} = -\frac{m^2}{2} + \frac{\alpha}{2}(1 - r) .$$

At $\alpha = \alpha_C$, $E = -0.5014$, whereas as $\alpha \to 0$, for finite m, $E \to -0.5$. For finite α the system is able to slightly lower its energy by relaxing a small fraction of the spins, to accommodate for fluctuations in the overlap of the other patterns.
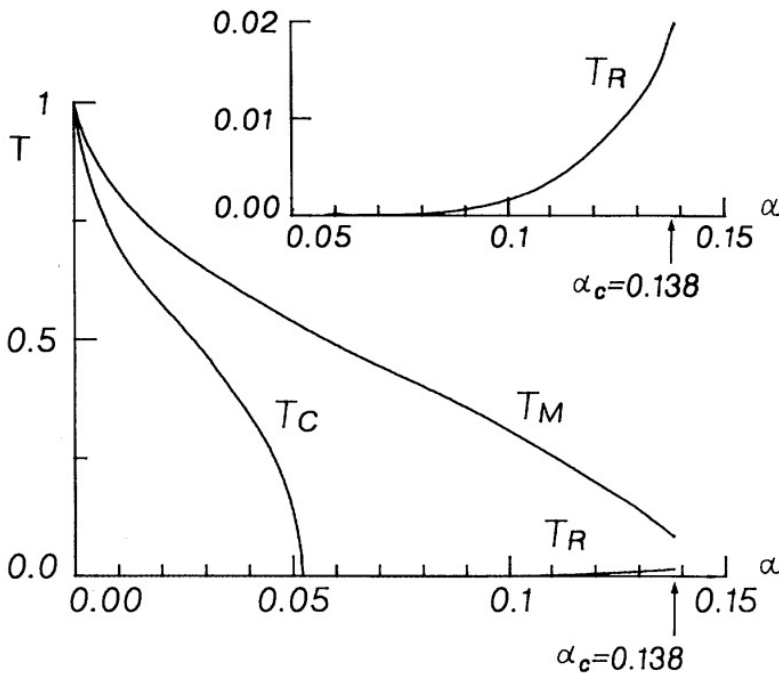
Figure 2.3: Phase diagram for the Hopfield model. The system exhibits three different phases. Below the curve T_C the phase is ferromagnetic: the states with $m \neq 0$ are the global minima of the free energy. The phase transition at T_C is a first-order phase transition. In the limit $T \to 0$ the phase is ferromagnetic for $\alpha < 0.051$. Above the curve T_M the system has a spin glass behavior: $m = 0$ and $q, r \neq 0$. In the limit $T \to 0$ the spin glass phase is observed for $\alpha > 0.138$. Between T_C and T_M the spin glass state is again the global minimum of the free energy. However ferromagnetic solutions are metastable states. These states start to appear just below T_M in a discontinuous way. The curve T_R in the main plot is the instability temperature for replica symmetric solutions and is showed on an expanded scale in the inset. This image is reproduced from [20].

Let us focus on the spin glass solution, where $m = 0$ and $q, r \neq 0$. These conditions

imply that:

$$r = \left[1 + \left(\frac{2}{\pi\alpha} \right)^{\frac{1}{2}} \right]^2 .$$

(2.30)

Moreover, using this last result, the energy of the spin glass state is equal to:

$$E = -\frac{1}{\pi} - \left(\frac{\pi\alpha}{2} \right)^{\frac{1}{2}} .$$

In the limit $\alpha \to 0$, $E \to -\frac{1}{\pi}$ and $C = \sqrt{\frac{2}{\pi\alpha r}} \to 1$. This limit coincides with the value of E of the symmetric solutions in the finite p case, where the state mixes n patterns, in the limit $n \to \infty$. This implies that, as $p \to \infty$, the numerous states which mix many patterns merge to form the spin glass phase. Comparing the energy of the spin glass and ferromagnetic states, the spin glass energy results to be lower in the range $0.051 < \alpha < 0.138$, whereas the ferromagnetic states becomes the absolute minima below 0.051. Thus at $\alpha = \alpha_C$ the spin glass state is definitely the ground state of the system.

The analytical calculation presented here can be numerically extended at non zero temperature, in order to produce the phase diagram of figure (2.3).

Both the SK model and the Hopfield network are intimately related with non-deterministic polynomial problems. In the next section we discuss qualitatively this connection.

2.5   Non-deterministic poynomial (NP) problems and the connection with spin glasses

In many cases, an optimization problem can be cast as a problem of minimizing a given cost or energy function $\mathcal{H}(S_1, S_2, ...S_N)$ with respect to N variables $S_1, S_2, ...S_N$ (sometimes subject to some constraints). The task is to find a set of values for these variables (a configuration) for which the function $\mathcal{H}(\{S_i\})$ has the minimum value. In many important optimization problems, the set of feasible configurations from which an optimum is to be chosen is a finite set (for finite N). In such a case, we say that the problem is combinatorial in nature. If the variables S_i are discrete and each takes on a finite number of values, then the problem is clearly a combinatorial one. Here we focus on this type of optimization problem, and assume that we have to minimize $\mathcal{H}(\{S_i\})$ with respect to the discrete set of the variables S_i [37].

An optimization problem is said to belong to the class P (P for Polynomial), if it can be solved in polynomial time (i.e., the evaluation time goes like some polynomial in N) using polynomially (in N, again) resources. Existence of such a polynomial bound on the evaluation time is somehow interpreted as the "easiness" of the problem. However, many important optimization problems seem to fall outside this class, like the famous traveling salesman problem (see Figure 2.4).

Another important class of problems which can be solved in polynomial time by non-deterministic machines. This class is the famous NP (Non-deterministic Polynomial) class. P is included in the NP class, since a deterministic Turing machine is just a special case of non-deterministic Turing machines. Unlike a deterministic machine, which takes a specific step deterministically at each instant (and hence follows a single computational
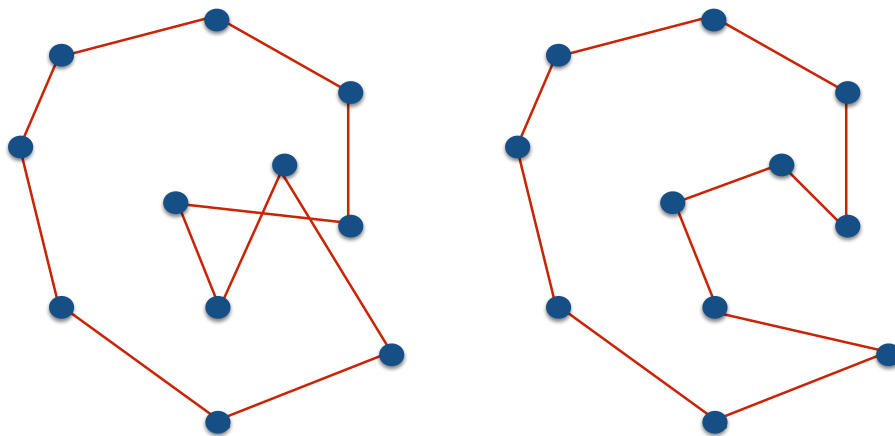
Figure 2.4: An instance of the Travelling salesman problem. The task is to find the shortest route connecting all the cities on the map (for instance with the euclidean metrics). This task is NP-hard. The solution on the left can be easily improved eliminating crossing lines. The improved solution is showed on the right.

path), a non-deterministic machine has a host of different 'allowed' steps at its disposal at every instant. At each instant it explores all the 'allowed' steps and if any of them leads to the goal, the job is considered to be done. Thus it explores in parallel many paths (whose number goes typically exponentially with time) and checks if any one of them reaches the goal.

Among the NP problems, there are certain problems (known as NP-complete problems) which are such that any NP problem can be "reduced" to them using a polynomial algorithm. For instance the *number partitioning* problem that we will define in the following is a representative of this class. This roughly means that if one has a routine to solve an NP-complete problem of size N then using that routine one can solve any NP problem at the cost of an extra overhead in time that grows only polynomially with N. The problems in this class are considered to be hard, since so far no one can simulate a general nondeterministic machine by a deterministic Turing machine without an exponential growth of execution time. In fact it is largely believed (though not proved yet) that it is impossible to do so (i.e., P≠NP) in principle.

There are some excellent deterministic algorithms for solving certain optimization problems exactly . These algorithms are, however, quite small in number and are strictly problem specific. For NP or harder problems, only approximate results can be found using these algorithms in polynomial time. These approximate algorithms too are strictly problem specific in the sense that if one can solve a certain NP-complete problem up to a certain approximation using some polynomial algorithm, then that does not ensure that one can solve all other NP problems using the same algorithm up to the said approximation in polynomial time.

Exact algorithms being scarce, one has to go for heuristics algorithms, which are based on certain intuitive moves, without guarantee on either the accuracy or the run time for the worst case instance. However, these algorithms are generally easy to formulate and are quite effective in solving most instances of the intended problems. A general approach towards formulating such approximate heuristics may be based on stochastic (randomized) iterative improvements. The easiest one in this family is the local minimization algorithm. In this algorithm one starts with a random configuration C_0 and makes some local changes in the configuration following some prescription (stochastic or deterministic) to generate a new configuration C_1 and calculates the corresponding change in the cost. If the cost is lowered by the change, then the new configuration C_1 is adopted. Otherwise the old configuration is retained. Then in the next step a new local change is attempted again, and so on. This reduces the cost steadily until a configuration is reached which minimizes the cost locally. This means that no further lowering of cost is possible by changing this configuration using any of the prescribed local moves: the algorithm essentially stops there. But generally, in most optimization problems (such as in spin glasses), there occur many local minima in the cost-configuration landscape and they are mostly far above the global minimum. It is likely that the algorithm therefore gets stuck in one of them and ends up with a poor approximation. One can then start afresh with some new initial configuration and end up with another local minimum. After repeating this for several times, each time with a new initial configuration, one may choose the best result from them. A better idea would be to get somehow out of shallow local minima. One can introduce some fluctuations or noise in the process so that the movement is not always towards lower energy configurations, but there is also a finite probability to go to higher energy configurations (the higher the final energy, the lower the probability to move to that), and consequently there appear chances to get out of the shallow local minima. Initially, strong fluctuations are adopted (i.e., the probability to go to higher energy configurations is relatively high) and slowly fluctuations are reduced until finally they are tuned off completely. In the mean time the system gets a fair opportunity to explore the landscape more exhaustively and settle into a reasonably deep cost or energy minimum. Kirkpartick et al. in 1983 [38] suggested an elegant way: A fluctuation is implemented by introducing an "artificial" temperature T into the problem such that the transition probability from a configuration C_i to a configuration C_f is given by $\min\{1, \exp-[\Delta_{if}/T]\}$, where $\Delta_{if} = E_f - E_i$, with E_k denoting the cost or energy of the configuration C_k. A corresponding Monte Carlo dynamics is defined, say, based on detailed balance, and the thermal relaxation of the system is simulated. In course of simulation, the noise factor T is reduced slowly from a very high initial value to zero following some annealing schedule. At the end of the simulation one is expected to end up with a configuration whose cost is a reasonable approximation of the global minimum one. If the temperature is decreased slowly enough, then the global minimum is attained with certainty in the limit $t \to \infty$ [39]. Even within a finite time and with a faster cooling rate, one can achieve a reasonably good approximation.

As has been mentioned already, many combinatorial optimization problems can be cast into the problem of finding the ground state of some classical (spin glass like) Hamiltonian $H(\{S_i\})$. In particular, finding the ground state of the SK model and of the Hop-
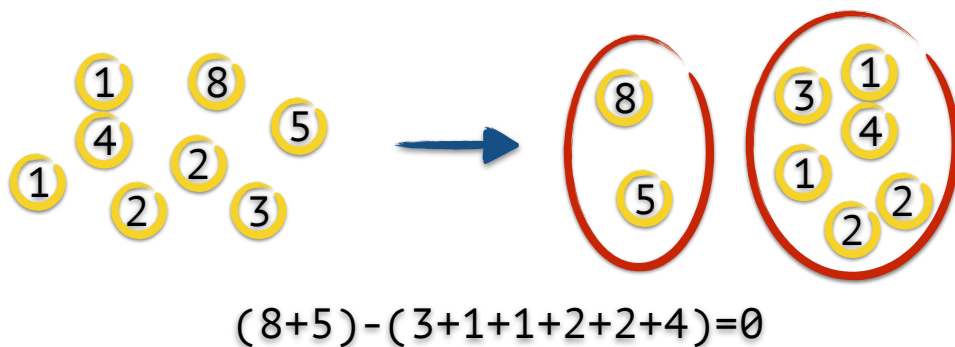
$(8+5)-(3+1+1+2+2+4)=0$

Figure 2.5: An instance of the Number Partitioning problem: a partition of a set of positive integer numbers is produced in such a way to minimize the absolute value of the difference of the sum of the elements of the two resulting sets. In this simple case a zero energy solution is found.

field network (in the spin glass phase) are both NP-hard problems. One can therefore analyze the problem by using statistical mechanics (as we did in the first sections) so as to apply Montecarlo techniques like simulated annealing.

In the last section of the chapter we define another famous NP-hard problem, number partitioning, that we mentioned above. This problem, as long as SK and Hopfield models, will play a role in the rest of the first part of this manuscript.

2.5.1   The number partitioning problem

Number partitioning asks the following: given a set of N positive numbers $S = \{n_i\}_{i=1}^{N}$, is there a partition of this set of numbers into two disjoint subsets R and $S - R$, such that the sum of the elements in both sets is the same? For example, can one divide a set of assets with values $n_1, \ldots, n_N$, fairly between two people? This is the *decision* version of the problem and is known to be NP-complete [37].

This problem can be phrased trivially as an Ising model as follows. Let n_i ($i = 1, \ldots, N = |S|$) describe the numbers in set S, and let

$$H = \left(\sum_{i=1}^{N} n_i \sigma_i \right)^2 \tag{2.31}$$

be an energy function, where $\sigma_i = \pm 1$ is an Ising spin variable.

It is clear that if there is a solution to the Ising model with $H = 0$, then there is a configuration of spins where the sum of the n_i for the $+1$ spins is the same for the sum of the n_i for the -1 spins. Thus, if the ground state energy is $H = 0$, there is a solution to the number partitioning problem.

This Ising glass has *degeneracies* – i.e., there are always at least two different solutions to the problem. This can be seen by noting that if σ_i^* denotes a solution to the problem, then $-\sigma_i^*$ is also a solution. Physically, this corresponds to the fact that we do not care which set is labeled as $\pm$. The existence of a symmetry transformation which leaves the

couplings unchanged (as there are no linear terms) implies that all energy levels of H are degenerate. It is possible that there are $2m$ ground states (with $m > 1$). This means that there are m physically distinct solutions to the computational problem. We can remove this double degeneracy by fixing $\sigma_1 = 1$. This also allows us to remove one spin: now only $\sigma_2, \ldots, \sigma_N$ are included on the graph, and σ_1 serves as an effective magnetic field. So in general, we require $N - 1$ spins, which live on a complete graph, to encode this problem.

If the ground state has $H > 0$, we know that there are no solutions to the partitioning problem, but the ground state we do find is (one of) the best possible solutions, in the sense that it minimizes the mismatch. Minimizing this mismatch is an NP-hard problem, and we see that we do not require any more fancy footwork to solve the optimization problem – the same Hamiltonian does the trick. The number partitioning problem, as long as many others spin glass problems, can be investigated with statistical mechanics techniques. This was done, for instance, in ref. [21].

Light-matter interaction at the quantum level: the Dicke model

In this chapter we review fundamental facts on *superradiance*, a concept introduced in 1954 by R. Dicke [40] in order to describe the collective spontaneous emission of photons from a collection of atoms. Loosely speaking superradiance occurs when a group of N emitters, such as excited two-level atoms, interact with a common light field. If the wavelength of the light is much greater than the separation of the emitters, then the emitters interact with the light in a collective and coherent fashion. Whenever this length scale separation is achieved, the atomic sample emits light as a high intensity pulse (with rate $\propto N^2$). This result is drastically different from the expected exponential decay (with rate $\propto N$) of a group of independent atoms radiating spontaneously.

Superradiance can be elegantly understood in a statistical mechanical framework as a quantum phase transition [41]. This was firstly highlighted by Hepp and Lieb [5], who solved the so called Dicke model. Here we present this solution following the more comprehensible and intuitive approach of Wang and Hioe [7].

This research field is source of renewed interest thanks to the advent of quantum simulators based on ultracold atoms. Recently several proposals and experiments have been put forward to simulate the toy Hamiltonian of the Dicke model. In this chapter we will try to review the state of the art, at the best of our knowledge. We stress that our original work is mainly motivated by some of these proposals.

3.1 Thermodynamics of the Dicke model: the superradiant phase transition

One of the primary goals of Quantum Optics is to understand the interaction between *qubits* (two-level systems) and quantized radiation fields. From this viewpoint, a benchmark model, widely investigated, is the Rabi model, whose Hamiltonian is given by ($\hbar = 1$)

$$H_R = \omega a^\dagger a + \Delta \sigma^z + \Omega \left(a + a^\dagger \right) \sigma^x . \tag{3.1}$$

The equation above describes the interaction (in the dipole approximation) of a monochromatic radiation field of frequency ω with a single two-level system with energy levels splitted by Δ. Photons are described by a single bosonic harmonic oscillator, whereas the atom is frozen at fixed position and therefore only internal degrees of freedom have

to be taken into account. For a two-level system these degrees of freedom are described, as usual, by Pauli matrices:

$$\sigma^x = \begin{pmatrix} 0 & 1 \\ 1 & 0 \end{pmatrix}, \qquad \sigma^y = \begin{pmatrix} 0 & -i \\ i & 0 \end{pmatrix}, \qquad \sigma^z = \begin{pmatrix} 1 & 0 \\ 0 & -1 \end{pmatrix}.$$

Despite its apparent simplicity, finding out the exact spectrum of the Hamiltonian operator in (3.1) is a formidable task: only recently it was proved that this model is *integrable* [42], in the sense that the spectrum is given by the zeros of a trascendental function whose power series in Ω is known.

A simpler version of this interacting quantum system is obtained in the weak coupling ($\Omega \ll \omega$) and quasi-resonant ($2\Delta \sim \omega$) regime. If these conditions are fullfilled we can perform a *rotating wave* approximation in order to obtain the so called Jaynes-Cummings Hamitonian

$$H_{JC} = \omega a^\dagger a + \Delta \sigma^z + \Omega \left(a \sigma^x + a^\dagger \sigma^- \right), \tag{3.2}$$

with: $\sigma^+ := (\sigma^x + i\sigma^y)/2$, $\sigma^- := (\sigma^x - i\sigma^y)/2$. Besides the energy itself, this systems is endowed with another conserved charge, generating a continuous $U(1)$ symmetry:

$$C = a^\dagger a + \frac{\sigma^z}{2}. \tag{3.3}$$

The existence of such a commuting operator allows to decompose the Hamiltonian operator as a direct sum on two-dimensional invariant subspaces, and therefore to exhibit explicit simple expressions both for the eigenvalues and the eigenvectors of the problem.

The Dicke model is a natural many-body extension of these single atom systems and describes a collection of N two level atoms interacting with a common quantized radiation field. Its Hamiltonian is given by

$$H_D = \sum_{s=1}^M \omega_s a_s^\dagger a_s + \frac{1}{2}\Delta \sum_{j=1}^N \sigma_j^z + \frac{1}{2\sqrt{V}} \left[\left(\sum_{s=1}^M \lambda_s'(a_s + a_s^\dagger) \right) \left(\sum_{j=1}^N (\sigma_j^+ + \sigma_j^-) \right) \right]. \tag{3.4}$$

Here atoms interact with M photonic modes of (in principle) different frequencies ω_s, V is the volume of the atomic cloud, and λ_s' is a mode-dependent coupling constant between the photons and the two-level systems. In the original formulation by Dicke, the coupling constants are

$$\lambda_s' = \Delta d \, (2\pi/\omega_s)^{\frac{1}{2}} \, (N/V)^{\frac{1}{2}}, \tag{3.5}$$

where d is the projection of the atomic dipole moment along the polarization vector of the electromagnetic field. Remarkably, the strenght of interaction can be tuned by varying the atomic density $\rho = N/V$. Loosely speaking we would like to prove that there exists a density threshold for which the macroscopic properties of the Dicke model abrubtly change, in order to understand how superradiance emerges from the interaction between the microscopic constituents of the system. As anticipated above, a natural framework for investigating this collective phenomenon is equilibrium statistical mechanics.

From now on, we will consider, for safe of clarity, a single mode ($M = 1$) Dicke Hamiltonian. For future convenience it is useful to measure all the parameters in (3.4) in units of ω. This amounts to study the following rescaled Hamiltonian

$$H = a^\dagger a + \sum_{j=1}^{N} \left[\frac{1}{2} \epsilon \, \sigma^z_{\, j} + \frac{\lambda}{2\sqrt{N}} (a + a^\dagger) \sigma^x_j \right], \qquad (3.6)$$

with $\epsilon = \Delta/\omega$ e $\lambda = \lambda' \rho / \omega$.

3.1.1 Partition function of the Dicke model

In this section we present the equilibrium statistical mechanical approach to the Dicke model, following the paper by Wang and Hioe [7], who simplified the original solution by Hepp and Lieb [5]. It is worth remarking that here we do not prove their method to be correct. For a mathematical proof see [6].

At equilibrium informations about the macroscopic properties of the system are entirely contained in the partition function $Z(N,T) = \mathrm{Tr}\, e^{-\beta H}$, where $\beta = 1/T$ is the inverse of the temperature. The trace is over the Hilbert spaces of both the photons and the atoms. In order to perform the calculation we need to choose a convenient basis.

For the bosonic degrees of freedom we choose the coherent states $|\alpha\rangle$, with the following properties:

1. $|\alpha\rangle$ is an eigenstate of the annihilation operator a

$$a |\alpha\rangle = \alpha |\alpha\rangle; \quad \langle\alpha| a^\dagger = \langle\alpha| \alpha^* \, .$$

2. The $|\alpha\rangle$'s are an (over)complete set of states:

$$\int \frac{\mathrm{d}^2\alpha}{\pi} |\alpha\rangle\langle\alpha| = 1 \, ,$$

with $\int \mathrm{d}^2\alpha := \iint \mathrm{d}(\mathrm{Im}(\alpha)) \, \mathrm{d}(\mathrm{Re}(\alpha))$.

By definition the partition function is

$$Z(N,T) = \sum_{s_1=\pm 1} \cdots \sum_{s_N=\pm 1} \int \frac{\mathrm{d}^2\alpha}{\pi} \langle s_1 \cdots s_N | \langle\alpha| e^{-\beta H} |\alpha\rangle | s_1 \cdots s_N \rangle \, . \qquad (3.7)$$

The first step is to evaluate the matrix element $\langle\alpha| e^{-\beta H} |\alpha\rangle$. We define the rescaled operators $b := a/\sqrt{N}$ and $b^\dagger := a^\dagger/\sqrt{N}$. These operators satisfy the commutation relations $[b, b^\dagger] = 1/N$. In terms of these rescaled variables, we can rewrite equation (3.6) as

$$H = \sum_{j=1}^{N} \left[b \, b^\dagger + \frac{\epsilon}{2} \sigma^z_{\, j} + \frac{\lambda}{2} (b + b^\dagger) \sigma^x_j \right]. \qquad (3.8)$$

Let us consider, as an example, the following string of b's:

$$bb^\dagger b^\dagger b = (b^\dagger b + \frac{1}{N}) b^\dagger b = b^\dagger b b^\dagger b + \frac{1}{N} b^\dagger b = b^\dagger (b^\dagger b + \frac{1}{N}) b + \frac{1}{N} b^\dagger b = b^\dagger b^\dagger b b + \frac{2}{N} b^\dagger b.$$

From this example we can argue that every contraction performed to obtain the normal ordered string can be discarded in the thermodynamic limit $N \to \infty$. Using this property, it turns out that

$$\langle \alpha | H^r | \alpha \rangle \simeq (\langle \alpha | H | \alpha \rangle)^r = \left[\alpha \alpha^* + \sum_{j=1}^{N} \left[\frac{\epsilon}{2} \sigma^z_j + \frac{\lambda}{2\sqrt{N}} (\alpha + \alpha^*) \sigma^x_j \right] \right]^r .$$

Therefore the photonic matrix element is

$$\begin{aligned} \langle \alpha | e^{-\beta H} | \alpha \rangle &= \langle \alpha | \sum_r \frac{(-\beta H)^r}{r!} | \alpha \rangle \\ &= \exp \left\{ -\beta \left[\alpha \alpha^* + \sum_{j=1}^{N} \left(\frac{\epsilon}{2} \sigma^z_j + \frac{\lambda}{2\sqrt{N}} (\alpha + \alpha^*) \sigma^x_j \right) \right] \right\} . \end{aligned} \tag{3.9}$$

The argument that we used here in order to obtain this result is purely heuristic and is not a formal proof. Hepp and Lieb proved rigorous bounds for the Dicke partition function in such a way to prove this result.

Once the photonic matrix element is evaluated, we consider the spin trace. It is convenient to define:

$$h_j = \frac{\epsilon}{2} \sigma^z_j + \frac{\lambda}{2\sqrt{N}} (\alpha + \alpha^*) \sigma^x_j .$$

Obviously this set of operators commute with each other. Using this definition and (3.9), it turns out that

$$\begin{aligned} \langle s_1 \cdots s_N | \langle \alpha | e^{-\beta H} | \alpha \rangle | s_1 \cdots s_N \rangle &= \\ &= e^{-\beta |\alpha|^2} \langle s_1 \cdots s_N | \exp \left(-\beta \sum_{j=1}^{N} h_j \right) | s_1 \cdots s_N \rangle \\ &= e^{-\beta |\alpha|^2} \langle s_1 \cdots s_N | \prod_{j=1}^{N} e^{-\beta h_j} | s_1 \cdots s_N \rangle \\ &= e^{-\beta |\alpha|^2} \prod_{j=1}^{N} \langle s_j | e^{-\beta h_j} | s_j \rangle , \end{aligned} \tag{3.10}$$

and the partition function (3.7) is written down as

$$\begin{aligned} Z(N,T) &= \int \frac{d^2\alpha}{\pi} \sum_{s_1 = \pm 1} \cdots \sum_{s_N = \pm 1} e^{-\beta |\alpha|^2} \prod_{j=1}^{N} \langle s_j | e^{-\beta h_j} | s_j \rangle \\ &= \int \frac{d^2\alpha}{\pi} e^{-\beta |\alpha|^2} \left(\langle +1 | e^{-\beta h} | +1 \rangle + \langle -1 | e^{-\beta h} | -1 \rangle \right)^N \\ &= \int \frac{d^2\alpha}{\pi} e^{-\beta |\alpha|^2} \left(\text{Tr}(e^{-\beta h}) \right)^N , \end{aligned} \tag{3.11}$$

with:

$$h = \frac{\epsilon}{2} \sigma^z + \frac{\lambda}{2\sqrt{N}} (\alpha + \alpha^*) \sigma^x .$$

The eigenvalues of h are easily found to be

$$\mu = \pm \left(\frac{1}{2}\epsilon\right)\left(1 + \frac{4\lambda^2[\text{Re}(\alpha)]^2}{\epsilon^2 N}\right)^{\frac{1}{2}}. \tag{3.12}$$

Using (3.12) in (3.11):

$$
\begin{aligned}
Z(N,T) &= \int \frac{d^2\alpha}{\pi} e^{-\beta|\alpha|^2} \left(e^{\beta|\mu|} + e^{-\beta|\mu|}\right)^N \\
&= \int \frac{d^2\alpha}{\pi} e^{-\beta|\alpha|^2} \left\{2\cosh\left[\left(\frac{1}{2}\beta\epsilon\right)\left(1 + \frac{4\lambda^2[\text{Re}(\alpha)]^2}{\epsilon^2 N}\right)^{\frac{1}{2}}\right]\right\}^N.
\end{aligned}
\tag{3.13}
$$

In conclusion we are able to write the partition function as a single integral

$$
\begin{aligned}
Z(N,T) &= \frac{\sqrt{N}}{\sqrt{\pi\beta}} \int_{-\infty}^{\infty} dy\, e^{-N\beta y^2} \left\{2\cosh\left[\left(\frac{1}{2}\beta\epsilon\right)\left(1 + \frac{4\lambda^2 y^2}{\epsilon^2}\right)^{\frac{1}{2}}\right]\right\}^N \\
&= \frac{\sqrt{N}}{\sqrt{\pi\beta}} \int_{-\infty}^{\infty} dy\, \exp\left[N\phi(y)\right],
\end{aligned}
$$

with

$$\phi(y) := -\beta y^2 + \log\left[2\cosh\left(\left(\frac{1}{2}\beta\epsilon\right)\left(1 + \frac{4\lambda^2 y^2}{\epsilon^2}\right)^{\frac{1}{2}}\right)\right]. \tag{3.14}$$

Finally we are able to evaluate the partition function with the saddle point method:

$$Z(N,T) \propto \max_{-\infty \le y \le \infty} \exp\left[N\phi(y)\right]. \tag{3.15}$$

3.1.2 Saddle point equations and superradiant phase transition

In this section we apply the saddle point method in order to investigate the behavior of the partition function. As a first step we evaluate the derivative of (3.14):

$$\phi'(y) = -2\beta y + \frac{2\beta\lambda^2 y}{\epsilon}\left(1 + \frac{4\lambda^2 y^2}{\epsilon^2}\right)^{-\frac{1}{2}}\tanh\left(\left(\frac{1}{2}\beta\epsilon\right)\left(1 + \frac{4\lambda^2 y^2}{\epsilon^2}\right)^{\frac{1}{2}}\right). \tag{3.16}$$

This equation has two different stationary points, the trivial one in $y = 0$ and the other one given by the solution of the following equation:

$$\frac{\epsilon}{\lambda^2}\eta = \tanh\left[\left(\frac{1}{2}\beta\epsilon\right)\eta\right], \tag{3.17}$$

with $\eta := \left(1 + 4\lambda^2 y^2/\epsilon^2\right)^{\frac{1}{2}}$. By direct inspection, it is straightforward to see that for $\lambda^2 < \epsilon$, equation (3.17) has no solution, and therefore in this case the only stationary point is the trivial one in $y = 0$. Let us consider (3.17) for $\lambda^2 > \epsilon$. There are two possible scenarios. For $\beta < \beta_c$, with β_c defined implicitly through

$$\frac{\epsilon}{\lambda^2} = \tanh\left[\left(\frac{1}{2}\beta_c\epsilon\right)\right],$$

the equation has no solution. On the other hand, if $\beta > \beta_c$, (3.17) has a single non-zero solution $\eta = \eta_0$. It is possible to show that this solution minimizes the free energy in the strong coupling ($\lambda^2 > \epsilon$) and low temperature ($\beta > \beta_c$) regime. This is the so called superradiant regime. From physical intuition, we expect that the mean number of photons $\bar{n}$, is a good order parameter to characterize the phase transition. By definition this observable is given by

$$\bar{n} = \left\langle \frac{a^\dagger a}{N} \right\rangle = \frac{\mathrm{Tr}\left[\left(\frac{a^\dagger a}{N} \right) e^{-\beta H} \right]}{Z(N,T)} \ . \tag{3.18}$$

A slight modification of the previous calculations allows to evaluate the order parameter:

$$\mathrm{Tr}\left[\left(\frac{a^\dagger a}{N} \right) e^{-\beta H} \right] = \frac{1}{N} \int \frac{\mathrm{d}^2\alpha}{\pi} |\alpha|^2 e^{-\beta|\alpha|^2} f(\mathrm{Re}(\alpha))$$
$$= \frac{1}{\pi N} \int_{-\infty}^{\infty} \mathrm{d}v \, v^2 e^{-\beta v^2} f(v) \int_{-\infty}^{\infty} \mathrm{d}w \, e^{-\beta w^2} +$$
$$+ \frac{1}{\pi N} \int_{-\infty}^{\infty} \mathrm{d}v \, e^{-\beta v^2} f(v) \int_{-\infty}^{\infty} \mathrm{d}w \, w^2 e^{-\beta w^2} \ ,$$

with $v := \mathrm{Re}(\alpha)$, $w := \mathrm{Im}(\alpha)$ and

$$f(x) := \left\{ 2\cosh\left[\left(\frac{1}{2}\beta\epsilon \right) \left(1 + \frac{4\lambda^2 x^2}{\epsilon^2 N} \right)^{\frac{1}{2}} \right] \right\}^N \ .$$

Within standard manipulations we end up with:

$$\bar{n} = \frac{\int_0^\infty \mathrm{d}y \, y^2 \exp\left\{ N\left[-\beta y^2 + \log\left[2\cosh\left(\left(\frac{1}{2}\beta\epsilon \right) \left(1 + \frac{4\lambda^2 y^2}{\epsilon^2} \right)^{\frac{1}{2}} \right) \right] \right] \right\}}{\int_0^\infty \mathrm{d}y \, \exp\left\{ N\left[-\beta y^2 + \log\left[2\cosh\left(\left(\frac{1}{2}\beta\epsilon \right) \left(1 + \frac{4\lambda^2 y^2}{\epsilon^2} \right)^{\frac{1}{2}} \right) \right] \right] \right\}} \ . \tag{3.19}$$

The saddle point method allows to identify two different regimes:

- If $\lambda^2 < \epsilon$ or if $\lambda^2 > \epsilon$ and $\beta < \beta_c$, then $\bar{n} = 0$.

- If $\lambda^2 > \epsilon$ and $\beta > \beta_c$, $\bar{n} = y_0^2 \neq 0$, with y_0 the maximum of ϕ in (3.14).

A straightforward analysis shows that the mean number of photons $\bar{n}$ is a continuous function, and therefore superradiance is a second order phase transition.

In the zero temperature limit $T \to 0$ ($\beta \to \infty$), all the equations of the previous section get simpler. For instance:

$$\lim_{\beta \to \infty} \phi(y) = \beta\left[-y^2 + \frac{1}{2}\epsilon\sqrt{1 + \frac{4\lambda^2 y^2}{\epsilon^2}} \right] ,$$

and thus, in order to characterize the transition we consider the following function:

$$\varphi(y) := -y^2 + \frac{1}{2}\epsilon\sqrt{1 + \frac{4\lambda^2 y^2}{\epsilon^2}} \ , \tag{3.20}$$

and its derivative:

$$\varphi'(y) = 2y \left[-1 + \frac{\lambda^2}{\epsilon} \left(1 + \frac{4\lambda^2 y^2}{\epsilon^2} \right)^{-\frac{1}{2}} \right].$$

The two stationary points are:

$$y = 0 \qquad \text{or} \qquad y^2 = \frac{1}{4\lambda^2} \left(\lambda^4 - \epsilon^2 \right).$$

and the second one exists if and only if $\lambda^2 > \epsilon$. Thus the energy of the superradiant ground state can be evaluated exactly in the thermodynamic limit.

3.2   Dicke quantum simulators: state of the art

The Dicke model was originally proposed in order to describe superradiance, i. e. how single atoms in a cloud (interacting with light) can cooperate in order to produce an enhancement of spontaneous emission. This phenomenon, as we tried to explain in the previous section, can be understood as a quantum phase transition. Nonetheless, in the Quantum Optics community there is an ongoing debate to understand whether this phase transition is physical rather than an artifact of approximations: this is the so called A^2-problem [43].

A possible loophole to circumvent this problem and realize a genuine superradiant phase transition is to provide quantum simulators that can mimic *effectively* the Dicke Hamiltonian (3.4) in all the parameter regimes. This is the same philosophy behind the ultracold atoms realization of the superfluid to Mott insulator phase transition in the Bose-Hubbard model [44]: something very difficult to observe in real life condensed matter systems may be fruitfully investigated in a completely tunable *analogic* version of the corresponding toy model.

In order to simulate the Dicke model, we mainly identify two large classes of quantum simulators: cavity QED with ultracold atoms and circuit QED with superconducting qubits. Both these platforms present advantages and limitations, that are currently mainstream reaserch topics. In the following we will focus out attention on the ultracold atoms proposals and realizations of the Dicke Hamiltonian.

A promising route to realize the superradiant transition has been proposed recently in the setting of cavity quantum electrodynamics by Carmichael and coworkers [45]. In their scheme strong coupling between two ground states of an atomic ensemble is induced by balanced Raman transitions involving a cavity mode and a pump field. This idea circumvents the thought to be unattainable condition for the Dicke quantum phase transition which requires a coupling strength on the order of the energy separation between the two involved atomic levels. This setup was recently implemented and evidences of a superradiant transition have been reported [46].

To date, however, the most popular implementation of an effective Dicke Hamiltonian is the experiment realized in Zurich by Esslinger's group in 2010 [22]. We stress that their implementation is rather different in spirit respect to the original Dicke model.

3.2.1   Self organization of a BEC in an optical cavity

Esslinger and coworkers considered a BEC placed inside an high-finesse optical cavity. Intuitively the cavity field is able to mediate an infinitely long range interaction between all the atoms in the sample. In such a setting a phase transition from a uniform Bose-Einstein condensate to a self-organized phase has been predicted once the atoms induce a sufficiently strong coupling between a pump field and an empty cavity mode. The experimental setup is schematically shown in Figure (3.1).

Remarkably the description of a BEC in an optical cavity is in one-to-one correspondence with the Dicke Hamiltonian [47]. Let us consider a zero-temperature BEC of a number of N atoms of mass m which is inside a high-Q optical cavity with a single quasi-resonant mode of frequency ω_C. The atoms are coherently driven from the side by a pump laser field. The pump laser frequency ω is detuned far below the atomic resonance frequency ω_A, so that the atom-pump (red) detuning $\Delta_A = \omega - \omega_A$ far exceeds the rate of spontaneous emission. One can then adiabatically eliminate the excited atomic level and the atom acts merely as a phase-shifter on the field [48]. The dispersive atom-field interaction has a strength $U_0 = g_0^2/\Delta_A$, where g_0 is the single-photon Rabi frequency at the antinode of the cavity mode. We describe the condensate dynamics in one dimension along the cavity axis x, where the cavity mode function is $\cos kx$. The motion perpendicular to the cavity axis requires a trivial generalization of the theory, and with a standing-wave side pump the self-organization effect occurs quite similarly in two and three dimensions.

The many-particle Hamilton operator in a frame rotating at the pump frequency ω and with $\hbar = 1$ reads [48]

$$H = -\Delta_C\, a^\dagger a + \int_0^L \Psi^\dagger(x)\left[-\frac{\hbar}{2\,m}\frac{d^2}{dx^2} + U_0\, a^\dagger a \cos^2(kx) + i\eta_t \cos kx(a^\dagger - a)\right]\Psi(x)dx, \quad (3.21)$$

where $\Psi(x)$ and a are the annihilation operators of the atom field and the cavity mode, respectively. The cavity length is L, the detuning $\Delta_C = \omega - \omega_C$ is the effective photon energy in the cavity. Atom-atom s-wave scattering is neglected. Besides the dispersive interaction term $U_0 \cos^2 kx$, there is another sinusoidal atom-photon coupling term describing an effective cavity-pump with the amplitude $\eta_t = \Omega g_0/\Delta_A$, where Ω is the Rabi frequency of the coupling to the transverse driving field.

Self-organization is a transition from the homogeneous to a λ-periodic distribution. The minimum Hilbert-space for the atom field required to describe this transition is spanned by two Fourier-modes,

$$\Psi(x) = \frac{1}{\sqrt{L}}c_0 + \sqrt{\frac{2}{L}}c_1 \cos kx\,, \quad (3.22)$$

where c_0 and c_1 are bosonic annihilation operators. In the low excitation regime these two modes can be assumed to form a closed subspace, so $c_0^\dagger c_0 + c_1^\dagger c_1 = N$ is a constant of motion giving the number of particles. On invoking the Schwinger-representation in
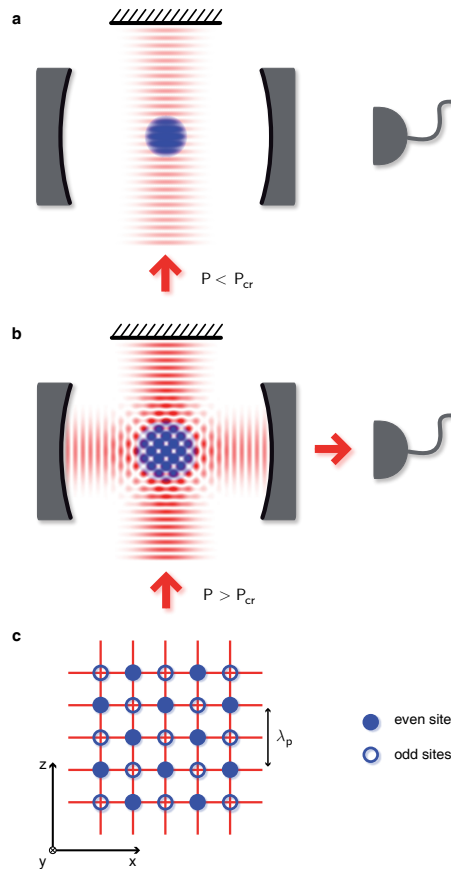
Figure 3.1: Esslinger's group experiment: a BEC is placed inside a single mode optical cavity and pumped in the transverse direction z with a standing wave laser. The frequency of the pump laser is far red-detuned with respect to the atomic transition line but close detuned to a particular cavity mode. Correspondingly, the atoms coherently scatter light into the cavity mode with a phase depending on their position within the combined pump–cavity mode profile. a) Below a critical pumping P_{cr} the density of the BEC is uniform along the cavity axis. The formation of a macroscopic cavity field is suppressed due to the destructive interference of individual scatterers. b) Above the critical pumping atoms self-organize in a checkerboard pattern (c) in order to maximize cooperative scattering. This results in the formation of a macroscopic cavity field, that can be measured outside the cavity.
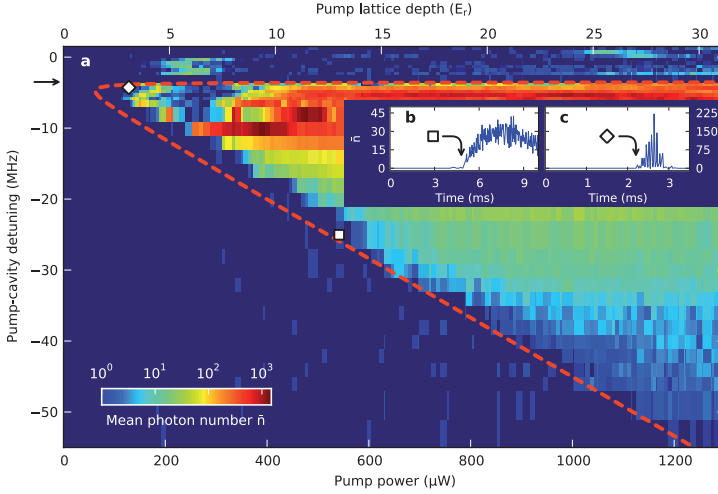
Figure 3.2: Experimental phase diagram: the mean intracavity photon number is displayed as a function of the pump power and of the pump-cavity detuning. Every pixel depicted in the plot is a single experiment run with different parameters. This result is in good agreement with the theoretical prediction of the Dicke model (red dashed curve).

terms of the spin $\hat{S}$ with components

$$\hat{S}_x = \frac{1}{2}\left(c_1^\dagger c_0 + c_0^\dagger c_1\right), \tag{3.23}$$

$$\hat{S}_y = \frac{1}{2i}\left(c_1^\dagger c_0 - c_0^\dagger c_1\right), \tag{3.24}$$

$$\hat{S}_z = \frac{1}{2}\left(c_1^\dagger c_1 - c_0^\dagger c_0\right), \tag{3.25}$$

the Hamiltonian Eq. (3.21) confined into the two-mode subspace reads

$$H = -\delta_C\, a^\dagger a + \omega_R \hat{S}_z + iy(a^\dagger - a)\hat{S}_x/\sqrt{N} + ua^\dagger a\left(\tfrac{1}{2} + \hat{S}_z/N\right), \tag{3.26}$$

where $\delta_C = \Delta_C - 2u$, $\omega_R = \hbar k^2/2m$, $u = N U_0/4$, and $y = \sqrt{2N}\eta_t$. In the first three terms we can recognize the Dicke-model Hamiltonian with a coupling constant y tunable via the transverse driving amplitude η_t. The last term is inherent to the BEC-cavity system, however, it does not essentially change the conclusions to be drawn here as long as $|u| < |\delta_c|$. The theoretical predictions of the Dicke model can be then compared with experiments, see Figure (3.2).

Once the mapping is exhibited, it is clear that this realization of the Dicke Hamiltonian is deeply different in spirit from the original model with two-level atoms. Here are the vibrational degrees of freedom of the BEC, as a whole, to form a collective angular momentum algebra (in the thermodynamics limit and at zero temperature) interacting with the cavity field.

In this thesis we are mostly interested in generalized Dicke simulators where the fundamental building blocks are genuine two-level atoms, in the spirit of Carmicheal
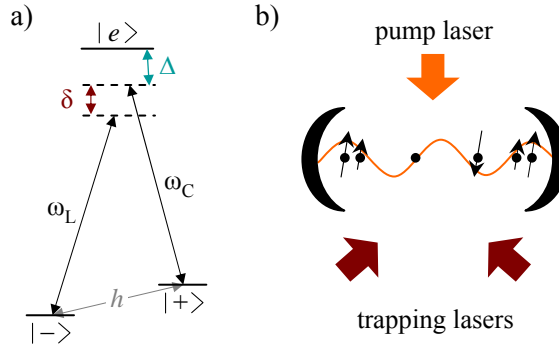
Figure 3.3: (a) Level structure of three-level Λ atoms, dressed by a pump laser at frequency ω_L, cavity mode(s) at frequency ω_C, and a microwave field represented by h. The detuning from two-photon resonance, δ, is assumed to be much smaller than the detuning of laser and cavity photons from the atomic transition, Δ. (b) Proposed experimental setup. Atoms are tightly trapped by trapping lasers, which are far detuned from the atomic transition, and pumped transversely. Spins are self-organized as discussed in the text for a single-mode cavity, with a sinusoidal mode function as depicted: spins at even antinodes interact ferromagnetically with spins at other even antinodes, but antiferromagnetically with spins at odd antinodes. Spin-spin interactions are strongest for spins trapped at antinodes; therefore, ordering is strongest at antinodes and weakest at nodes.

proposal, partly realized in [46]. This class of Dicke simulators, properly generalized, will be the subject of our investigations in Chapter 4. The main motivation of our work are the two paper by Lev and coworkers [3] and Strack and Sachdev [4], where they considered a multimomodal disordered generalization of Dicke simulators.

3.3 Multimode disordered Dicke simulators

In this section we briefly review the proposal by Gopalakrishnan, Lev and Goldbart. These authors suggest that ultracold atoms trapped in multimode optical cavities may be viable platforms for investigating spin glass phenomenology at the quantum level.

Let us consider Λ-type atoms whose lower levels (which will be our two spin states, $|+\rangle$ and $|-\rangle$) are separated by a microwave transition whereas the excited level, $|e\rangle$, is separated from both by an optical transition. The $|\pm\rangle$ states are assumed to be tightly confined at the intensity extrema of trapping lasers that are far detuned from the $|\pm\rangle \rightarrow |e\rangle$ transition; i.e., the atomic positional degrees of freedom are assumed to be frozen out. Disorder can be introduced using diffusers. The atoms are confined in an optical cavity having multiple degenerate modes, at a frequency red-detuned from the $|+\rangle \rightarrow |e\rangle$ transition by $\Delta \sim 1$ GHz; other modes are typically farther-detuned (e.g., by ~ 15 GHz for a 1 cm cavity). Additionally, the atoms interact with a pump laser oriented *transverse* to the cavity axis, red-detuned from the $|-\rangle \rightarrow |e\rangle$ transition by $\Delta + \delta$, where $\delta \simeq 10$ MHz is the detuning from two-photon resonance. The microwave $|+\rangle \leftrightarrow |-\rangle$ transition is driven at a weak Rabi frequency.

Under these conditions, the spin-spin interactions can be understood as follows: an

atom in the $|-\rangle$ state can scatter a laser photon into a cavity mode, thus changing its state to $|+\rangle$; this virtual cavity photon, being δ higher in energy than laser photons, is reabsorbed into the laser after a time $\sim 1/\delta$. The reabsorption involves flipping the state of a $|+\rangle$ atom (typically a different one from the initial atom) to $|-\rangle$. This entire process generates an interaction between two atoms arbitrarily far apart, and hence an effective long range spin model with couplings depending both on the position of the atoms and on the profiles of the cavity modes.

We further assume that the cavity photon leakage rate per mode, $\kappa \ll \delta$, and also that the atomic-excited-state decay rate, $\gamma \ll \Delta$. In this "*dispersive*" regime, the conservative virtual-excitation processes fall off as $1/\delta$ and $1/\Delta$ respectively, whereas the dissipative processes fall off as κ/δ^2 and γ/Δ^2 respectively. Generally, dissipation does not change the mean-field properties even beyond this regime.

Hence, upon *adiabatic elimination* [48] of the state $|e\rangle$, the Hamiltonian $\mathcal{H}$ of the atom-light system takes the form

$$\mathcal{H} = H_{\text{at}} + \sum_{\alpha=1}^{M} \omega_\alpha a_\alpha^\dagger a_\alpha + \frac{\Omega}{\Delta} \sum_{\alpha,i=1}^{N,M} g_\alpha(\mathbf{x}_i)\sigma_-^i a_\alpha^\dagger + \text{h.c.,} \tag{3.27}$$

where ω_α is the frequency of cavity mode α; a_α destroys a cavity photon; Ω is the strength (i.e., Rabi frequency) of the pump laser; $g_\alpha(\mathbf{x}_i)$ describes the coupling to mode α at the position $\mathbf{x}_i$ of atom i; and the σ operators are Pauli matrices acting on the atomic ground-state manifold. One can rewrite the coupling $g_\alpha(\mathbf{x}_i)$ as $g\Xi_\alpha(\mathbf{x}_i)$, where g is an overall coupling strength (assumed to be the same for all strongly-coupled modes) and $\Xi_\alpha(\mathbf{x}_i)$ a normalized mode profile. The terms in $H_{\text{at}} = \sum_i (h_x \sigma_x^i + h_z \sigma_z^i)$ represent transitions that do not involve the cavity, and are due to the $|+\rangle \leftrightarrow |-\rangle$ microwave driving: h_x is the microwave Rabi frequency, h_z is the detuning, and σ^i are the Pauli matrices for atom i. Note that the model described above, while similar in some ways to the multimode Dicke model, differs from it in the crucial respect that, in the present case, the different modes have *distinct spatial profiles*; it is this feature, not present in the multimode Dicke model, that enables frustration to be realized.

This proposal is the main motivation of the theoretical analysis that we perform in Chapter 4. Using an approach inspired from spin glasses, we show that the multimode disordered Dicke model is equivalent to a quantum Hopfield network. We propose variational ground states for the system at zero temperature, which we conjecture to be exact in the thermodynamic limit. These ground states contain the information on the disordered qubit-photon couplings. Our results lead to two intriguing physical implications. First, once the qubit-photon couplings can be engineered, it should be possible to build scalable pattern-storing systems whose dynamics is governed by quantum laws. Second, we argue with an example of how such Dicke quantum simulators might be used as solvers of "hard" combinatorial optimization problems.

Dicke simulators with emergent collective quantum computational abilities

In this chapter we present our original work. The following sections are an adaptation of our published results.

4.1 Replica symmetry breaking in cold atoms and spin glasses

Replica Symmetry Breaking (RSB) appeared for the first time as a necessary ingredient to solve the Sherrington-Kirkpatrick (SK) model for spin glasses [32], an Ising model characterized by a fully connected network and quenched random interactions. This model was introduced to be exactly solvable and not to reproduce a physical system. Nonetheless, through the years we have accumulated a number of examples of complex problems in biology, informatics, and economy in which RSB is found to play a fundamental role [8].

One of the reasons why the SK model received particular attention is that it allows for a solution via the celebrated Parisi *Ansatz* [35]. In a nutshell, Parisi suggested RSB as a consistent scheme to break the permutational symmetry of fictitious copies of the system (introduced with the *replica trick*). Physically, RSB in disordered spin systems is interpreted with the emergence of a spin-glass phase characterized by many pure states organized in an ultrametric structure [36, 49].

A fascinating proposal to observe glassy behaviour in a physical system came from the study of light propagation in Kerr-like disordered media [50, 51, 52], where the slowing-down as the critical point is approached is expected to occur on a much faster timescale than ordinary matter. Progress in this direction is encouraging: for instance, the observation of the mode-locking transition in Random Lasers has been recently reported [53]. A scheme to measure the Edwards-Anderson order parameter in interacting-replicas has been presented in [54] for a Bose gas. Despite these efforts, however, no conclusive results regarding the nature of the spin-glass phase have been presented so far.

In the last years, cold and ultracold atoms emerged as a powerful tool to test fundamental models of Condensed Matter physics [55] and disordered systems [56, 57, 58, 59]. Notable attention has been devoted to the Dicke model [40], describing the interaction

between M electromagnetic modes and N two-level systems. The superradiant quantum phase transition (QPT) of the single-mode Dicke model was predicted [47] and observed [22] in a Bose-Einstein Condensate with cavity-mediated long-range interactions, as detailed in the previous chapter. The appearance of quantum chaos at the Dicke QPT threshold was investigated in [60], and the Jaynes-Cummings-Hubbard model introduced in [61] can be rewritten as a multimodal Dicke model. This has been recently suggested as a quantum emulator for the fractional quantum Hall effect [62].

In the spirit outlined above we consider the multimode Dicke Hamiltonian introduced in [3, 4], where a spin-glass dynamics is obtained for a system of atoms placed in a multimode cavity. Here we focus our attention on the possible emergence of RSB in this setup, and the corresponding spin-glass observables. A simple and insightful result is obtained in the resonant, zero field regime (using the terminology adopted in [3]), where the system exactly realizes the SK Hamiltonian. In the case of a non-zero coupling one can also access the momenta of the overlap distribution and the ultrametric properties which characterize the Replica Symmetric broken phase. This opens up new interesting opportunities for the validation of spin-glass mean field theories and the observation of spin-glass transitions in a highly controllable system. We also wish to stress here that, from a theoretical standpoint, our mapping allows for an exact solution of the multimode Dicke model in the strong-field limit with quenched disordered interactions.

4.1.1 Model and zero-field limit

The Hamiltonian of the system is a multimode Dicke model with spatially-varying couplings for M photonic modes and N two-level systems [3, 4]:

$$H = H_{\text{at}} + \sum_{m=1}^{M} \omega_m a_m^\dagger a_m + \Omega \sum_{i=1}^{N} \sum_{m=1}^{M} g_{im}(a_m^\dagger + a_m)\sigma_i^x . \tag{4.1}$$

Here $H_{\text{at}} = h_x \sum_{i=1}^{N} \sigma_i^x + h_z \sum_{i=1}^{N} \sigma_i^z$, where h_x is the Rabi frequency and h_z is the detuning of the h field, see Fig. 4.1. The coupling coefficients appearing in the Hamiltonian (4.1) can be finely tuned, offering a high level of control. Disorder is introduced by the presence of many cavity modes, described by the the spatially-varying couplings g_{im}. We focus our analysis here on the case where a large number of modes can be supported by the cavity, as in confocal or concentric geometries [63].

Following [3, 4] we proceed by integrating out the photonic modes in order to obtain an effective spin model. In the resonant limit $h_z = 0$ (zero field limit), the partition function $Z(N, \beta) = \text{Tr}\, e^{-\beta H}$ (β being the inverse temperature) can be calculated as follows. First we operate a spin-dependent translation to the creation operators (analogous transformations apply to the annihilators):

$$a_m^\dagger \to a_m^\dagger + \frac{\Omega}{\omega_m} \sum_{i=1}^{N} g_{im}\sigma_i^x \quad \forall\, m = 1, \ldots, M .$$

We note that these transformations leave unaltered the commutation relations among the photonic modes. Using these new variables the partition function can be put in the
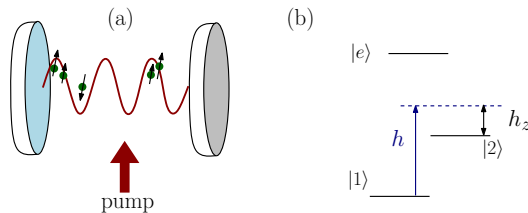
Figure 4.1: (a) Sketch of the multimode cavity setup. As in Ref. [3], N atoms are placed within a multimode cavity, kept at fixed positions by trapping beams (not shown in the figure) and pumped transversely. Ordering is strongest at the antinodes of the intra-cavity field (red full line), and atoms occupying even antinodes interact ferromagnetically with atoms at even antinodes, and antiferromagnetically with atoms at odd antinodes. (b) Upon adiabatic elimination of the upper state $|e\rangle$ [3], a Dicke interaction is realized by the $|1\rangle$ – $|2\rangle$ transition and a field h (Rabi frequency h_x, detuning h_z).

form $Z(N,\beta) = Z_{FB}(N,\beta)\,Z_{SK}(N,\beta)$, where Z_{FB} is a free boson partition function and Z_{SK} is given by:

$$Z_{SK}(N,\beta) = \sum_{\sigma_1=\pm 1} \cdots \sum_{\sigma_N=\pm 1} e^{-\beta\mathcal{H}_{SK}} ,$$

$$\mathcal{H}_{SK} = -\sum_{i,j=1}^{N} J_{ij}\sigma_i\sigma_j + h_x \sum_{i=1}^{N} \sigma_i \tag{4.2}$$

where the M-dependence is encoded in the local couplings:

$$J_{ij}\left(M,\{\omega_m\}\right) = \Omega^2 \sum_{m=1}^{M} \frac{g_{im}g_{jm}}{\omega_m} . \tag{4.3}$$

The Hamiltonian (4.2) describes an Ising model with spatially varying couplings in an external magnetic field. When $M \to \infty$, by the central limit theorem [4] the J_{ij}'s become independent random gaussian variables, and are distributed according to:

$$P\left(J_{ij}\right) = \frac{1}{(2\pi)^{1/2}J} \exp\left[(J_{ij} - J_0)^2/2J^2\right] .$$

We note that in order to obtain relevant disorder fluctuations in the thermodynamic limit ($N \to \infty$), we must require that $J_0 = \tilde{J}_0/N$, $J = \tilde{J}/\sqrt{N}$, $\tilde{J}_0$ and $\tilde{J}$ being intensive quantities. $\tilde{J}_0$ and $\tilde{J}$ parametrizes the disorder introduced by the g_{im}, their ratio representing a control parameter for the system (see Fig. 4.2). We remark that this condition implicitly imposes large number of modes ($M \sim N$) for the observation of spin-glass transitions, see also [3]. Since the couplings g_{im} evolve on the timescale of atomic motion, while the relevant light-atoms interactions occur on a much faster timescale, the random g_{im} coefficients are frozen in a single realization of the system. As a consequence, $\mathcal{H}_{SK}$ is exactly the Hamiltonian of the Sherrington-Kirkpatrick model [32] with an external field h_x (which does not play a fundamental rôle in what follows). We therefore conclude that in the resonant regime the thermodynamic properties of the disordered Dicke model (4.1) are described by the partition function Z_{SK}, so that the system (4.1) effectively realizes
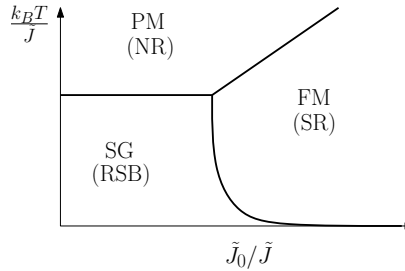
Figure 4.2: Phase diagram for the disordered multimode Dicke model, see [64]. At weak disorder (large $\tilde{J}_0/\tilde{J}$), a critical temperature is found below which the system is ferromagnetic (FM) and exhibits superradiance (SR). Above this critical temperature and for weak disorder, the system is paramagnetic (PM) and exhibits normal radiance (NR). At relatively low temperatures and strong disorder (small $\tilde{J}_0/\tilde{J}$), the system enters the spin-glass (SG) phase and displays RSB.

the SK model. The phase diagram for this model is well-known [64] and displays a spin-glass phase, so that RSB is expected also for the disordered multimode Dicke model (4.1) in the resonant regime (see Fig. 4.2).

   We now wish to turn our attention to the case of non-zero h_z. Restricting to a single photonic mode ($M = 1$) with uniform couplings ($\Omega g_i = g$, $\forall i$), the resonant case reduces to the fully connected Ising model and displays a classical paramagnetic (PM) to ferromagnetic (FM) phase transition. The only effect of introducing a non-zero external field h_z is the appearance of a threshold in the interaction strength $g^2 > h_z$ for the occurrence of the PM/FM transition [5, 6, 7]. Since the atomic density enters the expression of g, this suggests that in our disordered multimode case a non-zero h_z might introduce a threshold for the atomic density below which the phase is always paramagnetic, but this is not expected to change in a qualitative way the existence of a spin-glass phase. Indeed, as discussed below the system still realizes the SK model in the dispersive regime, with h_z acting as a relevant quantity in the detection of RSB.

4.1.2 Dispersive regime and RSB

To gain a first qualitative insight into the dispersive regime we consider the partition function for non-zero h_z and we use the Golden-Thompson inequality:

$$\text{Tr}[e^{-\beta(X+Y)}] \leq \text{Tr}[e^{-\beta X}e^{-\beta Y}], \tag{4.4}$$

which is valid for Hermitian operators X and Y. Assuming the inequality to be saturated in Eq. (4.4) and splitting the original Hamiltonian (4.1) as $X = h_z \sum_i \sigma_i^z$, $Y = H - X$, we recover the same bosonic decoupling as in the resonant limit and the partition function for the effective spin model can be approximated as:

$$Z(N, \beta) \simeq Z_{FB} \, \text{Tr}\left[e^{\beta \sum_{ij} J_{ij}\sigma_i^x \sigma_j^x} e^{-\beta h_z \sum_i \sigma_i^z}\right]. \tag{4.5}$$

In the following we will neglect the h_x term for simplicity, but our results are easily extended to the $h_x \neq 0$ case, leaving our conclusions unaffected. The symbol "Tr" has to be intended as the trace over the 2^N dimensional Hilbert space of the spins, the photonic

modes being already integrated out. We remark that Eq. (4.4) is saturated by requiring an appropriate relation between h_z and Ω, namely $\beta\Omega^2 = \lambda \tanh(2\beta h_z)$. This is a standard result in the context of the Hamiltonian formulation of spin models, such as the classical Ising model [65]. Given the partition function in the form (4.5), we are now able to establish a close connection with the usual observables employed in the characterization of the spin-glass phase. The key point in understanding this correspondence consists in rewriting the spin-glass observables in a transfer matrix language. Following [36], at fixed disorder it is possible to introduce an overlap between pure states (thermodynamic phases) α, β [66]:

$$q_{\alpha\beta} = \frac{1}{N} \sum_{i=1}^{N} m_i^\alpha m_i^\beta, \quad m_i^\alpha = \langle \sigma_i \rangle_\alpha,$$

where the thermal average $\langle \cdot \rangle_\alpha$ has to be intended only on configurations belonging to the pure state α. Given the number S of pure states of the system and P_α the probability that a typical configuration belongs to the state α, the probability distribution for two configurations to have an overlap q is given by:

$$P(q) = \sum_{\alpha,\beta=1}^{S} P_\alpha P_\beta \, \delta\left(q - q_{\alpha\beta}\right) \tag{4.6}$$

and acts as an order parameter for the spin-glass transition [36]. Intuitively, $q_{\alpha\beta}$ measures the 'similarity' between the thermodynamic phases α and β. The breaking of the permutational symmetry of the fictitious copies introduced by the replica trick is physically interpreted as the proliferation of pure states with different macroscopic properties and different overlaps. Hence, in the spin-glass phase $P(q)$ has a non-trivial behavior if Replica Symmetry is broken. In particular, the distribution $P(q)$ can be proven to be equivalent to the probability distribution of the overlap between fictitious replicas [36], which can be probed when computing the SK dynamics. We remark that $P(q)$ has been proven to be accessible in Monte Carlo simulations [67, 68, 69], and has the property of being a non self-averaging quantity in the presence of RSB [8]. The momenta $\langle q^n \rangle = \int dq \, q^n P(q)$ of the overlap distribution $P(q)$ can be calculated in a very physical way, introducing two replicated Hamiltonians of the SK model which interact ferromagnetically:

$$\mathcal{H}_2 = \mathcal{H}_{SK}\left[\sigma^{(1)}\right] + \mathcal{H}_{SK}\left[\sigma^{(2)}\right] - 2y \sum_{i=1}^{N} \sigma_i^{(1)} \sigma_i^{(2)}.$$

The corresponding partition function Z_2 can in fact be shown to be a generating function for the momenta $\langle q^n \rangle \sim \left[\partial \log Z_2 / \partial y^n\right]_{y=0}$ [36]. Another interesting feature of the spin-glass phase, the ultrametric topology of pure states [49], can be extracted looking at the partition function built with the following three-replicas Hamiltonian:

$$\mathcal{H}_3 = \mathcal{H}_{SK}\left[\sigma^{(1)}\right] + \mathcal{H}_{SK}\left[\sigma^{(2)}\right] + \mathcal{H}_{SK}\left[\sigma^{(3)}\right] +$$
$$- \sum_{i=1}^{N} \left(y_1 \sigma_i^{(1)} \sigma_i^{(2)} + y_2 \sigma_i^{(2)} \sigma_i^{(3)} + y_3 \sigma_i^{(3)} \sigma_i^{(1)}\right).$$
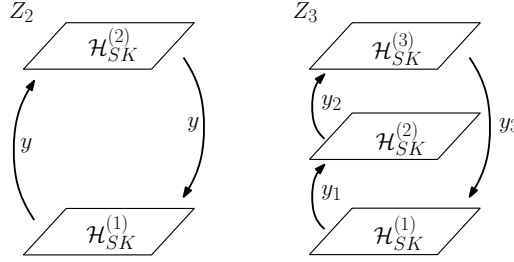
Figure 4.3: Graphical representation of the interacting-replicated partition functions, with Z_2 on the left and Z_3 on the right. Each layer represents a $\mathcal{H}_{SK}$ copy, interacting ferromagnetically with another replica with coupling strength y_i.

The replicated partition functions $Z_2(y)$ and $Z_3(y_1, y_2, y_3)$ can be rewritten within the transfer matrix formalism as $Z_2(y) = \mathrm{Tr}\left[T(y)^2\right]$, $Z_3(y_1, y_2, y_3) = \mathrm{Tr}\left[T(y_1)T(y_2)T(y_3)\right]$, where

$$T(h) = e^{\beta \sum_{ij} J_{ij} \sigma_i^x \sigma_j^x} e^{\beta h^* \sum_i \sigma_i^z} \tag{4.7}$$

is the transfer matrix and h^* is the solution of the equation: $\tanh h^* = e^{-2\beta h}$. [70] Graphically, the replicated partition functions can be visualized as different layers interacting with each other through the ferromagnetic coupling y_i as in Fig. 4.3. Since the multi-mode Dicke partition function (4.5) is written as $Z = \mathrm{Tr}[T(h_z^\star)]$ we find that the same operatorial content captures both the disordered Dicke model (4.1) and the interacting-replica systems $\mathcal{H}_2$ and $\mathcal{H}_3$. Therefore, a non-zero (generic) h_z enters the definition of the transfer matrix T, whose eigenvalues can be used to calculate the momenta of the overlap distribution and gain access to the observables of the spin-glass phase, at least in a Montecarlo simulation. From an experimental point of view the measure of the overlap distribution at fixed disorder proved to be challenging, because it requires in principle the capability to produce at least two copies of the system with the same disorder. A proposal in this direction came, for instance, in the context of Ref. [54] for Bose glasses. Essentially, the main idea we wish to convey is that the multimode Dicke model realizes SK in the resonant limit ($h_z = 0$), but switching on an additional field allows one to obtain information on the RSB phase via the overlap distribution $P(q)$, without having to create interacting copies of the system. We remark in fact that in our approach there are not two replicated SK hamiltonians interacting with each other as in the original Parisi works, but rather a single Hamiltonian with an additional parameter (h_z) playing the role of the coupling y. It would be nice to find at least one experimental observable in the unreplicated system which allows to gain information about the overlap distribution.

The previous discussion relies on the approximation taken in the Golden-Thompson inequality (4.4), and is therefore valid for intermediate values of h_z. We now wish to take into examination the dispersive limit $h_z \gg \Omega$, where as in the resonant case $h_z = 0$ we will find that the disordered multimode Dicke model realizes a SK dynamics.

Let us consider the original partition function $Z(N, \beta)$ for non-zero h_z and insert an identity in the form $\mathbb{1} = e^{\beta X} e^{-\beta X}$, where $X = h_z \sum_i \sigma_i^z$ as above. Applying the Baker-Campbell-Haussdorf formula (BCH), in the limit $h_z \gg \Omega$ the only contributions come

from commutators in the form:

$$[\beta X, [\beta X, [\cdots [\beta X, [\beta X, H]] \cdots]].$$

By making use of the explicit form of H we see that at first order $[X, H] \propto \sum_{ik} g_{ik}(a_k + a_k^\dagger)\sigma_i^y$, while $[X, [X, H]] \propto \sum_{ik} g_{ik}(a_k + a_k^\dagger)\sigma_i^x$, thus showing that these terms can be exactly resummed leading to the partition function

$$Z_{\text{disp}}(N, \beta) = \text{Tr}[e^{-\beta \tilde{H}} e^{-\beta h_z \sum_i \sigma_i^z}], \tag{4.8}$$

where the effective Hamiltonian $\tilde{H}$ is given by:

$$\tilde{H} = H_0 + \Omega \sum_{i,m} g_{im}(a_m + a_m^\dagger)(A(\beta h_z)\sigma_i^x + B(\beta h_z)\sigma_i^y).$$

Here we defined $H_0 = \sum_{m=1}^{M} \omega_m a_m^\dagger a_m$, while A and B are two functions whose Taylor series is determined through the explicit BCH calculation. An appropriate rotation of the Pauli matrices can be performed to recover the original form of the interaction $\sim \Omega_{\text{EFF}}(a_m^\dagger + a_m)\sigma_i^x$, provided that the coupling strength is rescaled as $\Omega_{\text{EFF}}(\beta h_z) = \Omega\sqrt{A^2 + B^2}$. Factorizing again the free boson partition function Z_{FB} as above, we find that Z_{disp} exactly reduces to the partition function (4.5). Alternatively, one can absorb the coupling Ω into the temperature as $\beta \to \bar{\beta} = \beta \Omega_{\text{EFF}}^2$. Given the partition function (4.8) we now make use again of the transfer matrix formalism and write it as $Z_{\text{disp}} = \text{Tr}\, T(h_z^\star)$. The transfer matrix is in the form $T = V_2 V_1$, and its elements can be explicitly written as [65]

$$\langle \sigma_1 \ldots \sigma_N | V_1 | \sigma_1' \ldots \sigma_N' \rangle = \prod_{k=1}^{N} e^{-\beta h_z \sigma_k \sigma_k'}$$

$$\langle \sigma_1 \ldots \sigma_N | V_2 | \sigma_1' \ldots \sigma_N' \rangle = \prod_{i=1}^{N} \delta_{\sigma_i, \sigma_i'} \prod_{i,j=1}^{N} e^{\bar{\beta} J_{ij} \sigma_i \sigma_j'}.$$

With these definitions, the trace operation reduces to a classical sum over the spin configurations $\{\sigma\}$ and we obtain

$$Z_{\text{disp}} = \text{Tr}(V_2 V_1) = Z_{FB} \sum_{\{\sigma\}\{\sigma'\}} \langle \sigma_1 \ldots \sigma_N | V_2 | \sigma_1' \ldots \sigma_N' \rangle \langle \sigma_1' \ldots \sigma_N' | V_1 | \sigma_1 \ldots \sigma_N \rangle =$$

$$= Z_{FB} \sum_{\{\sigma\}\{\sigma'\}} e^{\bar{\beta} \sum_{ij} J_{ij}\sigma_i\sigma_j} e^{-\beta h_z \sum_j \sigma_j \sigma_j'} \prod_{i=1}^{N} \delta_{\sigma_i \sigma_i'} = e^{-N\beta h_z} Z_{FB} Z_{SK}(N, \bar{\beta}). \tag{4.9}$$

The effective spin model emerging from the disordered multimode Dicke model (4.1) in the dispersive regime is therefore given again by the SK model, upon redefining the temperature as $\beta \to \bar{\beta}$. Once again, reintroducing h_x does not change this result in a qualitative way. The connection established above with spin-glass observables is therefore confirmed in the dispersive limit, as the partition function is in the form $Z_{\text{disp}} = \text{Tr}\, T$.

The derivation presented above shows that in the strong-field (dispersive) regime the SK model is exactly retrieved from a multimode Dicke dynamics. However, we note that in the regime $h_z \gg \Omega$ the spin glass phase is not accessible, because the system

is well below the usual strong coupling threshold of the Dicke model. This would in fact result in an effective temperature $\bar{\beta}$ whose value never approaches the critical one of the SK model. The main point we wish to make here is that the disordered Dicke model is thermodynamically equivalent to SK in both the zero-field ($h_z = 0$) and strong-field ($h_z \gg \Omega$) regimes. This suggests that this connection extends also for generic and intermediate values of h_z, as discussed earlier in this Section (see the discussion after Eq. (4.7)), in the same way as the multimode Dicke model with the same couplings is equivalent to a ferromagnetic fully-connected Ising model [5, 6, 7]. The results presented here are intended to be the first step in this direction.

To summarize, we analyzed a multimode Dicke model with quenched disorder, recently proposed for cold atoms in cavity setups [3, 4]. Spin-glass dynamics and frustrated interactions are expected, and we are able to prove that in the resonant (zero-field) regime the system exactly realizes the paradigmatic SK model (as already anticipated in the context of Ref. [3]). Quite surprisingly, in the dispersive (strong-field) regime this result stays unaffected upon a redefinition of the temperature. Moreover, for nonvanishing values of the coupling the operatorial content of the multimode Dicke model gives access to the spin-glass observables which characterize the Replica Symmetry broken phase. In the strong-field limit the equivalence between the multimode Dicke model and the SK model once again becomes exact, but the spin glass phase is not physically accessible. However, our work suggests that the connection between the SK and the multimode Dicke models extends into the domain of intermediate couplings, which will be the focus of the next section.

The system offers a high degree of tunability and control, and we stress that the dispersive regime might be more accessible experimentally as absorption and radiation pressure are reduced. From a theoretical standpoint, our approach provides an exact, strong-field solution of the multimode Dicke model with quenched disorder. With a view to the study and validation of spin-glasses mean field theory, dispersive cavity-mediated long range interactions in cold atomic gases appear as a promising benchmark for future research, as they allow for the physical realization of the paradigmatic SK model for spin glasses. The detection (in experiments or in Monte Carlo simulations) of the overlap distribution would in fact give information on the Replica Symmetry Broken phase in a highly tunable and controllable physical system.

Beyond the experimental investigation of spin glass physics, multimode disordered Dicke simulators may be interesting for quantum computation applications. This is the focus of our work (Dicke sim) that we present in the next section.

4.2   Dicke simulators with emergent collective quantum computational abilities

The connection of experimentally realizable quantum systems with computation contains promising perspectives from both the fundamental and the technological viewpoint [2, 71]. For example, quantum computational capabilities can be implemented by "quantum gates" [72] and by the so-called "adiabatic quantum optimization" technique [10, 73, 74]. Today's experimental technology of highly controllable quantum sim-

ulators, recently used for testing theoretical predictions in a wide range of areas of quantum physics [75, 76, 77], offers new opportunities for exploring computing power for quantum systems.

In the case of light-matter interaction at the quantum level, the reference benchmark is the Dicke model [40]. Studies of its equilibrium properties have predicted a superradiant transition to occur in the strong coupling and low temperature regime [5, 6, 7]. The superradiant phase is characterized by a macroscopic number of atoms in the excited state whose collective behaviour produces an enhancement of spontaneous emission (proportional to the number of cooperating atoms in the sample). Crucially, this phenomenology is in direct link with experimentally feasible quantum simulators. Recently, Nagy and coworkers [47] argued that the Dicke model effectively describes the self-organization phase transition of a Bose-Einstein condensate (BEC) in an optical cavity [22, 78]. Additionally, Dimer and colleagues [45] proposed a Cavity QED realization of the Dicke model based on cavity-mediated Raman transitions, closer in spirit to the original Dicke's idea. Evidence of superradiance in this system is reported in [46]. An implementation of generalized Dicke models in hybrid quantum systems has also been put forward [79]. More generally, Dicke-like Hamiltonians describe a variety of physical systems, ranging from Circuit QED [80, 81, 82, 83, 84] to Cavity QED with Dirac fermions in graphene [85, 86, 87, 88]. Additionally, disorder and frustration of the atom-photon couplings have an important role in the study of BEC in multimode cavities [89, 90]. Recent works [3, 4] discussed a multimodal-Cavity QED simulator with disordered interactions. The authors argue that these systems could be employed to explore spinglass properties at the quantum level [3, 4, 18]. In a follow-up work [91] Gopalakrishnan et al. found an interesting analogy with Hopfield networks at the perturbative level. However, the possible quantum computation applications of this new class of quantum simulators remain relatively unexplored.

Here we consider a multimode disordered Dicke model with finite number of modes. We calculate exactly (in the thermodynamic limit) the free energy of the system at temperature $T = 1/\beta$ and we find a superradiant phase transition characterized by the same free-energy landscape of the Hopfield model [33] in the so-called "symmetry broken" phase, with the typical strong-coupling threshold of the Dicke model. From the theoretical standpoint, our results generalize to the case of quenched disordered couplings the remarkable analysis performed by Lieb et al. [5, 6, 7]. The choice of frozen couplings is compatible with the characteristic time scales involved in light-matter interactions. The calculation of the partition function leads us to suggest variational ground states for the model, which we conjecture to be exact in the thermodynamic limit.

The physical consequences of this analysis are fascinating: once the multimode strong-coupling regime is reached and qubit-photon couplings are engineered, it should be possible to build a pattern-storing system whose underlying dynamics is fully governed by quantum laws. Moreover, Dicke quantum simulators here analyzed may be suitable to implement specific optimization problems, in the spirit of adiabatic quantum computation [10, 73, 74]. We point out a non-polynomial optimization problem [10, 73, 92], number partitioning, which could be implemented in a single mode cavity QED setup with controllable disorder. Computing applications based on cavity mediated interac-
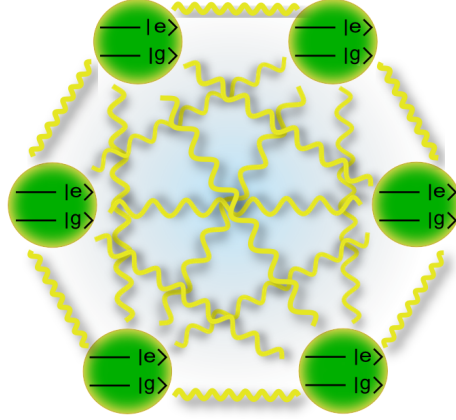
Figure 4.4: In the Dicke model, photons (yellow lines) mediate a long range interaction between qubits (green circles). The drawing sketches schematically a six qubits system within its fully-connected graph and its internal level structure. In the standard single-mode Dicke model the exchange coupling is fixed at the same value for every pair of qubits. In systems where both many modes and disorder are present, the exchange couplings are qubit-dependent and take the form given by Eq. (4.12).

tions might owns the advantage to be a viable way to generate entagled many-body states with remarkable scalability properties, as recently shown in Ref. [93].

Summarizing the results of Chapter 2, Hopfield's main idea [33] is that the retrieval of stored information, such as memory patterns, may emerge as a collective dynamical property of microscopic constituents ("neurons") whose interconnections ("synapses") are reinforced or weakened through a training phase (e.g. *Hebbian learning* [94, 95]). This is achieved in his model through a fictitious neuronal-dynamics whose effect is to minimize the Lyapunov cost function:

$$E = -\frac{1}{2} \sum_{i,j=1}^{N} T_{ij} S_i S_j \,, \tag{4.10}$$

where N is the number of neurons, $S_i = 1$ if the i-th neuron is active, and -1 otherwise, and the p stored patterns $\xi_i^{(k)} = \pm 1$ ($k = 1, \cdots, p$) determine the interconnections T_{ij} through the relation: $T_{ij} = 1/N \sum_k \xi_i^{(k)} \xi_j^{(k)} - p\,\delta_{ij}$. The analysis in Ref. [33] shows that the long-time dynamics always converges to one of the p stored patterns, i.e. these configurations are the global minima of the cost function (4.10). The interpretation of this result is that a suitable choice of the interconnections allows to store a given number of memory patterns into the neural network. Data retrieval is achieved through an algorithm that minimizes the energy function (4.10). A phase transition to a "complex" phase marks the intrinsic limitation on the number of patterns p that can be stored. If p exceeds the critical threshold $p \sim 0.14N$ many failures in the process of retrieval occur [9, 20].

Here we consider the following multimode Dicke Hamiltonian:

$$H = \sum_{k=1}^{M} \omega a_k^\dagger a_k + \Delta \sum_{i=1}^{N} \sigma_i^z + \sum_{i,k=1}^{N,M} \tilde{g}_{ik} \left(a_k + a_k^\dagger \right) \sigma_i^x \,, \tag{4.11}$$

effectively modelling quantum light-matter interaction of N two-level systems with detuning Δ and M electromagnetic modes supposed to be quasi-degenerate at the common frequency ω and with couplings that we parametrize for future convenience as $\tilde{g}_{ik} = \Omega g_{ik}/\sqrt{N}$, where Ω is the Rabi frequency and the dimensionless g_{ik}'s are both atom and mode-dependent. In Cavity QED realizations, ω represents the detuning between the cavity frequency and the pumping frequency and could be both positive or negative. A possible choice of the couplings is $g_{il} = \cos(k_l x_i)$, being k_l the wave vector of the photon and x_i the position of i-th atom [4].

4.2.1 Free energy of the multimode disordered Dicke model

We are interested in the thermodynamic properties of this system in the limit $M \ll N$, and thus in evaluating the partition function $Z = \operatorname{Tr} e^{-\beta H}$. This evaluation can be performed rigorously in the thermodynamic limit ($N \to \infty$) using the techniques introduced in Refs. [5, 6, 7]. We first consider the fully-commuting limit $\Delta = 0$. In this case the evaluation of the partition function is straightforward and we obtain $Z = Z_{FB} Z_H$, where Z_{FB} is a free boson partition function and Z_H is a classical Ising model with local quenched exchange interactions of the form:

$$
J_{ij} = -\frac{\Omega^2}{N} \sum_{k=1}^{M} \frac{g_{ik} \, g_{jk}}{\omega} \, . \tag{4.12}
$$

The physical interpretation of this result is that photons mediate long range interactions among the atoms, resulting in an atomic effective Hamiltonian described by a fully-connected Ising model (see Fig. 4.4). The role of the couplings g_{ik} can be understood from Eq. (4.10) in the context of the Hopfield network. They are the memory pattern stored in the system. By computing exactly the free energy of the model, we will show that this interpretation stays unaltered in the more complicated case $\Delta \neq 0$.

We now proceed to the evaluation of the quantum partition function. We use the method of Wang and coworkers [7, 96] (proved to be exact in the thermodynamic limit for $M/N \to 0$ [6]). We reviewed extensively this approach in Chapter 3. We introduce a set of coherent states $|\alpha_k\rangle$ with $\alpha_k = x_k + iy_k$, one for each electromagnetic mode k, and we expand the partition function on this overcomplete basis:

$$
Z = \int \prod_{k=1}^{M} \frac{d^2\alpha_k}{\pi} \operatorname{Tr}_A \langle\{\alpha\}| e^{-\beta H} |\{\alpha\}\rangle \, , \tag{4.13}
$$

where Tr_A is the atomic trace only. The only technical complication is the calculation of the matrix element in (4.13). This turns out to be equal, apart from non-extensive contributions, to the exponential of the operator in Eq (4.11) with the replacements a_k, $a_k^\dagger \to \alpha_k$, α_k^* [6, 7]. At this stage the trace over the atomic degrees of freedom can be easily performed. The integral over the imaginary parts of α_k's give an overall unimportant constant. Finally, defining the M-dimensional vectors $\mathbf{x} = (x_1, x_2, \cdots, x_M)$ and $\mathbf{g}_i = (g_{i1}, g_{i2}, \cdots, g_{iM})$, and with the change of variables $\mathbf{m} = \mathbf{x}/\sqrt{N}$, the partition function assumes a suitable form for performing a saddle-point integration, i.e. $Z =$

$\int d^M \mathbf{m}\, e^{-Nf(\mathbf{m})}$. Here f is the free energy

$$f(\mathbf{m}) = \beta \mathbf{m} \cdot \mathbf{m} - \frac{1}{N} \sum_{i=1}^{N} \log G(\mathbf{m}, \mathbf{g}_i) , \qquad (4.14)$$

with: $G(\mathbf{m}, \mathbf{g}_i) = 2 \cosh\left[\beta \left(\Delta^2 + \Omega^2 (\mathbf{g}_i \cdot \mathbf{m})^2 \right)^{\frac{1}{2}} \right]$.

The order parameter $\mathbf{m}$ describes the superradiant phase transition. Physically, it gives the mean number of photons in every mode [60]. Its value is determined by minimizing the free energy in Eq. (4.14). Solutions of this optimization problem are, in principle, $\mathbf{g}_i$-dependent, but in the thermodynamic limit both the free energy and the saddle-point equation are self-averaging [9]. Thus we conclude that the free energy and the saddle point equations are given by

$$f(\mathbf{m}) = \beta \mathbf{m} \cdot \mathbf{m} - \langle \log G(\mathbf{m}, \mathbf{g}) \rangle_{\mathbf{g}} ,$$
$$\mathbf{m} = \frac{\Omega^2}{2} \left\langle \frac{(\mathbf{g} \cdot \mathbf{m}) \mathbf{g}}{\mu(\mathbf{g})} \tanh\left(\beta \mu(\mathbf{g}) \right) \right\rangle_{\mathbf{g}} , \qquad (4.15)$$

with: $\mu(\mathbf{g}) = \left(\Delta^2 + \Omega^2 (\mathbf{g} \cdot \mathbf{m})^2 \right)^{\frac{1}{2}}$ and $\langle \cdots \rangle_{\mathbf{g}}$ representing the average over the disorder distribution. Eq. (4.15) reduces to the mean-field equations for the Hopfield model for $\Delta \to 0$ [9]. Thus, Δ may be intended as a quantum annealer parameter. To fully specify the model, the probability distribution for the couplings is needed. In the following we will assume

$$P(\mathbf{g}) = \prod_{k=1}^{M} \left(\frac{1}{2} \delta \left(g_k - 1 \right) + \frac{1}{2} \delta \left(g_k + 1 \right) \right) , \qquad (4.16)$$

but we have verified that the results are qualitatively robust as long as the disorder is not too peaked around zero in accordance with the classical results of Ref. [9]. To locate the critical point it suffices to expand in Taylor series Eqs. (4.15). As in the conventional Dicke model, a temperature-independent threshold $\Omega_c^2 = 2\Delta$ emerges. For $\Omega < \Omega_c$, the phase transition is inhibited at all temperatures. Whenever the magnitude of the coupling exceeds this threshold value, the critical temperature is located at $T_c = \Delta / \operatorname{arctanh}\left(2\Delta/\Omega^2 \right)$.

Above the critical temperature T_c the only solution to (4.15) is a paramagnetic state, with $m_k = 0$ for all k. Below T_c, different solutions appear. We now set out to classify these solutions and their stability under temperature decrease. For this analysis, we considered both the Hessian matrix $\partial^2 f / \partial m_k \partial m_l$ and numerical optimization (Figure 4.5) . The key point, as mentioned above is that in this "symmetry-broken" phase the system takes $2M$ degenerate ground states (as well as many metastable states energetically well separated from the ground states). In other words, also in this fully quantum limit the free-energy landscape still closely resembles that of the Hopfield model [9].

The ground state solutions have the explicit form:

$$\mathbf{m}_k = m^{(1)} (\underbrace{0, 0, \cdots, 0,}_{k-1 \; times} \; \underbrace{1, 0, \cdots, 0}_{M-k+1 \; times}) . \qquad (4.17)$$
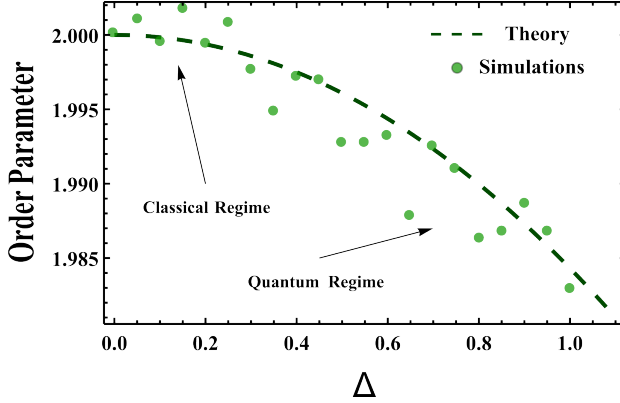
Figure 4.5: Order parameter $m^{(1)}$ in Eq. (4.18) as a function of Δ in the ultrastrong coupling regime ($\Omega > \Omega_c$) at $T = 0$. On the theoretical curve (dashed line) are superposed the results (green dots) of a naive numerical optimization algorithm minimizing the ground state energy ansatz in Eq. (4.20). The parameters of the simulation are $\Omega = 4$, $N = 100$, $M = 10$. Green dots are the result of a single realization of the disorder. This plot suggests that at $N = 100$ the system is already close to the thermodynamic limit behavior. The classical Hopfield model is recovered in the limit $\Delta \to 0$.

Equation (4.15) for the order parameter $m^{(1)}$ reduces to: $2\mu(m^{(1)}) = \Omega^2 \tanh\left(\beta\mu(m^{(1)})\right)$, where $\mu(m^{(1)}) = \sqrt{\Delta^2 + \Omega^2(m^{(1)})^2}$. In the zero temperature limit the order parameter can be evaluated exactly:

$$m^{(1)} = \pm\sqrt{\frac{\Omega^2}{4} - \frac{\Delta^2}{\Omega^2}} \,. \tag{4.18}$$

4.2.2 Zero temperature limit: Dicke simulators as quantum memories and quantum annealers

At zero temperature the most interesting state is the ground state (GS) of the Hamiltonian (4.11). Inspired by the calculation above we propose the variational ansatz for the GS:

$$|GS\rangle = |\alpha_1, \alpha_2, \cdots, \alpha_M\rangle |\text{spin}(\alpha_1, \cdots, \alpha_M)\rangle \,, \tag{4.19}$$

where $|\alpha_1, \alpha_2, \cdots, \alpha_M\rangle$ is the product of M coherent states and the spin part is factorized. The mean value of the energy in this GS is given by:

$$E_{GS}(\mathbf{m}) = \mathbf{m} \cdot \mathbf{m} - \left\langle\sqrt{\Delta^2 + \Omega^2(\mathbf{g} \cdot \mathbf{m})^2}\right\rangle_{\mathbf{g}} \,. \tag{4.20}$$

This expression exactly equals the free-energy computed previously in the limit $\beta \to \infty$, which leads us to conjecture that our factorized variational ansatz is exact. The quantum phase transition is located at the critical coupling $\Omega = \Omega_c = \sqrt{2\Delta}$, at which the paramagnetic solution becomes unstable. In the symmetry-broken phase we have $2M$ degenerate ground states of the form

$$|GS\rangle_k = |\underbrace{0, 0, \cdots, 0}_{k-1\,times}, \pm m^{(1)}, \underbrace{0, \cdots, 0}_{M-k\,times}\rangle |\text{spin}(\pm m^{(1)})\rangle_k \,, \tag{4.21}$$

with $k = 1, \cdots M$. The spin wave function is also factorized $|\text{spin}(\pm m^{(1)})\rangle_k = \prod_i |s_i\rangle_k$, with

$$|s_i\rangle_k = \frac{1}{\mathcal{N}} \left(-\frac{-\Delta + \sqrt{\Delta^2 + \beta_{ik}^2}}{\beta_{ik}} |e_i\rangle + |g_i\rangle \right), \tag{4.22}$$

where $\mathcal{N}$ a normalization, $\beta_{ik} = g_{ik} m^{(1)}$ and $|e_i\rangle$, $|g_i\rangle$ are σ_i^z's eigenstates. It is worth noting that, as expected, the ground state energy is a self-averaging quantity, whereas the ground states are not, being disorder-dependent also in the thermodynamic limit.

The above calculation shows that in the superradiant phase the ground state of the system is a quantum superposition of the $2M$ degenerate eigenvectors given by Eqs. (4.21) and (4.22). Their explicit form suggests that at fixed disorder and mode number the information about the disordered couplings belonging to the k-th mode is *printed* on the atomic wave function. Moreover, the photonic parts of the wave functions are all orthogonal for $k_1 \neq k_2$ in the thermodynamic limit. This implies that in principle a suitable measure on the photons-subsystem causes the collapse over one of the $2M$ ground states and gives thus the possibility to retrieve information ("patterns") stored in the atomic wave function.

One may wonder how these ideas may translate into a feasible experimental scheme. As mentioned above, a single-mode Dicke model has been recently realized with cavity-mediated Raman transitions in cavity QED with ultracold atoms [46]. A multimode cavity QED setup supporting disordered couplings has been proposed in refs. [3, 4], and preliminary evidence of superradiance in this system was found in [97]. Setups operating in multimode regime were recently suggested also in circuit QED [98, 99, 100]. Thus, the ideas on quantum pattern retrieval may directly apply on cavity-QED experimental setups similar to the ones studied in refs. [3, 91, 101]. The only missing ingredient is a concrete strategy to tune the atom-photon interactions. While this step might be technically involved, single-atom manipulation techniques are rapidly developing [102]. This technology should make it possible to fix the position of the atoms, and thus tune the coupling constants.

We surmise that multimode Dicke quantum setups with controllable disorder could be used beyond storage, to simulate specific optimization problems. Indeed, finding the ground state of classical spin models with disordered interactions is equivalent, in most cases, to finding solutions of computationally expensive non-polynomial (NP) problems [92]. For example, the *simplest* NP-hard problem, number partitioning, could be implemented in a single-mode cavity QED setup with controllable disorder as follows. Number partitioning can be formulated as an optimization problem [21]: given a set $\mathcal{A} = \{a_1, a_2, \ldots, a_N\}$ of positive numbers, find a partition, i.e. a subset $\mathcal{A}' \subset \mathcal{A}$, such that the residue: $E = |\sum_{a_j \in \mathcal{A}'} a_j - \sum_{a_j \notin \mathcal{A}'} a_j|$ is minimized. A partition can be defined by numbers $S_j = \pm 1$: $S_j = 1$ if $a_j \in \mathcal{A}'$, $S_j = -1$ otherwise. The cost function can be replaced by a classical spin hamiltonian: $H = \sum_{i,j=1}^N a_i a_j S_i S_j$, whose ground state is equivalent to the minimum partition. In a single-mode cavity QED network, couplings have the simple form $g_i = \cos(kx_i)$ [4]. By the definition of $a = \max_{\mathcal{A}} a_j$ and $\tilde{a}_j = a_j/a$, single-atom manipulation techniques might make possible to *engineer* the g_i's in order to implement a given instance of the problem, provided that the cavity is in the "blue" detuned regime and hence the couplings have appropriate sign (see Eq. 4.12). With a suitably slow an-

nealing of the atomic detuning Δ (to ensure applicability of the adiabatic theorem), the system should collapse on qubit configurations that are solutions of the corresponding optimization problem.

4.3 Conclusions and future directions

In the previous section we provided the first rigorous analysis of the multimode disordered Dicke model, valid beyond the weak-coupling regime and exact in the thermodynamic limit. The equivalence between multimodal disordered Dicke model and a quantum Hopfield network [103], together with the proposal of a cavity QED setup implementing a non-polynomial optimization problem, demonstrates the possibility of quantum computational abilities of this new class of quantum simulators. Our proposal is conceptually complementary to a standard quantum computation perspective [104, 105]. Indeed, the information can be "written" on the qubits through a quantum annealing on the detuning Δ, similarly to what happens for adiabatic quantum computation [10, 73, 74]. Another important point is that this multimode cavity QED setup is an *all to all* architecture, which means that the effective spin system is fully connected. This is particularly relevant, because the most part of NP problems allow for a representation in terms of Ising Hamiltonian with fully connected couplings and it is completely non-trivial to map such a problem on a *local* architecture.

Before discussing possible future directions of our work, we point out two recent proposals which share the same spirit of our ideas. The first one is by Lewenstein group [106]: the authors suggest a trapped ions setup, in order to implement number partitioning and Mattis spin glasses (a simplified version of an Hopfield network). The second one (especially interesting in our opinion) is by Lechner, Hauke and Zoller [107]: they suggest a quantum annealer with local interactions only, but able to produce an all to all architecture. If we understand correctly, the trick to achieve this result is the following: a local lattice gauge theory is implemented on a set of extended (physical plus auxiliary) qubits and the input of the optimization problem is encoded in the gauge fields. On the other hand the output of the problem is printed on the physical qubits, that effectively experience a long-range interaction because of the gauge constraints.

In conclusion we want to point out possible further developments of our work:

- for the moment we proposed two models in the spin glass realm (Hopfield netwok and number partitioning), that seem suitable for implementation in a cavity QED setup. It would be interesting to understand if other spin glass problems can be mapped naturally on a cavity QED architecture;

- we do not understand, looking at Lev proposal, if at the moment it is possible to discuss a concrete strategy to implementing controllable disorder;

- in order to overcome this problem, other viable quantum platforms may be more suitable to implement a Dicke simulator. Among the others, we cite architectures based on photonic crystals [108] or circuit QED with superconducting qubits [98].

Part II

Devil's staircase phase diagram of the fractional quantum Hall effect in the thin-torus limit and beyond

One dimensional lattice gases with long range repulsive interactions

5.1   The one dimensional repulsive lattice gas model

In 1982 Bruinsma and Bak [12] introduced and solved (at zero temperature) a one dimensional model of lattice gas with repulsive long range interactions:

$$E(\boldsymbol{n}) = \frac{1}{2} \sum_{j \neq i} V(|i - j|) n_i n_j - \mu \sum_i n_i \,, \tag{5.1}$$

where μ is the chemical potential and $n_i = 0, 1$ are the occupation numbers. This model is trivially dual to an antiferromagnetic long range Ising model in an external magnetic field and exhibits a peculiar phase transition at zero temperature: the mean density (magnetization) as a function of the chemical potential (external magnetic field) has a complete *devil's staircase* structure (see Figure (5.1)). This means that tuning μ, the system undergoes an infinite (fractal) series of second order phase transitions.

The physical reason for this weird phenomenon is the following: at fixed rational density, the ground state of the model is a different periodic configuration, with the property to be *incompressible*. The devil's staircase structure of the phase diagram is a byproduct of this hierarchy of incompressible ground states. This statement can be understood looking at the standard definition of incompressibility.

The compressibility is defined as the relative volume decrease per unit increase in pressure;

$$\kappa \equiv -\frac{1}{V} \frac{\partial V}{\partial P} \tag{5.2}$$

It is usually more convenient to calculate thermodynamic properties as a function of volume rather than as a function of pressure so that the following expression is often more useful:

$$\kappa^{-1} \equiv -V \frac{\partial P}{\partial V} = V \frac{\partial^2 E}{\partial V^2}. \tag{5.3}$$

For systems of many particles the energy in the thermodynamic limit is an extensive quantity and the energy per particle depends on the volume and the particle number only through the particle density, $E = N\epsilon(n)$ where $n = N/V$ is the density. This relationship allow us to connect the compressibility with the chemical potential; $\mu = \partial E/\partial N =$

$d(n\epsilon(n))/dn$. Comparing with Eq. (5.3) we find that

$$\kappa^{-1} = n^2 \frac{d\mu}{dn} \tag{5.4}$$

When we say that the system is incompressible we mean that $\kappa = 0$. This occurs whenever the chemical potential of the system increases discontinuously as a function of density. That is what we really mean by incompressibility.

Whenever the ground state is incompressible the increase in energy when a particle is added to the system and the decrease in energy when a particle is removed from the system differ even in the thermodynamic limit. It follows that it costs a finite energy to create particle-hole pairs which are not bound to each other. In this circumstance we say that the system has a 'gap'.

Our strategy will be the following: firstly we will review the explicit construction of the ground states of (5.34). This is due to Hubbard [23]. Then we will give a formal proof of the incompressibility of these ground states [12, 24].

5.2   Explicit construction of the Hubbard ground states

In a remarkable paper Hubbard [23] studied orderings of electrons in one dimensional conductors. When the electrostatic energy is dominant, a 1D lattice-gas model results, and Hubbard gave a general method to determine the exact ground state.
Consider a chain of N sites. The particle configuration is a vector $\boldsymbol{n}$ of occupation numbers $n_i = 0, 1$ ($i = 1, \dots, N$). Particles interact via two-body forces that depend on their distance, and not with themselves. Hubbard's Hamiltonian is:

$$E(\boldsymbol{n}) = \frac{1}{2} \sum_{j \neq i} V(|i - j|) n_i n_j \tag{5.5}$$

We search for the configuration (GS) that minimizes $E(\boldsymbol{n})$, at fixed number of particles $m = \sum_{i=1}^{N} n_i$, or density $\rho := m/N$. Since the potential is repulsive, intuition suggests to allocate particles on the lattice as far as possible from each other. However, the prescription of the density does not allow to do this evenly. Hubbard analytically solved the problem for the infinite chain and for potentials satisfying the two conditions:

$$V(r) \to 0 \quad \text{as} \quad r \to \infty \tag{5.6}$$
$$V(r + 1) + V(r - 1) \geq 2V(r) \quad \text{for all} \quad r > 1 \tag{5.7}$$

The convexity condition is satisfied by the Coulomb potential and by $V(|i - j|) = |i - j|^{-\alpha}$, $\alpha > 0$. Hubbard's solutions are called *generalized Wigner lattices* or *most uniform configurations*. They are independent of any further detail of the interaction potential.

Let's extend the N-site chain into an infinite one with particle density ρ, and search for ground states that are N-periodic, with ρN particles per period. We thus impose the periodic boundary conditions (pbc)

$$n_{i+N} =: n_i \quad i = 1, \dots, N \tag{5.8}$$

and the bound

$$\sum_{i=j}^{N+j} n_i = m \quad \forall j \tag{5.9}$$

The N-site chain is a loop, and it interacts with the rest of the lattice, i.e. with an infinite number of self-copies. A complete rotation of the loop corresponds to a shift of one period of the infinite chain.

Let's label the particles round the loop as $\nu = 1, \ldots, m$ and define $r_\nu^{(0)}$ as the position of particle ν, and $r_\nu^{(1)}$ as the interval between particles ν and $\nu + 1$. Then $r_\nu^{(1)} =: r_{\nu+1}^{(0)} - r_\nu^{(0)}$. Because of pbc, we can obtain the position of a generic particle in the infinite chain, i.e. $r_{\nu+m}^{(0)} = r_\nu^{(0)} + N$. It follows that $r_{\nu+m}^{(1)} = r_\nu^{(1)}$.

The distance between particle ν and $\nu + \mu$ is

$$r_\nu^{(\mu)} =: r_{\nu+\mu}^{(0)} - r_\nu^{(0)} = \sum_{\tau=\nu}^{\nu+\mu-1} r_\tau^{(1)} = \sum_{\tau=0}^{\mu-1} r_{\nu+\tau}^{(1)} \tag{5.10}$$

From this we obtain the useful properties

$$r_{\nu+m}^{(\mu)} = r_\nu^{(\mu)} \quad \text{for all } \mu \tag{5.11}$$

$$r_\nu^{(\mu+m)} = r_\nu^{(\mu)} + N \quad \text{for all } \mu \tag{5.12}$$

$\{n_i\}$	configuration	$\{r_\nu^{(1)}\}$
1111100000000	● ● ● ● ● ○ ○ ○ ○ ○ ○ ○ ○	$\{1,1,1,1,9\}$
1001001001010	● ○ ○ ● ○ ○ ● ○ ○ ● ○ ● ○	$\{3,3,3,2,2\}$
0000110100110	○ ○ ○ ○ ● ● ○ ● ○ ○ ● ● ○	$\{1,2,3,1,6\}$
$\vdots$	$\vdots$	$\vdots$
1010010100100	● ○ ● ○ ○ ● ○ ● ○ ○ ● ○ ○	$\{2,3,2,3,3\}$

Table 5.1: Examples of microscopic configurations for a loop of $N = 13$ sites, $\rho = 5/13$

The energy only depends on relative positions, $\{r_\nu^{(\mu)}\}$. Therefore the vector $\mathbf{r}^{(1)} =: \{r_\nu^{(1)}\}$ defines a system's configuration and satisfies $\sum_{\nu=1}^m r_\nu^{(1)} = N$. It defines a configuration up to transformations like $r_\nu^{(1)} \to r_{\nu+\tau}^{(1)}$, and a configuration satisfies $\sum_{\nu=\tau}^{m+\tau} r_\nu^{(1)} = N$, that implies $\sum_{\nu=\tau}^{m+\tau} r_\nu^{(\mu)} = \mu N$.

How can we express energy (5.5) in term of $\mathbf{r}^{(1)}$? The interaction energy between particle ν and particle $\nu + \mu$ is $V(r_\nu^{(\mu)})$. Therefore, the interaction energy between particle ν and the rest is

$$\sum_\mu V(r_\nu^{(\mu)}) = \sum_{\mu=1}^m V(r_\nu^{(\mu)}) + V(r_\nu^{(\mu+m)}) + V(r_\nu^{(\mu+2m)}) + \ldots = \sum_k \sum_{\mu=1}^m V(r_\nu^{(\mu+km)})$$

that we can simplify using property (5.12)

$$\sum_\mu V(r_\nu^{(\mu)}) = \sum_k \sum_{\mu=1}^m V(r_\nu^{(\mu)} + kN) \tag{5.13}$$

The energy of the system

$$E(\boldsymbol{r}^{(1)}) = \frac{1}{2} \sum_\nu \sum_\mu V(r_\nu^{(\mu)})$$

$$= \frac{1}{2} \sum_{\nu=1}^m \sum_k \sum_{\mu=1}^m V(r_\nu^{(\mu)} + kN) + V(r_{\nu+m}^{(\mu)} + kN) + \dots$$

can be simplified using property (5.11)

$$E(\boldsymbol{r}^{(1)}) = A \sum_k \sum_{\nu=1}^m \sum_{\mu=1}^m V(r_\nu^{(\mu)} + kN) = A \sum_k \sum_{\mu=1}^m U^k(\boldsymbol{r}^{(\mu)}) \tag{5.14}$$

where A it is a factor that depends on lenght of the chain, $\boldsymbol{r}^{(\mu)} =: \{r_\nu^{(\mu)}\}$ and

$$U^k(\boldsymbol{r}^{(\mu)}) =: \sum_{\nu=1}^m V(r_\nu^{(\mu)} + kN) \tag{5.15}$$

We now have the basic ingredients to solve the problem. The first task is to look for an algorithm to minimize (5.14) with the condition

$$\sum_{\nu=1}^m r_\nu^{(1)} = N \tag{5.16}$$

This problem is similar to m problems in which we separately minimize the inner sum (5.15) with the condition

$$\sum_{\nu=1}^m r_\nu^{(\mu)} = \mu N \tag{5.17}$$

If such a solution exists, it also minimizes (5.14). To obtain the solution for inner problems we need the following theorem:

Theorem 5.2.1. *If $\{r_i\} = r_1, \dots, r_m$ is a set of m integers such that*

$$\sum_{i=1}^m r_i := R = mr + a, \quad 0 \le a < m \tag{5.18}$$

and if $V : \mathbb{N} \mapsto \mathbb{Z}$ is an integer function such that it is strictly convex, then

$$(m-a)V(r) + aV(r+1) \le \sum_{i=1}^m V(r_i) \tag{5.19}$$

Proof. First we suppose that $\{r_i\}$ is a set such that $|r_i - r_j| \le 1$ for all pairs i, j; such a set will be called *minimal*. We define $\hat{r} =: \min(r_i)$. For a minimal set we have $\hat{r} \le r_i \le \hat{r} + 1$ for all i: r_i can assume only values $\hat{r}$ or $\hat{r} + 1$. Let $\hat{n}$ be the number of r_i that assume the value $\hat{r}$. Then $m - \hat{n}$ is the number of r_i that assume value $\hat{r} + 1$. Calculating

$$\sum_{i=1}^m r_i = \hat{n}\hat{r} + (m - \hat{n})(\hat{r} + 1) = m\hat{r} + m - \hat{n} \tag{5.20}$$

by the uniqueness of the modular decomposition, we obtain $\hat{r} \equiv r$ and $m - \hat{n} \equiv a$. So it follows at once that, for minimal sets, the equality in (5.19) is satisfied.

Now let C be a non minimal set $\{r_i\}$; then, for some $s \neq t$ one has $r_s > r_t + 1$. We construct the set C' by taking C and moving only r_s and r_t: $r_i' =: r_i$ for all $i \neq s, t$, $r_s' =: r_s - 1$, $r_t' =: r_t + 1$. We see that C' satisfy the condition (5.18) and, by using the lemma (5.2.2), we obtain

$$V(r_t') + V(r_s') \leq V(r_s) + V(r_t) \quad \Rightarrow \quad \sum_{i=1}^{m} V(r_i') \leq \sum_{i=1}^{m} V(r_i) \tag{5.21}$$

If C' isn't minimal we repeat the procedure to obtain a C'' with $\sum_{i=1}^{m} V(r_i'') \leq \sum_{i=1}^{m} V(r_i') \leq \sum_{i=1}^{m} V(r_i)$ and so on, until one arrives at a minimal set C^0. Using inequalities between $C^0, \ldots, C$ one proves the thesis $\qquad \square$

Lemma 5.2.2. *Let $V : \mathbb{N} \mapsto \mathbb{Z}$ an integer function such that it is strictly convex i.e. $V(r+1) + V(r-1) \geq 2V(r)$ for all $r > 1$ then*

$$V(s+1) + V(t-1) \leq V(s) + V(t) \quad \text{for all } s \text{ such that } s < t \tag{5.22}$$

%endalign*

If $\{r_\nu^{(\mu)}\}$ is a minimal set, it minimizes the energy (5.15). We need to fabricate such set. Starting from (5.17), we calculate integers $r^{(\mu)}$ and $a^{(\mu)}$, by decomposing the fraction μ/ρ into the sum of a non-zero integer and a proper fraction:

$$\sum_{\nu=1}^{m} r_\nu^{(\mu)} = \mu N = m r^{(\mu)} + a^{(\mu)} \quad \Rightarrow \quad \frac{\mu}{\rho} = r^{(\mu)} + \frac{a^{(\mu)}}{m} \tag{5.23}$$

We obtain $r^{(\mu)} = \lfloor \mu/\rho \rfloor$ ($\lfloor x \rfloor$ means interger part of x). If $r_\nu^{(\mu)} \in S^\mu(\rho) := [r^{(\mu)}, r^{(\mu)} + 1] = [\lfloor \mu/\rho \rfloor, \lfloor \mu/\rho \rfloor + 1]$ then $\{r_\nu^{(\mu)}\}$ is a minimal set. There are $m - a^{(\mu)}$ of $r_\nu^{(\mu)}$ that take value $\lfloor \mu/\rho \rfloor$ and $a^{(\mu)}$ of $r_\nu^{(\mu)}$ that take value $\lfloor \mu/\rho \rfloor + 1$. Therefore a set of solutions that minimize (5.15) exists for each $\mu = 1, \ldots, m$, and for all fixed ρ, the energy (5.14) is minimised when $r_\nu^{(\mu)} \in S^\mu(\rho)$ for each $\mu = 1, \ldots, m$.

Example 5.2.1. $m = 5$ *and* $N = 13$ *($\rho = 5/13$).*
Calculating $r^{(\mu)}$ and $a^{(\mu)}$ we obtain minimal configuration for each μ. Results are in the table.

μ	$r^{(\mu)}$	$m - a^{(\mu)}$	$r^{(\mu)} + 1$	$a^{(\mu)}$	$\{r_\nu^{(\mu)}\}$
1	2	2	3	3	{2,2,3,3,3}
2	5	4	6	1	{5,5,5,5,6}
3	7	1	8	4	{7,8,8,8,8}
4	10	3	11	2	{10,10,10,11,11}
5	13	5	14	0	{13,13,13,13,13}

Table 5.2: Minimal sets for U, $m = 5$ and $N = 13$

Each set of $r_\nu^{(\mu)}$ minimizes the energy (5.15) indipendently from the internal order of numbers. For example both $\{2, 2, 3, 3, 3\}$ and $\{2, 3, 2, 3, 3\}$ minimize $U(\boldsymbol{r}^{(1)})$. But from $\{r_\nu^{(1)}\} =$

$\{2, 2, 3, 3, 3\}$ *it descends that the* $\{r_\nu^{(2)}\}$ *configuration* $\{4, 5, 6, 6, 5\}$ *is not a minimal set for* $U(\mathbf{r}^{(2)})$. *Therefore, to minimize energy (5.14) we need to combine results in table and choose only one* $\{r_\nu^{(1)}\}$ *configuration, i.e. to specify the* $r_\nu^{(1)}$ *ordering, up to rotations.*

In the example we have only two inequivalent configurations. They generate the chain of configurations

$$\{2, 2, 3, 3, 3\} \to \{4, 5, 6, 6, 5\} \to \{7, 8, 9, 8, 7\} \to \{10, 11, 11, 10, 10\} \to \{13, 13, 13, 13, 13\}$$
$$\{2, 3, 2, 3, 3\} \to \{5, 5, 5, 6, 5\} \to \{7, 8, 8, 8, 8\} \to \{10, 11, 10, 11, 10\} \to \{13, 13, 13, 13, 13\}$$

The configuration that minimises the total energy is $\{r_\nu^{(1)}\} = \{2, 3, 2, 3, 3\}$. *It is the most uniform configuration for* $\rho = 5/13$. *We can write this result in a compact notation:* $\{2, 3, 2, 3, 3\}$ =: $(10100)^2 (100) = (23)^2 (3)$

We proved that, for each μ there is a set of configurations that minimize $U(\mathbf{r}^{(\mu)})$ and we know how to construct it. We don't have yet a method to choose the one that minimises the total energy (5.14), but we can fabricate it. We start using $\mu = 1$, i.e. we minimize the nearest-neightbor energy $U(\mathbf{r}^{(1)})$. We obtain the set of minimal configurations by applying the algorithm of the theorem. We calculate $r^{(1)}$ and $a^{(1)}$ from the decomposition

$$\frac{1}{\rho} = r^{(1)} + \frac{a^{(1)}}{m} \tag{5.24}$$

and then we have the set of configurations that minimises $U(\mathbf{r}^{(1)})$, i.e. $\{r_\nu^{(1)}\}$ such that there are $m - a^{(1)}$ times $r^{(1)}$ and $a^{(1)}$ times $r^{(1)} + 1$.

For example, if $a^{(1)} = 0$, i.e. $\rho = 1/r^{(1)}$ (the simplest possibility), we have only one configuration that satisfies the problem: particles are distributed uniformly, one every $r^{(1)}$ sites. Indeed $\{r_\nu^{(1)}\}_{\rho=1/r^{(1)}} = \{r^{(1)}, r^{(1)}, \ldots, r^{(1)}\}$. This microstate solves the general problem, as we can verify by comparing the chain of configurations that the solution generates with sets of configurations that minimize $U(\mathbf{r}^{(\mu)})$:

$$\{r^{(1)}, r^{(1)}, \ldots, r^{(1)}\} \to \{r^{(2)} = 2r^{(1)}, r^{(2)}, \ldots, r^{(2)}\} \to \ldots$$

Let's introduce a new notation to indicate the set of configurations that minimises $U(\mathbf{r}^{(1)})$. An element $r_\nu^{(1)}$ can be $r^{(1)}$ or $r^{(1)} + 1$. To identify only one system's configuration we have to know the pattern of $r_\nu^{(1)}$ in the vector $\{r_\nu^{(1)}\}$, up to rotations. However, knowing that $r_\nu^{(1)} = r^{(1)}$ means that after particle ν we must have $r^{(1)} - 1$ holes. In terms of occupation numbers, when we find $r_\nu^{(1)}$ we fix a part of the configuration, that we indicate with round brackets. We have only two types of partial configurations: $(10^{(r^{(1)}-1)})$ and $(10^{(r^{(1)})})$. If we assume that a particle is always at the beginning of the string, we can compact the notation for partial configurations using $(10^{(r^{(1)}-1)})$ =: $(r^{(1)})$ or $(10^{(r^{(1)})})$ =: $(r^{(1)} + 1)$. A choice of configuration means fixing the order of partial configurations. A minimal configuration for $U(\mathbf{r}^{(1)})$ is part of

$$M_1 := \left\{ \{n_i\} : \begin{array}{l} (r^{(1)}) \times [m - a^{(1)}] \\ (r^{(1)} + 1) \times [a^{(1)}] \end{array} \right\} \tag{5.25}$$

To understand the notation let us consider examples.

Example 5.2.2. *$m = 5$ and $N = 13$ ($\rho = 5/13$). We obtain $r^{(1)} = 2$, so the partial configurations are (10) and (100). Minimal configurations for $U(\boldsymbol{r}^{(1)})$ are*

$$\{2,3,2,3,3\} = (10)(100)(10)(100)(100) = (23)^2(3)\,,$$
$$\{2,2,3,3,3\} = (10)(10)(100)(100)(100) = (2)^2(3)^3.$$

Example 5.2.3. *$\rho = 1/n$ ($m = N/n$). We obtain $r^{(1)} = n$, so the partial configurations are (10^{n-1}) and (10^n). Minimal configuration for $U(\boldsymbol{r}^{(1)})$ is $\{n,\dots,n\} = (10^{n-1})^m = (n)^m$.*

Let us observe that the smallest possible partial configurations are (1) and (0) (that we call 0-particles). Then, a generic configuration is part of:

$$M_0 := \left\{ \{n_i\} \; : \; \begin{array}{l} (0) \times [N - m] \\ (1) \times [m] \end{array} \right\} \tag{5.26}$$

Knowing the minimal sets for $U(\boldsymbol{r}^{(1)})$ (i.e. ρ density decomposition) permits a first ordering of 0-particles in bigger partial configurations $M_1 \subset M_0$:

$$\left\{ \{n_i\} \; : \; \begin{array}{l} (0) \times [N - m] \\ (1) \times [m] \end{array} \right\} \longrightarrow \left\{ \{n_i\} \; : \; \begin{array}{l} (r^{(1)}) \times [m - a^{(1)}] \\ (r^{(1)} + 1) \times [a^{(1)}] \end{array} \right\} \tag{5.27}$$

How can we select the configuration that minimises (5.14) among those (5.25) that minimise $U(\boldsymbol{r}^{(1)})$? If $a^{(1)} = 0$ we know the solution: we have only one configuration in the set (5.25) that is a GS. If $a^{(1)} \neq 0$ the second term $a^{(1)}/m$ in the continued fraction decomposition represents the density of $(r^{(1)} + 1)$-site intervals which can be regarded as particles, within the $(r^{(1)})$-site intervals, which can be regarded as holes. In this way we define two types of 1-particles. Therefore we want to find Hubbard GS for a density $\rho = a^{(1)}/m$. We know which is the first step to solve this problem: we calculate $s^{(1)}$ and $b^{(1)}$ from the decomposition

$$\frac{m}{a^{(1)}} = s^{(1)} + \frac{b^{(1)}}{m} \tag{5.28}$$

If $\{s_\nu^{(1)}\}$ is the vector of distance between 1-particles, i.e. it indicates how many $(r^{(1)})$ sites intervals there are between $(r^{(1)} + 1)$ sites intervals, we have $m - b^{(1)}$ of $s_\nu^{(1)}$ that are $s^{(1)}$ and $b^{(1)}$ of $s_\nu^{(1)}$ that are $s^{(1)} + 1$. So we obtain two types of 2-particles

$$((r^{(1)} + 1)(r^{(1)})^{(s^{(1)}-1)}) \qquad ((r^{(1)} + 1)(r^{(1)})^{(s^{(1)})}) \tag{5.29}$$

and a subset of M_1 that minimises also $U(\boldsymbol{r}^{(2)})$

$$M_2 := \left\{ \{n_i\} \; : \; \begin{array}{l} ((r^{(1)} + 1)(r^{(1)})^{(s^{(1)}-1)}) \times [m - b^{(1)}] \\ ((r^{(1)} + 1)(r^{(1)})^{(s^{(1)})}) \times [b^{(1)}] \end{array} \right\} \tag{5.30}$$

If $b^{(1)} = 0$ we have only one configuration that is a solution. If $b^{(1)} \neq 0$ the second term $b^{(1)}/m$ in the $a^{(1)}/m$ density decomposition represents the density of (1) 2-particles within the (0) 2-particles. We can repeat the algorithm used before for 1-particles. And so on, as long as we find a null density fraction for k-particles. Indeed in such case we have only one configuration in M_k, that is a GS.

Example 5.2.4. $m = 5$ *and* $N = 13$ $(\rho = 5/13)$. *We start from the set of* 0-*particles*

$$M_0 := \left\{ \{n_i\} \; : \; \begin{matrix} (0) \times [8] \\ (1) \times [5] \end{matrix} \right\}$$

From 5/13 *decomposition we obtain the set of* 1-*particles*

$$\frac{13}{5} = 2 + \frac{3}{5} \longrightarrow M_1 := \left\{ \{n_i\} \; : \; \begin{matrix} (2) \times [2] \\ (3) \times [3] \end{matrix} \right\}$$

From 3/5 *decomposition we obtain the set of* 2-*particles*

$$\frac{5}{3} = 1 + \frac{2}{3} \longrightarrow M_2 := \left\{ \{n_i\} \; : \; \begin{matrix} (3) \times [1] \\ (32) \times [2] \end{matrix} \right\}$$

From 2/3 *decomposition we obtain the set of* 3-*particles*

$$\frac{3}{2} = 1 + \frac{1}{2} \longrightarrow M_3 := \left\{ \{n_i\} \; : \; \begin{matrix} (32) \times [1] \\ (323) \times [1] \end{matrix} \right\}$$

Finally from 1/2 *decomposition we obtain the set of* 4-*particles*

$$2 = 2 + \frac{0}{1} \longrightarrow M_4 := \{\{n_i\} \; : (32332) \times [1]\}$$

Example 5.2.5. $m = 11$ *and* $N = 47$ $(\rho = 11/47)$. *We start from the set of* 0-*particles*

$$M_0 := \left\{ \{n_i\} \; : \; \begin{matrix} (0) \times [36] \\ (1) \times [11] \end{matrix} \right\}$$

From 11/47 *decomposition we obtain the set of* 1-*particles*

$$\frac{47}{11} = 4 + \frac{3}{11} \longrightarrow M_1 := \left\{ \{n_i\} \; : \; \begin{matrix} (4) \times [8] \\ (5) \times [3] \end{matrix} \right\}$$

From 3/11 *decomposition we obtain the set of* 2-*particles*

$$\frac{11}{3} = 3 + \frac{2}{3} \longrightarrow M_2 := \left\{ \{n_i\} \; : \; \begin{matrix} (544) \times [1] \\ (5444) \times [2] \end{matrix} \right\}$$

From 2/3 *decomposition we obtain the set of* 3-*particles*

$$\frac{3}{2} = 1 + \frac{1}{2} \longrightarrow M_3 := \left\{ \{n_i\} \; : \; \begin{matrix} (5444) \times [1] \\ (5444544) \times [1] \end{matrix} \right\}$$

Finally from 1/2 *decomposition we obtain the set of* 4-*particles*

$$2 = 2 + \frac{0}{1} \longrightarrow M_4 := \{\{n_i\} \; : (54445445444) \times [1]\}$$

Remarks:

1) The algorithm has an end. As we are representing the rational number ρ as a continued fraction, it is known that every finite continued fraction is a rational number, and a rational number can be represented by a finite continued fraction in precisely two different ways.

2) If $\rho = (mp)/(Np)$ where m and N are coprime, and $p > 1$, the GS that is obtained by the algorithm is the same one as $\rho = p/N$. Then it is sufficient to obtain GS for densities in which numerator and denominator are coprime.

3) Particle-hole symmetry makes it sufficient to obtain the GS for $\rho \leq \frac{1}{2}$.

Let us summarize Hubbard's algorithm for a filling fraction ρ. First ρ is represented as a continued fraction,

$$\rho = \cfrac{1}{u_1 + \cfrac{1}{u_2 + \dots}} =: [0; u_1, \dots, u_k] \tag{5.31}$$

Then we define n-particle Y_n and n-hole X_n recursively

$$X_n := (Y_{n-1})(X_{n-1})^{u_n - 1} \tag{5.32}$$

$$Y_n := (Y_{n-1})(X_{n-1})^{u_n} \tag{5.33}$$

The initial conditions are 0-particle and 0-hole, $X_0 := (0)$ and $Y_0 := (1)$. Hubbard's ground state is X_k.

ρ	X_k	configuration
$\frac{1}{3}$	(3)	● ○ ○ ● ○ ○ ● ○ ○ ● ○ ○ ● ⋯
$\frac{3}{7}$	(322)	● ○ ○ ● ○ ● ○ ● ○ ○ ● ○ ● ⋯
$\frac{5}{13}$	$(32)^2(3)$	● ○ ○ ● ○ ● ○ ○ ● ○ ● ○ ○ ⋯

Table 5.3: Hubbard ground states for three different filling fractions: $\rho = 1/3$, $\rho = 3/7$ and $\rho = 5/13$.

5.3 The Burkov-Sinai formula: a formal proof of incompressibility

In the previous section we obtained the periodic ground states for the Hamiltonian (5.5): fixing rational density (or filling fraction or particles number) corresponds to choose one ground state (up to translations) with that density of particles. From now on we want to study our system in the grandcanonical ensemble, i.e. we want to change the particles number. Therefore we add the chemical potential μ in order to obtain the Bak Hamiltonian 5.1, i.e. if we consider Hubbard model, we have an infinite chain (chain of length N with periodic boundary conditions) and periodic configurations

$$E(\boldsymbol{r}^{(1)}) = A\left(-2\mu m + \sum_k \sum_{\mu=1}^{m} U^k(\boldsymbol{r}^{(\mu)})\right). \tag{5.34}$$

For each value of μ we have only one *stable* (and incompressible) periodic ground state (to be chosen from the set built up above). In order to understand if a given ground state is incompressible, we analyze the energy cost of insert or extract one excitation from a given configuration. If both operations increase the energy, the configuration is stable. The solution was given by Bak in [12]. A mathematical proof of this result is due to Burkov and Sinai [24].

Let us calculate the region of the parameter space μ in which Hubbard ground state for $\rho = m/N$ is stable. We suppose to inserting or extracting one excitation on pN sites, obtaining an Hubbard configuration with filling fraction $\rho' = pm + 1/pN$ or $\rho'' = pm - 1/pN$, where we have to find p such that we don't disturb too much the order, i.e. we are demanding that distances between particles change little. So, our hipothesis are

$$
\begin{cases}
r^\mu\left(\rho'\right) = \left\lfloor \frac{\mu pN}{pm+1} \right\rfloor = \left\lfloor \frac{\mu N}{m} \right\rfloor = r^\mu\left(\rho\right) & \forall\mu \;(\mathrm{mod}\; m) = 1, \ldots, m-1 \\[2ex]
r^\mu\left(\rho'\right) = \left\lfloor \frac{\mu pN}{pm+1} \right\rfloor = \left\lfloor \frac{\mu N}{m} \right\rfloor - 1 = kN - 1 & \forall\mu = km
\end{cases}
$$

$$(5.35)$$

$$
\begin{cases}
r^\mu\left(\rho''\right) = \left\lfloor \frac{\mu pN}{pm-1} \right\rfloor = \left\lfloor \frac{\mu N}{m} \right\rfloor = r^\mu\left(\rho\right) & \forall\mu \;(\mathrm{mod}\; m) = 1, \ldots, m-1 \\[2ex]
r^\mu\left(\rho''\right) = \left\lfloor \frac{\mu pN}{pm-1} \right\rfloor = \left\lfloor \frac{\mu N}{m} \right\rfloor = kN & \forall\mu = km
\end{cases}
$$

$$(5.36)$$

where $r^\mu\left(\rho\right)/r^\mu\left(\rho'\right)/r^\mu\left(\rho''\right)$ is the minimal distance that we obtain with Hubbard algorithm for $\rho/\rho'/\rho''$.

Since we know that all states are of Hubbard kind, we know the configurations structure. We know that we have $m - a^\mu\left(\rho\right)$ distances ($r^\mu\left(\rho\right)$) and $a^\mu\left(\rho\right)$ distances ($r^\mu\left(\rho\right) + 1$) for ρ; we can suppose to have $m + 1 - a^\mu\left(\rho'\right)$ distances ($r^\mu\left(\rho'\right)$) and $a^\mu\left(\rho'\right)$ distances ($r^\mu\left(\rho'\right) + 1$) for ρ' and $m - 1 - a^\mu\left(\rho''\right)$ distances ($r^\mu\left(\rho''\right)$) and $a^\mu\left(\rho''\right)$ distances ($r^\mu\left(\rho''\right) + 1$) for ρ''. Our second hypothesis is that all states satisfy Hubbard bond (we don't change the lenght of chain, when we change density):

$$
\sum_{v=1}^{m(\rho)} r^\mu_v\left(\rho\right) = \mu N,
$$

$$(5.37)$$

then

$$
\sum_{v=1}^{m} r^\mu_v\left(\rho\right) = \mu N = m r^\mu\left(\rho\right) + a^\mu\left(\rho\right),
$$

$$(5.38)$$

$$
\sum_{v=1}^{m+1} r^\mu_v\left(\rho'\right) = \mu N = (m + 1 - a^\mu\left(\rho'\right)) r^\mu\left(\rho'\right) + a^\mu\left(\rho'\right)\left(r^\mu\left(\rho'\right) + 1\right) =
$$
$$
= m r^\mu\left(\rho'\right) + r^\mu\left(\rho'\right) + a^\mu\left(\rho'\right),
$$

$$(5.39)$$

$$
\sum_{v=1}^{m-1} r^\mu_v\left(\rho''\right) = \mu N = (m - 1 - a^\mu\left(\rho''\right)) r^\mu\left(\rho''\right) + a^\mu\left(\rho''\right)\left(r^\mu\left(\rho''\right) + 1\right) =
$$
$$
= m r^\mu\left(\rho''\right) - r^\mu\left(\rho''\right) + a^\mu\left(\rho''\right),
$$

$$(5.40)$$

from which we obtain two equations

$$mr^{\mu}(\rho') + r^{\mu}(\rho') + a^{\mu}(\rho') = mr^{\mu}(\rho) + a^{\mu}(\rho) \ , \tag{5.41}$$

$$mr^{\mu}(\rho'') - r^{\mu}(\rho'') + a^{\mu}(\rho'') = mr^{\mu}(\rho) + a^{\mu}(\rho) \ . \tag{5.42}$$

Replacing values of $r^{\mu}(\rho')/r^{\mu}(\rho'')$ we evaluate $a^{\mu}(\rho')/a^{\mu}(\rho'')$.

$$\begin{cases} a^{\mu}(\rho') = a^{\mu}(\rho) - r^{\mu}(\rho) & \forall \mu \ (\mathrm{mod}\ m) = 1, \dots, m-1 \\ a^{\mu}(\rho') = m+1-kN & \forall \mu = km \end{cases} \tag{5.43}$$

$$\begin{cases} a^{\mu}(\rho'') = a^{\mu}(\rho) + r^{\mu}(\rho) & \forall \mu \ (\mathrm{mod}\ m) = 1, \dots, m-1 \\ a^{\mu}(\rho'') = kN & \forall \mu = km \end{cases} \tag{5.44}$$

Throughout, $r^{\mu} := r^{\mu}(\rho)$ and $a^{\mu} := a^{\mu}(\rho)$. Therefore inserting one excitation matches to transform Hubbard GS with $m - a^{\mu}$ distances (r^{μ}) and a^{μ} distances ($r^{\mu}+1$) in Hubbard GS with $m - a^{\mu} + 1 + r^{\mu}$ distances (r^{μ}) and $a^{\mu} - r^{\mu}$ distances ($r^{\mu}+1$); we are replacing r^{μ} distances ($r^{\mu}+1$) by $r^{\mu}+1$ distances (r^{μ}). With the same logic one understands that extracting excitation from the system will replace $r^{\mu}+1$ distances (r^{μ}) by r^{μ} distances ($r^{\mu}+1$). In a schematic way we can write:

	$\mu \ (\mathrm{mod}\ m) = 1, \dots, m-1$	$\mu = km$
$\rho \rightarrow$	$(r^{\mu}) \times m - a^{\mu}$ $(r^{\mu}+1) \times a^{\mu}$	$(kN) \times m$
$\rho' \rightarrow$	$(r^{\mu}) \times m - a^{\mu} + 1 + r^{\mu}$ $(r^{\mu}+1) \times a^{\mu} - r^{\mu}$	$(kN-1) \times kN$ $(kN) \times m + 1 - kN$
$\rho'' \rightarrow$	$(r^{\mu}) \times m - a^{\mu} - (1 + r^{\mu})$ $(r^{\mu}+1) \times a^{\mu} + r^{\mu}$	$(kN) \times m - 1 - kN$ $(kN+1) \times kN$

$$\tag{5.45}$$

If we evalutate the energy on an Hubbard ground state we have

$$E(\rho) = -2\mu m + \sum_{k=1}^{\infty} \sum_{\mu=1}^{m} (m - a^{\mu}) V(r^{\mu} + kN) + a^{\mu} V(r^{\mu} + kN + 1) \tag{5.46}$$

that directly depends on number of particles m.

Until now, starting from a given ρ configuration, we have constructed two Hubbard phases ρ' and ρ'' to be compared with ρ. Now we have all the ingredients to obtain the energy difference between ρ' GS and ρ GS (inserting excitation):

$$\begin{aligned} \Delta E_+ &= E(\rho') - E(\rho) = \\ &= -2\mu_+ + \sum_{k=1}^{\infty} \sum_{\mu=1}^{m-1} (r^{\mu} + kN + 1) V(r^{\mu} + kN) - (r^{\mu} + kN) V(r^{\mu} + kN + 1) + \\ &\quad + \sum_{k=1}^{\infty} (1 - kN) V(kN) + (kN) V(kN - 1) \ , \end{aligned} \tag{5.47}$$

and similarly the energy difference between ρ'' GS and ρ GS (extracting excitation):

$$\Delta E_- = E(\rho'') - E(\rho) =$$

$$= 2\mu_- - \sum_{k=1}^{\infty} \sum_{\mu=1}^{m-1} (r^\mu + kN + 1)V(r^\mu + kN) - (r^\mu + kN)V(r^\mu + kN + 1) + \tag{5.48}$$

$$+ \sum_{k=1}^{\infty} (kN)V(kN+1) - (1+kN)V(kN) \,.$$

The interval in μ, $\Delta\mu(\rho) = \mu_+ - \mu_-$, where the ground state is stable is determined simply by setting (5.47) and (5.48) equal to zero, because we demand that $\Delta E_+ \geq 0$ for all ρ' and $\Delta E_- \geq 0$ for all ρ''; respectively

$$\frac{1}{2}\Delta\mu = \sum_{k=1}^{\infty} (kN) \left[V(kN+1) + V(kN-1) - 2V(kN) \right] \,. \tag{5.49}$$

Note that $\Delta\mu(\rho)$ is indipendent the numerator m and non zero for every Hubbard ground state, thus proving their incompressibility.

5.4   Devil's staircase phase diagram at zero temperature

Using (5.49) we can plot the phase diagram for (5.34) for a strictly convex potential. Operatively we set a minimum cut-off for the density. We assume there exists some density $\rho_0 = 1/N$ that is stable for $\mu = 0$, with high N. It is useful to choose N with a lot of divisors.

Now we construct the phase diagram. We suppose $\mu_-(\rho_0) = 0$. We calculate $\mu_+(\rho_0)$ using (5.49) with a larger number of term. Now we flip one spin up, because over $\mu_+(\rho_0)$, the phase ρ_0 isn't stable. So we consider $\rho_1 = 2/N$ and we fix $\mu_-(\rho_1) := \mu_+(\rho_0)$. We calculate $\rho_1 = 2/N$ stability interval and so on. The algorithm to construct phase diagram is recursive. Our initial conditions are:

$$\begin{cases} \rho_0 := \frac{1}{N} \\ \mu_-(\rho_0) := 0 \end{cases} \tag{5.50}$$

then we have to apply recursively:

$$\begin{cases} \mu_+(\rho_i) := \mu_-(\rho_i) + \Delta\mu(\rho_i) \\ \rho_{i+1} := \rho_i + \frac{1}{N} \\ \mu_-(\rho_{i+1}) := \mu_+(\rho_{i+1}) \end{cases} \tag{5.51}$$

Results are in Figure (5.1).
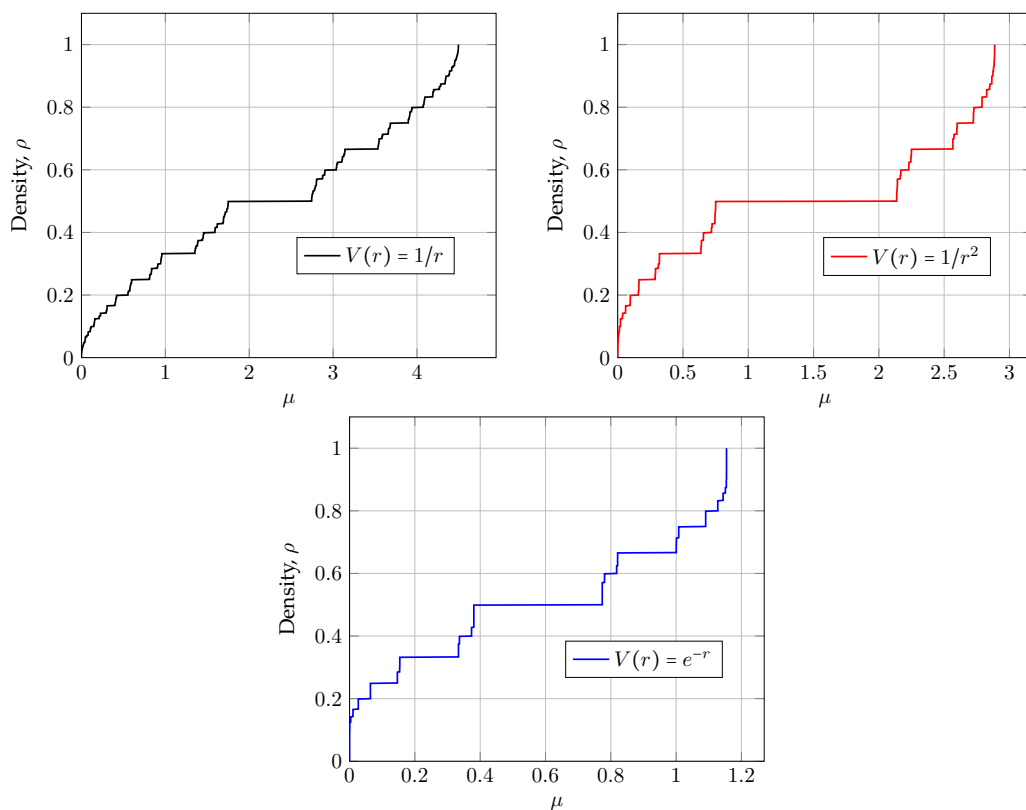
Figure 5.1: Phase diagram with the *Devil's staircase* for different potentials. The density of particle ρ is plotted against the chemical potential μ. The structure of the staircase is qualitatively similar for the three potentials. However the length of the plateaux is not universal. In the case $V(r) = 1/r$ the result shown is misleading: increasing N the devil's staircase is pushed toward infinity along the orinzontal axes. This is a byproduct of the non-extensivity of the Coulomb problem. In order to obtain sensible results we should regularize the potential.

Quantum Hall problem in the lowest Landau level

In this chapter we introduce the fundamental background to understand correlated electrons in two dimensions. The take-home messages are mainly two:

1. the quantum Hall Hamiltonian projected on the lowest Landau level [14] undergoes a sort of *dimensional reduction* when written down in the second quantization formalism. This fact is indipendent of the gauge choice and also of the geometry;

2. many fractional quantum Hall states, such as Laughlin [16], Moore-Read [109] or Read-Rezayi [110] wavefunctions, are specific realizations of *Jack polynomials* [111]. This observation is recent [25] and allows to obtain recurrence relations for the coefficients of the decomposition in Slater determinant of these states [112], previously unknown.

Both observations are fundamental for our original work, that we will present in the last Chapter.

6.1 Non-interacting electrons in $2D$ in a constant magnetic field: Landau levels

In this section we introduce the quantum description of an electron (more in general of a charged particle) in an electromagnetic field in two-dimensions. Ignoring spin degrees of freedom, the single particle Hamiltonian is

$$H_{EM} = \frac{(\boldsymbol{p} - q_e \boldsymbol{A})^2}{2m_e} + q_e V \,, \tag{6.1}$$

where $\boldsymbol{p}$ is the canonical momentum operator that satisfies canonical commutation relations $[r_a, p_b] = i\hbar \delta_{ab}$ and $(V(\boldsymbol{r},t), \boldsymbol{A}(\boldsymbol{r},t))$ is the potential of the electromagnetic field:

$$\boldsymbol{E} = -\nabla V - \frac{\partial \boldsymbol{A}}{\partial t} \,, \qquad \boldsymbol{B} = \nabla \times \boldsymbol{A} \,. \tag{6.2}$$

In absence of electromagnetic field, electrons are free particles on the (x, y) plane and they are described by plane waves with energy $E_k = \hbar^2 \boldsymbol{k}^2 / 2m_e$ and wave vector $\boldsymbol{k} = \frac{2\pi}{L}(n_x, n_y)$.

We are interested in finding eigenstates and eigenvalues for the Hamiltonian H_{EM}, setting $V = 0$ and $\boldsymbol{A} = \boldsymbol{A}(\boldsymbol{r})$, such that the magnetic field $\boldsymbol{B} = (0, 0, B)$ is homogeneous and constant. If we define the gauge invariant momentum $\boldsymbol{\pi}$, the covariant momentum, that correspond to the classical generalized momentum is:

$$\boldsymbol{\pi} := m_e \boldsymbol{v} = \boldsymbol{p} - q_e \boldsymbol{A} \tag{6.3}$$

and the Hamiltonian reads

$$H_{EM} = \frac{\boldsymbol{\pi}^2}{2m_e} = \frac{1}{2m_e} (\pi_x^2 + \pi_y^2) . \tag{6.4}$$

The components of $\boldsymbol{\pi}$ satisfy the following commutations relations

$$[\pi_x, \pi_y] = i \frac{\hbar}{\ell^2} , \tag{6.5}$$

where the magnetic lenght $\ell = \sqrt{\hbar/q_e B}$, is the fundamental length scale ($B = 10T$ means $\ell \simeq 100A$). We observe that in a magnetic field the operators of covariant momentum components do not commute. Furthermore, using these operatos, we can define a creation and an annihilation operator, for which $[a, a^\dagger] = 1$,

$$a := \frac{\ell}{\sqrt{2}\hbar} (\pi_x - i\pi_y), \qquad a^\dagger := \frac{\ell}{\sqrt{2}\hbar} (\pi_x + i\pi_y) . \tag{6.6}$$

The Hamiltonian has the same algebraic structure of an harmonic oscillator:

$$H_{EM} = \hbar\omega_c \left(aa^\dagger + \frac{1}{2} \right) , \tag{6.7}$$

where $\omega_c = q_e B/m_e$ is the cyclotron frequency. The eigenstates of H_{EM} are the same of the number operator $N = a^\dagger a$, i.e. $N |n\rangle = n |n\rangle$). Creator and annihilation operators generate whole ladder of states as usual:

$$a |n\rangle = \sqrt{n} |n-1\rangle , \qquad a^\dagger |n\rangle = \sqrt{n+1} |n\rangle , \tag{6.8}$$

and $|0\rangle$ is the ground state such that $a |0\rangle = 0$. Energy levels $E_n = \hbar\omega_c \left(n + \frac{1}{2} \right)$ are degenerate. They are called *Landau levels*.

To eliminate the degeneration we need to define the guiding center coordinate (center of cyclotron motion) χ, that represents the barycentric coordinate

$$\chi_x := x + \frac{1}{q_e B} \pi_y, \qquad \chi_y := y - \frac{1}{q_e B} \pi_x , \tag{6.9}$$

that satisfies

$$[\chi_x, \chi_y] = -i\ell^2 . \tag{6.10}$$

We observe, since the operators of guiding center components do not commute, the particle position can not be determined more accurately than the area $2\pi\ell^2$. Furthermore

$$[\chi_x, \pi_x] = [\chi_x, \pi_y] = [\chi_y, \pi_x] = [\chi_y, \pi_y] = 0 , \tag{6.11}$$

so the guiding center χ and the covariant momentum π are entirely indipendent variables. We can construct one creation and one annihilation operator for which $[b, b^\dagger] = 1$,

$$b = \frac{1}{\sqrt{2}\ell}(\chi_x - i\chi_y), \qquad b^\dagger := \frac{1}{\sqrt{2}\ell}(\chi_x + i\chi_y). \tag{6.12}$$

We observe that

$$[a, b] = [a^\dagger, b] = 0, \tag{6.13}$$

so we have another indipendent harmonic oscillator $b^\dagger b |m\rangle = m |m\rangle$. The eigenstates of H_{EM} are the same of the number operator $M = b^\dagger b$, then the general eigenstate of the Hamiltonian, with energy $E_n = \hbar\omega_c \left(n + \frac{1}{2}\right)$ is a linear superposition of the following states, which we call the *Landau sites*

$$|n, m\rangle = \sqrt{\frac{1}{n!m!}} (a^\dagger)^n (b^\dagger)^m |0, 0\rangle \tag{6.14}$$

where $|0, 0\rangle$ is the vacuum. Their orthonormal completeness condition reads

$$\langle n_1, m_1 | n_2, m_2 \rangle = \delta_{n_1, n_2} \delta_{m_1, m_2}, \qquad \sum_{n,m} |n, m\rangle \langle n, m| = 1 \tag{6.15}$$

The motion of an electron within one Landau level is specified by the guiding center χ. Since the coordinates χ_x and χ_y do not commute, we can not diagonalize both of them simultaneously.

6.1.1 Landau levels in the symmetric gauge

We now consider the same analysis in the symmetric gauge:

$$\boldsymbol{A}(\boldsymbol{r}) = \left(-\frac{1}{2}By, \frac{1}{2}Bx, 0\right). \tag{6.16}$$

Since the system has a disk geometry, it is appropriate to diagonalize the symmetric combination $\chi_x^2 + \chi_y^2$. This is equivalent to diagonalize the number operator $b^\dagger b$:

$$\chi_x^2 + \chi_y^2 = (2b^\dagger b + 1)\ell^2. \tag{6.17}$$

The Landau site $|n, m\rangle$ is an eigenstate of the operator $\chi_x^2 + \chi_y^2$

$$\left(\chi_x^2 + \chi_y^2\right)|n, m\rangle = (2m + 1)\ell^2 |n, m\rangle. \tag{6.18}$$

The angular momentum operator is given by

$$L = xp_y - yp_x = (b^\dagger b - a^\dagger a)\hbar, \tag{6.19}$$

so the state $|n, m\rangle$ has the angular momentum $(m - n)\hbar$ in a given Landau level n. b and $b^\dagger$ are the ladder operators increasing or decreasing angular momentum.

Using a complex number $z := \frac{1}{\ell}(x + iy)$ for electron position, the general solution for the states in the *lowest Landau level* (LLL), i.e. states which satisfie $a|0, m\rangle = 0$, is

$$\psi_{0,m}(\boldsymbol{r}) = h(z) \exp\left[-|z|^2/4\right], \tag{6.20}$$

where $h(z)$ is an arbitrary analytic function. All these states are degenerate.

The state $|0, 0\rangle$ statisfies $b |0, 0\rangle = 0$, which is solved as

$$\psi_{0,0}(\boldsymbol{r}) = \frac{1}{\sqrt{2\pi\ell^2}} \exp\left(-\frac{r^2}{4\ell^2}\right) . \tag{6.21}$$

The state $|0, m\rangle$ is described by the wave function

$$\psi_{0,m}(\boldsymbol{r}) = \sqrt{\frac{2^m}{2\pi\ell^2 m!}} z^m e^{-|z|^2/4} . \tag{6.22}$$

It represent an electron circularly localized. The probability of finding the electron at $r = 2\ell|z|$ in the lowest Landau level is given by

$$|\psi_{0,m}(r)|^2 \propto r^{2m} \exp\left(-\frac{r^2}{2\ell^2}\right) , \tag{6.23}$$

which has a sharp peak at $r_m = \sqrt{2m}\ell$. These states are represented by rings on a disk geometry, where a ring is labeled by the angular momentum $m\hbar$. The area of each ring is

$$\Delta S = \pi r_{m+1}^2 - \pi r_m^2 = 2\pi\ell^2 . \tag{6.24}$$

The position of the electron cannot be localized within an area smaller than ΔS.

6.1.2   Landau levels in the Landau gauge

Now we consider the Landau Gauge. We suppose to have translational invariance in y direction.

$$\boldsymbol{A}(\boldsymbol{r}) = (0, Bx, 0) . \tag{6.25}$$

Since we have $p_y = (\hbar/\ell^2)\chi_x$ conservation, we can diagonalize χ_x:

$$p_y |k_y\rangle = \hbar k_y |k_y\rangle , \qquad \chi_x |k_y\rangle = k_y\ell^2 |k_y\rangle . \tag{6.26}$$

Here k_y is a wave number in y direction. To obtain the lowest Landau levels, we have to apply LLL condition $a |k_y\rangle = 0$. Solving that differential equation is a trivial problem so:

$$\phi_{0,k_y}(\boldsymbol{r}) = \frac{1}{\pi^{1/4}\ell^{1/2}} \exp(ik_y y) \exp\left[-\frac{1}{2\ell^2}(x - k_y\ell^2)^2\right] . \tag{6.27}$$

This is a plane wave in y direction with momentum $\hbar k_y$. The probability of finding an electron at x has a sharp peak at $x = k_y\ell^2$. These states are represented by strips on a rectangular geometry, where a strip is labeled by the wave number k_y, located at $x = k_y\ell^2$, and has width $\delta x = \ell^2 \delta k_y$. Here $\delta k_y = 2\pi/L_y$, because the wave number is quantized as $k_y = 2\pi/L_y s_y$, where s_y is an integer and L_y is the y size of the sistem. The area of each strip is equal to

$$\Delta S = L_x \Delta y = 2\pi\ell^2 . \tag{6.28}$$

6.1.3   Flux quanta and filling factor

Due to the Pauli exclusion principle only one electron can occupy a single Landau site (in the spinless theory). Each of them has area $\Delta S = 2\pi\ell^2$, so that each energy level has a degenaracy per unit area ρ_Φ

$$\rho_\Phi = \frac{N_\Phi}{S} = \frac{1}{2\pi\ell^2} \,, \tag{6.29}$$

where S is the area of the total system and N_Φ is the number of states $S/\Delta S$. If we define the Dirac flux quantum Φ_D as the magnetic flux on the area ΔS,

$$\Phi_D := 2\pi\ell^2 B = \frac{2\pi\hbar}{q_e} \,, \tag{6.30}$$

the density of states is equal to the density of flux quanta

$$\rho_\Phi = \frac{N_\Phi}{S} = \frac{\Phi_{TOT}}{S\Phi_D} = \frac{B}{\Phi_D} \,. \tag{6.31}$$

The filling fraction of the energy level is defined by the ratio

$$\nu = \frac{\text{Number of particles}}{\text{Number of states}} = \frac{S\rho_0}{S\rho_\Phi} = 2\pi\ell^2\rho_0 = \frac{2\pi\hbar\rho_0}{q_e B} = \frac{\rho_0\Phi_D}{B} \,. \tag{6.32}$$

At $\nu = 1/q$ there are q flux quanta per electron, $B/\rho_0 = q\Phi_D$. The filling factor is called the *Landau level filling factor*, or simply the filling factor. When $\nu = 1$ the Landau level is full.

6.2   Integer and fractional quantum Hall effect

Edwin Hall discovered in 1879 [113], while he was working on his doctoral degree, that in a conductor travelled by electric current and immersed in a magnetic field perpendicular to the current, a voltage difference (the Hall voltage) appears across the electrical conductor, transverse to the electric current.

Classically, electrons moving with velocity $\boldsymbol{v}$ in an xy plane (2D-system) in magnetic field $\boldsymbol{B}$, obey the equation of motion

$$m_e\dot{\boldsymbol{v}} = -q_e(\boldsymbol{E} + \boldsymbol{v} \times \boldsymbol{B}) \tag{6.33}$$

where m_e is the electron mass and q_e is the electron charge. It implies that $\boldsymbol{E} = -\boldsymbol{v} \times \boldsymbol{B}$, for static current, i.e. $\dot{\boldsymbol{v}} = 0$. The current density is $\boldsymbol{J} = -q_e\rho_0\boldsymbol{v}$ in a homogeneous electron gas with areal density ρ_0. It means that

$$J_x = \frac{q_e\rho_0}{B_\perp}E_y, \qquad J_y = -\frac{q_e\rho_0}{B_\perp}E_x \tag{6.34}$$

with $B_\perp := -B_z > 0$. The current $\boldsymbol{J}$ flows in a direction perpendicular to the electrical field $\boldsymbol{E}$.

We take the electric field along the y axis; then $E_x = 0$ and $E_y \neq 0$. It follows that the classical Hall resistivity ρ_{xy} is

$$\rho_{xy} = -\rho_{yx} = \frac{E_y}{J_x} = \frac{B_\perp}{q_e\rho_0} = \frac{2\pi\hbar}{q_e^2}\frac{1}{\nu} \tag{6.35}$$
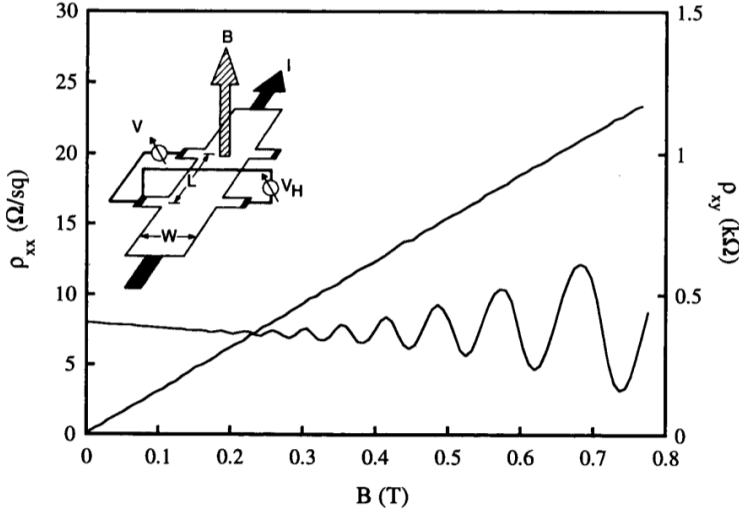
Figure 6.1: Classic Hall effect: low temperature and moderately low B. The insert shows the measurement geometry. The voltages V_x and V_y are respectively measured in the two perpendicular directions on the sample. ρ_{xx} is the resistivity across the square. $\rho_{xy} = V_y/I$ is the Hall resistivity. Image taken from [114].

with

$$\nu := \frac{2\pi\hbar\rho_0}{q_e B_\perp} \tag{6.36}$$

while the diagonal resistivity ρ_{xx} is

$$\rho_{xx} = \rho_{yy} = \frac{E_x}{J_x} = 0 \tag{6.37}$$

The classical Hall resistivity is a linear function of the perpendicular magnetic field $B_\perp$ for fixed density ρ_0. It is a common knowledge that the resistivity depends sensitively on details of a sample such as its composition, geometry and impurities. Experimental results are strikingly different, though they are obtained in dirty solid-state samples. The resistivity is insensitive to details of samples at particular values of parameter ν, where the Hall resistivity ρ_{xy} is quantized and develops a series of plateaux, and the diagonal resistivity ρ_{xx} shows a series of dips. This is known as QH effect. The number of observed Hall plateaux increases as the sample becomes purer.

The integer QH effect (IQHE), i.e. at $\nu \in \mathbb{N}$, was discovered by von Klitzing [115] in 1980 in a 2D electron gas at low temperature, a century after the discovery of the Hall effect. The discovery was preceded by a theoretical suggestion due to Ando and an experimental indication due to Kawaji, but no one seems to have foreseen the exact quantization of the Hall conductivity. The fractional QH effect (FQHE), i.e. at $\nu = p/q$ with integer p and odd integer q, was discovered by Tsui, Stormer and Gossard [116] in 1982. While the IQHE can be understood within an independent electron theory of a disordered system, the FQHE is based on strong electron correlations. Both effects are
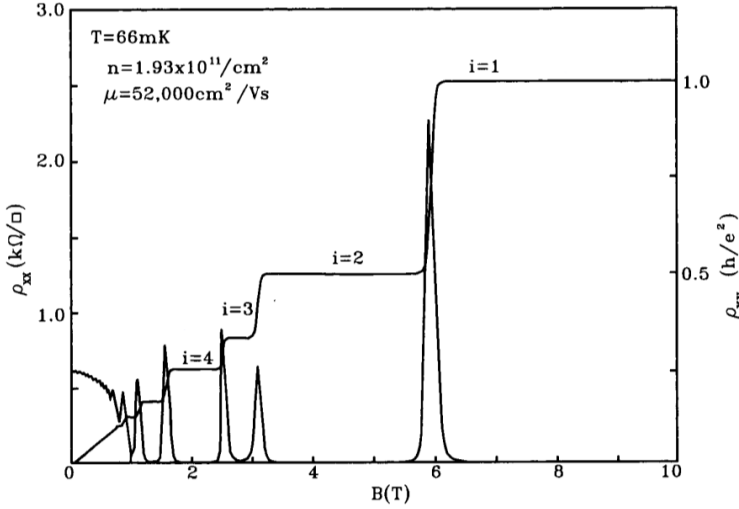
Figure 6.2: The integer QH effect (IQHE). In a classical electron gas the Hall resistivity ρ_{yx} is proportional to the magnetic field $B_\perp$. However, the Hall resistivity ρ_{xy} shows a stair case in an actual sample, with the plateau crossing the classical line at $\nu = 1, 2, 3, \ldots$. The diagonal resistivity ρ_{xx} vanishing at these points. Image taken from [114].

found in GaAs/Ge$_x$Ga$_{1-x}$As heterostructures of silicon field-effect transistors when a magnetic field B is applied perpendicularly to the two-dimensional electron liquid.

While the actual experimental data are affected by the thermal motion, theoretically it is believed that in the zero temperature limit, the Hall resistivity is given by

$$\rho_{yx} = \frac{1}{\nu} R_K \qquad \text{with} \qquad R_K := \frac{2\pi\hbar}{q_e^2} = 25812.8074434(84)\Omega \qquad (6.38)$$

Because its precise measurement is possible rather easily in QH systems, since 1990 this has been used as the standard resistance with a definite choice of R_K, called the von Klitzing constant.
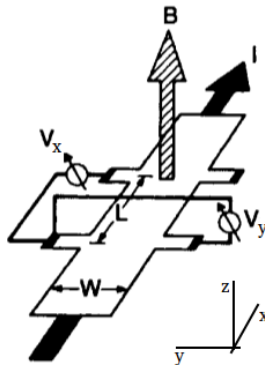

Figure 6.3: Experimental arrangement for measuring the quantum Hall effect.

The Hall resistivity ρ_{yx} and the diagonal resistivity ρ_{xx} are determined in a rectangular sample by feeding a constant current $J_{tot} = J_x W$ along the x axis and measuring the voltage V_y perpendicular to it (see Figure 6.3). It is arranged so that no current flows in the y direction, $J_y = 0$. The electric field reads

$$E_x = -\rho_{xx} J_x = -\rho_{xx}\frac{J_{tot}}{W}, \qquad E_y = -\rho_{yx} J_x = \rho_{xy}\frac{J_{tot}}{W} \tag{6.39}$$

where $E_y = V_y/W$ and $E_x = V_x/L$. It follows that

$$\rho_{xy} = \frac{V_y}{J_{tot}}, \qquad \rho_{xx} = -\frac{W V_x}{L J_{tot}} \tag{6.40}$$

The Hall resistivity ρ_{xy} depends only on the current J_{tot} and the voltage V_y. Hence, it can be determined very accurately. They take peculiar values,

$$\rho_{xy} = \frac{R_K}{\nu}, \qquad \rho_{xx} = 0 \tag{6.41}$$

in the QH state at ν. In weak magnetic field, the Hall resistivity is described well by the classical theory, $\rho_{xy} = B_\perp/q_e\rho_0$, which is used experimentally to determine the electron density ρ_0 of a sample.

6.2.1   Qualitative explanation of the IQHE

To avoid unnecessary complications we ignore the dynamical degree of freedom associcated with spin by assuming that all spins are polarized and frozen by the Zeeman effect: it is a spin frozen system. The electron gas is described by the following Hamiltonian:

$$H = \sum_i H_{EM}(\boldsymbol{r}_i, \boldsymbol{p_i}) + H_C, \tag{6.42}$$

where $H_{EM}(\boldsymbol{r}_i, \boldsymbol{p_i})$ is the electromagnetic Hamiltonian for the i-th electron and H_C is the Coulomb energy contribution. Our first attempt to symplify the problem is neglecting the Coulomb energy, i.e. we use indipendent single-particle approximation. So we consider an hamiltonian

$$H = \sum_i H_{EM}(\boldsymbol{r}_i, \boldsymbol{p}_i). \tag{6.43}$$

Each electron can occupy only one Landau site, and the total eigenstate is a Slater determinant of single particle eigenstates. Working with this idealized system it can be demonstrated that we obtain classical prediction about Hall resistivity, because $\langle \boldsymbol{v}_i \rangle$ (mean i-th electron's speed value calculated on Landau sites) has the same behavior of the classical speed.

To understand IQHE it is necessary to introduce the interaction of the system with impurities, defects and inhomogeneity [117]. This theory was provided by Laughlin in 1981 [14]. We need strong magnetic fields so that Landau levels do not intersect. Essentially the interaction wih impurities partially splits Landau sites and broadens Landau levels. However new single-particle states of the system are not equivalent. States in the tail of new Landau levels are Anderson localizated, thus they are ensnared in a specific

microscopic region of the system. So disorder traps electrons wave functions. At the opposite, states near the center of new Landau levels are not localized, they are extended on all the system.

Only extended wave functions contribute to the current flow. Let us analize the behaviour of a low temperature system by tuning the particle density. For low densities, all particles occupy localized states and current flow is impossible. Adding particles, Fermi energy reaches first possible Landau level, a region with extended states, and conductivity gains one quantum $e^2/\hbar$. Next density level cross the other tail of Landau level that is a region with localized states. So conductivity remains constant and displays a plateau. Increasing density means refreshing the sequence. At each Landau level conductivity has a leap. Laughlin connects changes in magnetic field to density mutations through flux quanta filling fraction [118].

6.3 Quantum Hall problem in the lowest Landau level

At the beginning of the fractional quantum Hall era, only a small number of plateaux were observed, the first one being the $\nu = 1/3$. Nowadays the picture is completely different: more than fifty different plateaux are observed only in the lowest Landau level [119].
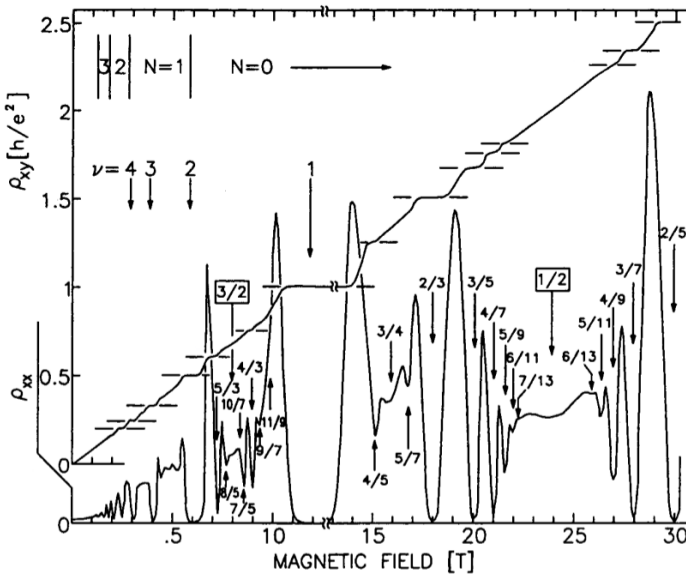
Figure 6.4: The celebrated fractional QH landscape. Many fractional QH states are observed in pure samples. It easy to identify them by searching for dips in the diagonal resistance ρ_{xx} rather than plateaux in the Hall resistance ρ_{xy}. Image taken from [114].

The qualitative explanation of the previous section does not apply to plateaux at fractional fillings. In order to understand fractional quantum Hall effect, Coulomb repulsion between electrons can not be ignored and must be taken into account.

A measure of the Coulomb interaction is roughly $U = e^2/4\pi\ell$, which is proportional to $\sqrt{B}$. The separation between the Landau levels is $\hbar\omega_c$ and thus it is proportional to B. Therefore in the limit of strong magnetic field, the ciclotron frequency is much larger than the Coulomb repulsion, $\hbar\omega_c \gg U$. This condition is barely satisfied in real sample at $B = 10T$. It is widely accepted that the fractional quantum Hall effect in the lowest Landau level can be understood in this regime, where the *mixing* between different Landau levels can be safely ignored. This observation leads to important simplifications when we consider the interacting Hamiltonian, which is the sum of the kinetic energy plus the Coulomb interaction:

$$H = H_{K.E.} + \sum_{i<j} V_{ij} \,. \tag{6.44}$$

This Hamiltonian can be written down in the Fock space. We use the basis of the non-interacting problem. The states in this basis, indipendently from the gauge and from the geometry, are always labelled by two indices: an index L that labels different Landau levels, and an index m for the degenerate Landau sites. For the disk geometry the latter labels states with different angular momentum. In the second quantization formalism we obtain:

$$H_{K.E.} = \hbar\omega_c \sum_{L=0}^{\infty} \sum_m \left(L + \frac{1}{2} \right) a_{L,m}^\dagger a_{L,m} \,, \tag{6.45}$$

$$H_{int} = \sum_{L_1,m_1} \sum_{L_2,m_2} \sum_{L_3,m_3} \sum_{L_4,m_4} \langle L_1,m_1; L_2,m_2| V_{12} |L_3,m_3; L_4,m_4 \rangle \times$$
$$\times a_{L_1,m_1}^\dagger a_{L_2,m_2}^\dagger a_{L_4,m_4} a_{L_3,m_3} \,. \tag{6.46}$$

This is the general expression. In the limit of strong magnetic field we can restrict the Hilbert space, under the assumption that the mixing between different Landau levels is negligible, which means that the non-diagonal terms of the potential are small. When we consider only the lowest Landau level, we obtain:

$$H_{K.E.} = \hbar\omega_c/2 \sum_m a_{0,m}^\dagger a_{0,m} \,, \tag{6.47}$$

$$H_{int} = \sum_{m_1,m_2,m_3,m_4} \langle 0,m_1; 0,m_2| V_{12} |0,m_3; 0,m_4 \rangle \times$$
$$\times a_{0,m_1}^\dagger a_{0,m_2}^\dagger a_{0,m_4} a_{0,m_3} \,. \tag{6.48}$$

This Hamiltonian is a quantum lattice gas, whose sites are the Landau sites of the lowest LL. Moreover a dimensional reduction took place during the no-mixing approximation: the geometry of this lattice is effectively one dimensional.

The first problem is to identify ground states of this Hamiltonian at fixed filling fraction ν. Laughlin was the first able to overcome this problem [16].

In order to minimize the Coulomb repulsion of the electrons he proposed to find a proper superposition of Slater determinants of single particle states in the lowest LL. The general wavefunction (in the symmetric gauge) for a single particle in the lowest LL is

$$\psi_{0,m}(\boldsymbol{r}) = h(z) \exp\left[-|z|/4^2 \right] \,. \tag{6.49}$$

He assumed that this superposition of Slaters was a Jastrow function:

$$\psi(\boldsymbol{r}_1, \ldots, \boldsymbol{r}_N) = \prod_{i<j} f(z_i - z_j) \exp\left[-\sum_i |z_i|^2/4\right]. \tag{6.50}$$

Using symmetry assumptions (angular momentum conservation and Pauli principle) the wavefunction is completely constrained:

$$\psi(\boldsymbol{r}_1, \ldots, \boldsymbol{r}_N) = \prod_{i<j} (z_i - z_j)^m \exp\left[-\sum_i |z_i|^2/4\right], \qquad m = 1, 3, 5, \ldots. \tag{6.51}$$

This correlated wavefunction exhibit remarkable properties [120]:

- it is an extremely accurate approximation of the exact ground state of the interacting system for filling fractions $\nu = 1/(2m+1)$. Its overlap with the exact GS (for small system size) is larger than 0.995;

- it displays no solid nor superfluid order;

- it is the exact ground state of the so called Trugman-Kivelson Hamiltonian, the first term in a short range expansion of the long range interaction.

After the incredible insight by Laughlin, a plethora of fractional quantum Hall states were proposed to describe quantum Hall liquids at different filling fractions [120].

In the following we describe the *modern* characterization of these states through Jack polynomials, which is due firstly to Haldane and Bernevig [25]. This representation allows to discover a number of previously unknown properties of the fractional quantum Hall states in their Fock space representation: among the others, a remarkable recurrence relation for the coefficients of the Slater decomposition of Laughlin states [112]. We will use this result in the last Chapter.

The presentation of the next section closely follows a recent pedagogical (eh eh..) paper by Bernevig and coworkers [121].

6.4 The connection between fractional quantum Hall states and Jack polynomials

As anticipated above, finding model wave functions for Fractional Quantum Hall (FQH) states, has been one of the dominant lines of consideration in the field. Most prominently, Laughlin's trial wave function for the FQH state at $\nu = 1/3$ filling initiated the foundation of a new level of microscopic understanding of the FQH phases. Trial states, as one of many insights, have been significantly contributing to the development of concepts like fractional Abelian statistics as found in the $\nu = 1/m$ Laughlin states [122], composite fermions [123], as well as non-Abelian statistics as in the Moore-Read (MR) [109] and Read-Rezayi (RR) states [110], which promise realization of topological quantum computation [124].

However, these trial states all share an ambiguous nature: While they are explicitly available in terms of analytical polynomial wave function expressions, it has remained

elusive to decompose them into a non-interacting basis of occupation number states being Slater determinants for fermionic states and monomials for bosonic states. As such, neither stringent comparison to mean field theories nor use of large scale numerical methods like Monte Carlo methods has proved practicable. This is why any quantitative analysis of these states has centrally relied on exact diagonalization methods [120]. There, the general pursuit is as follows: One starts with a trial Hamiltonian and generates the lowest Landau Level Hilbert space. The computational effort of diagonalization algebraically depends on the Hilbert space dimension which factorially grows with system size setting the decisive size limit constraint. For the Laughlin $1/3$ state there exist previous attempts to identify zero weight coefficients of the free basis. However, since these concepts only enabled to erase $O(1/N!)$ of the zero weight coefficients, the reduced basis dimensions obtained this way in the non-interacting basis still by far exceeds the basis reduction reachable by exact diagonalization subblock decomposition to interacting basis sets [125, 126].

6.4.1   Bosonic states

FQH states are analytic functions (except for the exponential prefactor) of the positions of electrons in a magnetic field. The single-particle orbitals in the lowest Landau Level are given by

$$\phi_m(z) = (2\pi m! 2^m)^{-1/2} z^m \exp(-|z|^2/4) \tag{6.52}$$

with angular momentum $L_z = m\hbar$, although from now we will neglect the trivial Gaussian multiplication factors. A non-interacting N-particle basis state can be indexed by a partition λ - an ordered list of the L_z angular momentum of the occupied orbitals. The corresponding occupation number configuration is [25]

$$n(\lambda) = \{n_m(\lambda), m = 0, 1, 2, \dots\}, \tag{6.53}$$

where m labels the individual single-particle orbitals and $n_m(\lambda)$ is the multiplicity of orbital m in λ. We consider FQH states decomposed in this many-body basis, either of bosons (permanents) or fermions (slaters) with expansion coefficients c_λ.

We now define a two-body operation on the many-body basis: for a pair of particles in the orbitals m_1 and m_2, with $m_1 < m_2 - 1$, the elementary *squeezing* operation consists of the two particles shifted to different momentum orbitals as

$$n_{m_{1,2}} \rightarrow n_{m_{1,2}} - 1, \tag{6.54}$$

$$n_{m_{1,2}\pm 1} \rightarrow n_{m_{1,2}\pm 1} + 1. \tag{6.55}$$

This means that both particles in the m_1, m_2 orbitals are shifted "inwards" the partition (as shown in Fig. 6.5). The squeezing defines a partial ordering relation between two partitions $\lambda > \mu$ when μ is generated by squeezing operations acting on λ [111]. This ordering yields a tree hierarchy a complete example of which is shown in Fig. 6.6 for the Laughlin state with $N = 4$ electrons and $\nu = 1/3$. By contrast, when λ and μ do not relate by squeezing, no ordering relation is set between these partitions.

The trial FQH states we consider are all squeezed polynomials. They possess a unique partition, called the root partition, dominating all other partitions. This means
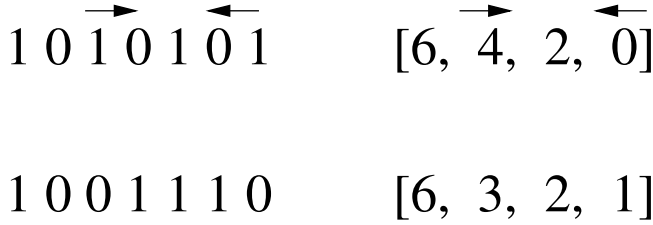
$$1\ 0\ \overrightarrow{1\ 0}\ 1\ 0\ \overleftarrow{0}\ 1 \qquad [6,\ \overrightarrow{4},\ 2,\ \overleftarrow{0}]$$

$$1\ 0\ 0\ 1\ 1\ 1\ 0 \qquad [6,\ 3,\ 2,\ 1]$$

Figure 6.5: Pictorial example of the squeezing operation in occupation language (left) and partition language (right). The squeezing operation takes the first row into the second.
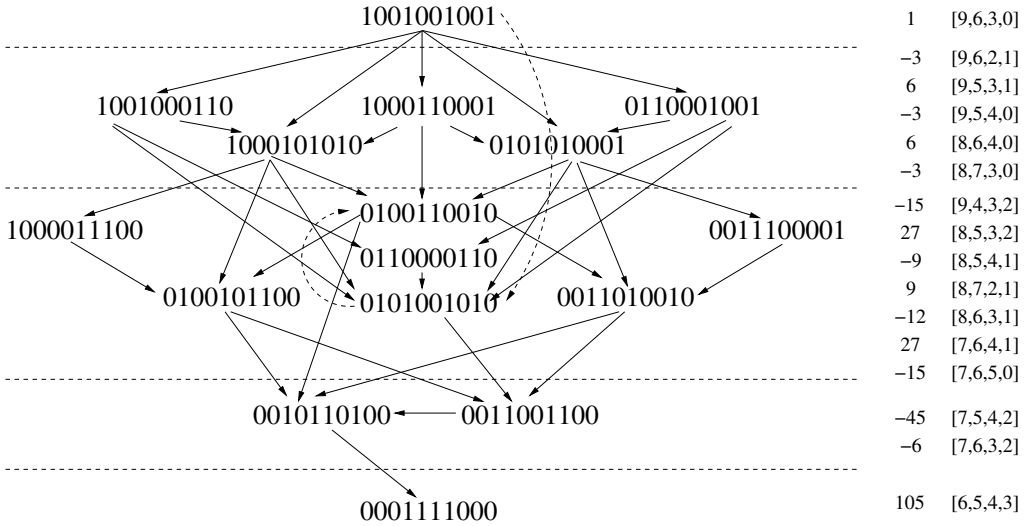

1	[9,6,3,0]
−3	[9,6,2,1]
6	[9,5,3,1]
−3	[9,5,4,0]
6	[8,6,4,0]
−3	[8,7,3,0]
−15	[9,4,3,2]
27	[8,5,3,2]
−9	[8,5,4,1]
9	[8,7,2,1]
−12	[8,6,3,1]
27	[7,6,4,1]
−15	[7,6,5,0]
−45	[7,5,4,2]
−6	[7,6,3,2]
105	[6,5,4,3]

Figure 6.6: Monomial decomposition of $N = 4$ particle $\nu = 1/3$ Laughlin state. The particle positions are denoted by 1. The coefficients of the Slater partitions are computed according to (6.70), with $\alpha = -2$. The arrows denote a squeezing relation from the upper to the lower partition. In total, there are 4 squeezing levels till the maximally squeezed partition is reached.

that all partitions with possible (but not guaranteed) non-zero weight are generated by subsequent squeezing operations acting on the root partition. In many cases, this already allows us to omit a significant (more than half) part of the Hilbert space (see Table 6.1).

In this Section, we focus on the bosonic FQH states. The non-interacting basis is given by monomials

$$\mathcal{M}_\lambda(z_1, \dots, z_N) = \mathrm{Per}(z_i^{\lambda_j}) / \prod_m n_m(\lambda)!, \tag{6.56}$$

where λ_j is the momentum index of the j-th particle in the partition λ and Per is the permanent. It was shown [25] that the N-particle bosonic Read-Rezayi k series of states (which includes the Laughlin and MR state) are a special class of symmetric polynomials. Specifically, this class is called the $r = 2$ single *Jack* polynomials $J_\lambda^\alpha(z_1, \dots, z_N)$ of parameter $\alpha = -\frac{k+1}{r-1}$ and root partition $\lambda = [k0^{r-1}k \dots k0^{r-1}k]$. The Jack wave functions can be related to conformal field theories with extended symmetry WA_{k-1}.

nbr particles	full dim.	squeezed dim.
4	18	16
5	73	59
6	338	247
7	1656	1111
8	8512	5302
9	45207	26376
10	246448	135670
11	1371535	716542
12	7764392	3868142
13	44585180	21265884
14	259140928	118741369
15	1521967986	671906876
16	9020077206	3846342253
17	53885028921	22243294360

Table 6.1: Size of the monomial basis for the bosonic Laughlin state $\nu = 1/2$ up to $N = 17$ particles. The second column is the complete size. The third column is the number of partitions allowed by the squeezing operation from the root partition $1010101\ldots0101$.

Jacks are eigenstates of the Laplace Beltrami (LB) operator [111]:

$$\mathcal{H}_{\mathrm{LB}} = \sum_i \left(z_i \frac{\partial}{\partial z_i} \right)^2 + \frac{1}{\alpha} \sum_{i<j} \frac{z_i + z_j}{z_i - z_j} \left(z_i \frac{\partial}{\partial z_i} - z_j \frac{\partial}{\partial z_j} \right). \tag{6.57}$$

In particular, as stated above, some of them are found to correspond to bosonic FQH trial states for the ground state of the quantum Hall problem in the lowest LL.

We expand the Jacks into the monomial basis :

$$J_\lambda^\alpha = \sum_{\kappa \leq \lambda} c_{\lambda\kappa}(\alpha) \mathcal{M}_\kappa, \tag{6.58}$$

where κ runs over all monomial partitions squeezed from the root partition λ. There is a known recurrence relation for the expansion coefficients $c_{\lambda\kappa}(\alpha)$ [111]:

$$c_{\lambda\kappa}(\alpha) = \frac{2/\alpha}{\rho_\lambda(\alpha) - \rho_\kappa(\alpha)} \sum_{\kappa < \mu \leq \lambda} \left((l_i + t) - (l_j - t) \right) c_{\mu\kappa}(\alpha), \tag{6.59}$$

where $\kappa = [l_1, \ldots, l_i, \ldots, l_j, \ldots]$ and $\mu = [l_1, \ldots, l_i + t, \ldots, l_j - t, \ldots]$ denote partitions. We arrange the momentum orbitals denoted above in decreasing order from left to right, i.e. $l_1 \geq l_2 \geq l_i \geq l_j \ldots$ in κ, and a possible rearrangement occurs in μ depending on t. All partitions μ are understood to be reordered in this way. The sum in (6.59) extends over all partitions μ strictly dominating κ but being dominated (squeezed from) or equal to λ that can be generated by unsqueezing (i.e. the inverse operation to squeezing). The ρ's are defined as:

$$\rho_\lambda(\alpha) = \sum_i \lambda_i \left(\lambda_i - 1 - \frac{2}{\alpha}(i-1) \right). \tag{6.60}$$

This recurrence relation is extremely useful numerically, because it allows for exact computations of bosonic trial wavefunctions without the need of exact diagonalization methods. This recurrence relation was recently extended to polarized fermionic states by Bernevig and Regnault [112]. This derivation is described in the next section.

6.4.2 Polarized fermionic states

Similar to the bosonic case in Sec. 6.4.1, we start with single particle orbitals of the lowest Landau level in equation (6.52) . However, for the many-body state, we now assume that the particles described by the first quantized wave functions obey fermionic statistics. As a consequence, the non-interacting free fermion basis is given by Slater determinant states:

$$\text{sl}_\lambda = \mathcal{A}_z(z_1^{\lambda_1} z_2^{\lambda_2} \dots z_N^{\lambda_N}) = \text{Det}(z_i^{\lambda_j}),\tag{6.61}$$

where sl_λ is the unnormalized orthogonal Slater determinant and $\mathcal{A}$ denotes the anti-symmetrization over all z coordinates. Different normalizations can be applied to put the polynomial wave function on different manifolds such as the plane or the sphere. As in the bosonic case, we describe the free many body states by partitions (or occupation numbers). We again assume the partition $\lambda = [\lambda_1, \dots, \lambda_N]$ to be ordered by decreasing order in angular momentum λ_i of the ith particle. As before, the squeezing operation shifts two particles inwards (towards each other) in the partition. For fermions, multiple occupancy is forbidden due to the Pauli principle.

In first quantized notation, bosonic and fermionic trial states can be transformed into each other by multiplication with a Vandermonde determinant. In terms of single particle coordinates, this polynomial is the Jastrow factor, which is the antisymmetric homogeneous polynomial of degree 1. Starting from a Jack polynomial J_λ^α, the transformation reads

$$J_\lambda^\alpha \to S_\lambda^\alpha := J_\lambda^\alpha \prod_{i<j}(z_i - z_j).\tag{6.62}$$

The S_λ^α polynomials are the exact fermionic analogue of the bosonic (Jack) trial state J_λ^α. For example, the $\nu = 1/2$ bosonic Laughlin state (Jack of $(k, r) = (1, 2)$) becomes the $\nu = 1/3$ fermionic Laughlin state. The filling always changes from bosonic filling $\nu = p/q$ to fermionic filling $\nu = p/(p+q)$. However, in second quantized notation, multiplication by the Vandermonde determinant does not transform a single monomial to a single Slater. To obtain a one-to-one correspondence between a bosonic basis and fermionic Slaters, one would first have to transform the monomials to Schur functions.

We define the decomposition of the S_λ^α polynomials into Slaters:

$$S_\lambda^\alpha(z_1, \dots, z_N) = J_{\lambda_B}^\alpha \prod_{i<j}^N (z_i - z_j) = \sum_{\mu \leq \lambda} b_{\lambda\mu}\text{sl}_\mu.\tag{6.63}$$

To avoid confusion, λ_B denotes the bosonic root partition and λ the associated fermionic root partition. All partitions μ are squeezed from the fermionic partition λ that is related to the bosonic partition by $\lambda_i = \lambda_i^B + (N - i)$. We now use that the Jack part of S_λ^α is an eigenstate of the LB operator, i.e. $\mathcal{H}_{\text{LB}} J_{\lambda_B}^\alpha = E_{\lambda_B}(\alpha) J_{\lambda_B}^\alpha$. We then relate the derivatives

acting on $J_{\lambda_B}^\alpha$ to derivatives on S_λ^α:

$$
\begin{aligned}
E_{\lambda_B}(\alpha) S_\lambda^\alpha &= \prod_{k<l}(z_k - z_l)\left[\sum_i\left(z_i\frac{\partial}{\partial z_i}\right)^2 + \frac{1}{\alpha}\sum_{i<j}\frac{z_i+z_j}{z_i-z_j}\left(z_i\frac{\partial}{\partial z_i} - z_j\frac{\partial}{\partial z_j}\right)\right]J_{\lambda_B}^\alpha \\
&= \left[\sum_i\left(z_i\frac{\partial}{\partial z_i}\right)^2 - 2\sum_{\substack{i,m \\ m\neq i}}\frac{z_i}{z_i-z_m}z_i\frac{\partial}{\partial z_i} + \frac{1}{\alpha}\sum_{i<j}\frac{z_i+z_j}{z_i-z_j}\left(z_i\frac{\partial}{\partial z_i} - z_j\frac{\partial}{\partial z_j}\right)\right]S_\lambda^\alpha \\
&\quad + \left[\sum_{\substack{i,m \\ i\neq m}}\frac{z_i(z_i+z_m)}{(z_i-z_m)^2} + \sum_{\substack{i,m,n \\ i\neq m\neq n}}\frac{z_i^2}{(z_i-z_m)(z_i-z_n)} + \right. \\
&\quad \left. + \frac{1}{\alpha}\sum_{i<j}\frac{z_i+z_j}{z_i-z_j}\left(\sum_{m\neq i}\frac{z_i}{z_i-z_m} - \sum_{m\neq j}\frac{z_j}{z_j-z_m}\right)\right]S_\lambda^\alpha.
\end{aligned}
\tag{6.64}
$$

Simplifying several polynomial sums that yield constants, we can define a fermionic Laplace Beltrami operator that diagonalizes S_λ^α, i.e.

$$
\mathcal{H}_{\text{LB}}^{\text{F}}(\alpha)S_\lambda^\alpha(z_1,\ldots,z_N) = E_\lambda(\alpha)S_\lambda^\alpha(z_1,\ldots,z_N),
\tag{6.65}
$$

with

$$
E_\lambda(\alpha) = \sum_i \lambda_i\left(\lambda_i - 2\left(\frac{1}{\alpha}-1\right)i\right) + \left(\frac{1}{\alpha}-1\right)\left((N+1)\sum_i\lambda_i - N(N-1)\right),
\tag{6.66}
$$

$$
\begin{aligned}
\mathcal{H}_{\text{LB}}^{\text{F}}(\alpha) &= H_K + \frac{1}{2}\left(\frac{1}{\alpha}-1\right)H_I = \sum_i\left(z_i\frac{\partial}{\partial z_i}\right)^2 + \\
&\quad + \frac{1}{2}\left(\frac{1}{\alpha}-1\right)\left[\sum_{i\neq j}\frac{z_i+z_j}{z_i-z_j}\left(z_i\frac{\partial}{\partial z_i} - z_j\frac{\partial}{\partial z_j}\right) - 2\frac{z_i^2+z_j^2}{(z_i-z_j)^2}\right].
\end{aligned}
\tag{6.67}
$$

We now diagonalize the above operator in the basis of Slater determinants. The action of the kinetic part yields $\sum_i H_K\text{sl}_\mu = (\sum_i \mu_i^2)\text{sl}_\mu$, where the μ_i denotes the polynomial power of the ith particle in the partition. The action of the interaction part H_I is non-diagonal in Slater determinant basis and demands further calculation. First we realize that, due to its two-body nature, the action of H_I on any Slater determinant decomposes into the sum of two-particle interaction terms. It is thus sufficient to look at the action on the two-particle Slater determinant

$$
\text{sl}_{\mu=(\mu_1,\mu_2)} = z_1^{\mu_1}z_2^{\mu_2} - z_2^{\mu_1}z_1^{\mu_2}.
\tag{6.68}
$$

Assume $\mu_1 > \mu_2$, and define $p = \mu_1 - \mu_2$:

$$
\begin{aligned}
\frac{H_I \mathrm{sl}_{(\mu_1,\mu_2)}}{z_1^{\mu_2} z_2^{\mu_2}} &= p \frac{z_1 + z_2}{z_1 - z_2}(z_1^p + z_2^p) - 2\frac{z_1^2 + z_2^2}{(z_1 - z_2)^2}(z_1^p - z_2^p) \\
&= \frac{1}{z_1 - z_2}\Big(p(z_1^{p+1} + z_2^{p+1} + z_1^p z_2 + z_2^p z_1) + \\
&\quad - 2\sum_{s=1}^{p/2}\big(z_1^{p-s}z_2^{s+1} + z_2^{p-2}z_1^{s+1} + z_1^{p-s+2}z_2^{s-1} + z_2^{p-s+2}z_1^{s-1}\big)\Big) \\
&= \frac{1}{z_1 - z_2}2\sum_{s=1}^{p/2}\big(z_1^{p-s+2}(z_1^{s-1} - z_2^{s-1}) + z_2^{p-s+2}(z_2^{s-1} - z_1^{s-1}) + z_1^{p-s}z_2(z_1^s - z_2^s) + \\
&\quad + z_2^{p-s}z_1(z_2^s - z_1^s)\big) \\
&= 2\sum_{s=1}^{p/2}(z_1^{p-s+2} - z_2^{p-s+2})\sum_{t=1}^{(s-1)/2}(z_1^{s-t-1}z_2^{t-1} + z_2^{s-t-1}z_1^{t-1}) + \\
&\quad + 2\sum_{s=1}^{p/2}(z_1^{p-s}z_2 - z_2^{p-s}z_1)\sum_{t=1}^{s/2}(z_1^{s-t}z_2^{t-1} + z_2^{s-t}z_1^{t-1})
\end{aligned}
\tag{6.69}
$$

The two terms are already grouped to yield two-particle Slater determinants. Collecting all prefactors, this gives:

$$
H_I \mathrm{sl}_{(\mu_1,\mu_2)} = (\mu_1 - \mu_2 - 2)\mathrm{sl}_{(\mu_1,\mu_2)} + 2\sum_{s=1}^{(\mu_1-\mu_2)/2}(\mu_1 - \mu_2 - 2s)\mathrm{sl}_{(\mu_1-s,\mu_2+s)}.
\tag{6.70}
$$

Eq. (6.70) has a particular form: it only scatters "inwards" the two-particle basis of Slater determinants, i.e. towards decreasing relative momentum of the particles, and thus to a squeezed partition. Let us now look at the total action of $H_{\mathrm{LB}}^{\mathrm{F}}$ on S_λ^α expanded in Slaters. The above scattering Hamiltonian and the linear independence of Slater determinants provide a recurrence relation for the coefficients $b_{\lambda\mu}$ in (6.63). We collect all diagonal terms and invert the sum over s in Eq. (6.70) to a sum over all dominating partitions:

$$
b_{\lambda\mu} = \frac{2(\frac{1}{\alpha} - 1)}{\rho_\lambda^{\mathrm{F}}(\alpha) - \rho_\mu^{\mathrm{F}}(\lambda)} \sum_{\theta;\ \mu < \theta \le \lambda}(\mu_i - \mu_j)b_{\lambda\theta}(-1)^{N_{\mathrm{SW}}},
\tag{6.71}
$$

where $\rho_\lambda^{\mathrm{F}}(\alpha) = \sum_i \lambda_i(\lambda_i + 2i(1 - 1/\alpha))$. Similar to the bosonic recurrence formula in (6.59), the sum in (6.71) extends over all partitions $\theta = [\mu_1, \ldots, \mu_i + s, \ldots, \mu_j - s, \ldots, \mu_N]$ that dominate the partition $\mu = [\mu_1, \ldots, \mu_N]$ and are squeezed from the root partition λ. A new factor $(-1)^{N_{\mathrm{SW}}}$ appears: a sign according to the even/oddness of the number of transpositions (swaps) of particles from a given dominating partition θ back to μ. This term appears since the reordering of the partition in Slater determinant language may cause a minus sign due to the fermionic anticommutation relations. N_{SW} starts from zero for partition μ and advances by one unit every time the momentum of the unsqueezed electron passes through the value of the momentum for another electron. As a further difference from the bosonic Jack recurrence relation, the terms summed in Eq. 6.71 do not explicitly depend on the partition θ. This is because the rescaling of the s in (6.70) exactly cancels the term's dependence on s. For $\alpha = -(k + 1)$, (6.71) gives the coefficients

Occupation Number	Angular Momentum	N=4 Laughlin State
9 8 7 6 5 4 3 2 1 0		$\alpha = -2$
1001001001	=[9,6,3,0] ⟶	$\rho^{\mathrm{F}}_{\lambda=[9,6,3,0]} = 216$
0100110010	=[8,5,4,1] ⟶	$\rho^{\mathrm{F}}_{\mu=[8,5,4,1]} = 208$

unsqueezed partitions θ:

$$\overleftarrow{1000}1100\overrightarrow{01} \qquad b_{\mu\lambda} = \frac{-3}{216-208}\Big[(8-1)b_{[9,5,4,0]}$$

$$\overleftarrow{1000}1\overrightarrow{01010} \qquad\qquad +(8-4)b_{[9,5,3,1]}$$

$$010\overleftarrow{1}010\overrightarrow{01} \qquad\qquad +(5-1)b_{[8,6,4,0]}$$

$$010\overleftarrow{1}00\overrightarrow{1}010 \qquad\qquad +(5-4)b_{[8,6,3,1]}$$

$$01\overleftarrow{1}0000\overrightarrow{1}10 \qquad\qquad +(5-4)b_{[8,7,2,1]}\Big] = -9$$

Figure 6.7: The recurrence relation (6.70) for the $N = 4$ particle $\nu = 1/3$ Laughlin state. The partitions are written in decreasing order of orbital angular momentum, which ranges from 9 to 0 in the case considered. The coefficient of the partition $\mu = 0100110010$ is computed with the knowledge of the coefficient for the partitions dominating μ.

of the fermionic Read-Rezayi states (an example computation of the partition coefficient for the $\nu = 1/3$ Laughlin state is shown in Fig. 6.7).

Devil's staircase phase diagram of the fractional quantum Hall effect in the thin-torus limit and beyond

In this Chapter we present our originial work. The first part is an adaptation of a draft currently under review. The second part is a preliminary result that we obtained recently.

7.1 Devil's staircase phase diagram of the FQHE in the thin-torus limit

The Fractional Quantum Hall Effect (FQHE) [127] is among the most fascinating quantum phenomena involving strongly correlated electrons. It attracts and fuels research in many directions since its discovery [128]. Lately, much interest is directed to quantum Hall states as experimentally accessible prototypes of topological states of matter, which have promising applications for quantum computation [124, 129, 130].

The physics of the FQHE is well-understood phenomenologically thanks to the pioneering work by Laughlin and his celebrated ansatz (LA) for $1/m$ filling fractions [16]. The approach was generalized to more complicated fractions through the introduction of composite fermions [120, 123] and a hierarchy of quasi-particles with fractional statistics [122, 131, 132, 133], or by conformal invariance arguments [25, 109, 110, 134]. A huge amount of results were obtained in the years, confirming the validity of the phenomenological approach [128, 135, 136, 137].

In contrast, a systematic microscopic theory of the FQHE is still lacking, despite the considerable effort. An intrinsic difficulty is the absence of an evident perturbative parameter, a common hindrance in strongly-correlated systems [120]. In 1983 Tao and Thouless (TT) observed [17] that electrons in a strong magnetic field could form a one-dimensional *Wigner crystal* [138] in the lattice of degenerate states in the lowest Landau level (LL), and suggested that this mechanism may explain the fractional quantization of the Hall resistivity. However, the resulting many-body ground state displays long-range spatial correlations, in conflict with Laughlin's results. This route to a microscopic theory of the FQHE was abandoned (by Thouless himself [139]), as the LA offers several advantages, e.g. its high overlap with the exact low-density ground state, and the fact that it constrains very naturally the filling fractions to have odd denominators. The TT framework was recently reconsidered by Bergholtz and co-workers [15, 140, 141]. They found that TT states become the exact wavefunctions of the problem in the quasi one-dimensional (thin-torus) limit (aggiungere anche citazione a bernevig).

Nowadays experiments in ultrahigh mobility 2D electron systems point toward a *Devil's staircase* scenario for the Hall resistivity as a function of the magnetic field: indeed more than fifty filling fractions are observed only in the lowest LL, some of them out both from Laughlin and Jain series.

In this Chapter, we study the thin-torus limit of the quantum Hall Hamiltonian in the lowest LL, and show that it realises a repulsive gas on the reciprocal lattice of degenerate Landau states, with the magnetic field acting as a chemical potential. The zero-temperature statistical mechanics of this class of models was studied extensively [12, 24, 142, 143]. It is characterized by an infinite series of second-order phase transitions, occurring at critical (non-universal) values of the chemical potential μ. The density of particles $\rho(\mu)$ is the *order parameter*, and takes a different rational value in each phase, thus producing a *complete devil's staircase* (a self-similar function with plateaux at rational values) when plotted against μ [12]. There is a revived interest in these models, for potential applications to quantum simulators with ultracold Rydberg gases [11, 13, 144].

Our mapping allows to

1. explicitly write the ground states in the thin torus limit, which take the form of generalized Wigner crystals on the reciprocal lattice;

2. derive a selection rule forbidding odd denominators, using a result derived recently by Seidel [145];

3. interpret the dependence of transverse conductivity as a function of magnetic field as a fractal diagram of phase transitions, peculiar to 1D repulsive lattice gases;

4. provide a theoretical justification of the relative widths of different Hall plateaux.

We consider the standard two-dimensional gas of N_e interacting electrons in a uniform positive background, providing electrical neutrality. We make the assumptions that in strong magnetic fields the mixing between different Landau levels is suppressed, i.e. we work in the regime $e^2/\ell \ll \omega_c$, where $\ell = 1/(eB)^{1/2}$ is the magnetic length and $\omega_c = eB/m$ is the cyclotron frequency ($\hbar = c = 1$) and spin degrees of freedom are frozen in the lowest spin level. We take the system to have area $L_x L_y$ and to be periodic in the y direction, so that the single-particle wave functions may be written in the form

$$\phi_s(x,y) = (\pi^{1/2}\ell L_y)^{-1/2} e^{-\frac{2\pi i s y}{L_y} - \frac{1}{2}\left(\frac{x}{\ell} - \frac{2\pi s \ell}{L_y}\right)^2}, \tag{7.1}$$

with $s = 1, 2, \ldots, N_s = \frac{L_x L_y}{2\pi \ell^2}$. The filling fraction $\nu = N_e/N_s$ is less than one.

In second quantisation the Coulomb interaction between the electrons in the lowest LL is

$$H_c = \sum_{s_1,s_2,s_3=1}^{N_s} V_{s_1-s_3,s_2-s_3} a_{s_1}^\dagger a_{s_2}^\dagger a_{s_1+s_2-s_3} a_{s_3}, \tag{7.2}$$

where $a_s^\dagger$, a_s are fermionic creation and annihilation operators, and momentum conservation in the periodic direction is manifest. The Coulomb matrix element was parametrized

in a useful form by TT [17]:

$$V(s_1 - s_3, s_2 - s_3) = \frac{e^2}{L_y} \int_{-\infty}^{\infty} dq \, \frac{\exp\left[-\frac{\ell^2}{2}\left(q^2 + \frac{4\pi^2(s_1 - s_3)^2}{L_y^2}\right) + \frac{2\pi i q \ell^2 (s_2 - s_3)}{L_y}\right]}{\sqrt{q^2 + \frac{4\pi^2(s_1 - s_3)^2}{L_y^2}}}. \tag{7.3}$$

A possible way to obtain it is to consider periodic boundary conditions in both directions (torus geometry) [146, 147] and to take the continuum limit in the x direction.

The starting point of our analysis is the observation that this matrix element can be evaluated exactly in the thin-torusl limit $\ell/L_x \gg 1$, via the saddle-point approximation. The calculation, detailed below, shows that the matrix element, when it is non zero, is $V_{s_1 - s_3, s_2 - s_3} = e^2/\ell \, W_{s_1 - s_3}$, for all $s_2 - s_3$ (with $W_{s_1 - s_3}$ positive).

7.1.1 Coulomb matrix element and the thin torus limit

The earliest numerical calculations of the ground state for FQHE including Coulomb interactions for various filling fractions were done by Yoshioka et al. [146, 147]. Here we provide the details of their evaluation of eq.(7.6) The geometry is that of a periodic array of rectangles with sides L_x and L_y and area $L_x L_y = 2\pi \ell^2 N_s$, where N_s is a natural number; ω is the rectangle $[0, L_x] \times [0, L_y]$. From the N_s degenerate LLL eigenstates with centers in ω

$$\psi_s(\mathbf{r}) = \frac{1}{\sqrt{L_y}} \frac{1}{\pi^{\frac{1}{4}}\sqrt{\ell}} \exp\left[-\frac{1}{2}\left(\frac{x}{\ell} - \frac{2\pi\ell}{L_y}s\right)^2 - i\frac{2\pi}{L_y}sy\right], \quad 0 \le s \le N_s - 1 \tag{7.4}$$

one constructs a basis of orthonormal quasi-periodic eigenstates:

$$\theta_s(\mathbf{r}) = \sum_{m \in \mathbb{Z}} \psi_{s + m N_s}(\mathbf{r}) \tag{7.5}$$

An electron in ω interacts with electrons in ω as well as with their copies. The Coulomb interaction depends on $\mathbf{r} = \mathbf{r_1} - \mathbf{r_2}$ and is a periodic function of the lattice;

$$v(\mathbf{r}) = \sum_{\mathbf{m} \in \mathbb{Z}^2} \frac{e^2}{\sqrt{(x + m_x L_x)^2 + (y + m_y L_y)^2}}$$

It has Fourier expansion $v(\mathbf{r}) = \frac{1}{L_x L_y} \sum_{\mathbf{q}} v(\mathbf{q}) e^{i\mathbf{q} \cdot \mathbf{r}}$ where $q_x = \frac{2\pi}{L_x} n_x$ and $q_y = \frac{2\pi}{L_y} n_y$ and $v(\mathbf{q}) = \int_\omega d\mathbf{r} \, v(\mathbf{r}) e^{-i\mathbf{q} \cdot \mathbf{r}} = \frac{2\pi e^2}{|\mathbf{q}|}$. In the Fourier representation the integrals for Coulomb matrix elements factorise:

$$\langle s_1, s_2 | v | s_3, s_4 \rangle = \iint_{\omega^2} d\mathbf{r}_1 d\mathbf{r}_2 \, \overline{\theta_{s_1}(\mathbf{r}_1)} \, \overline{\theta_{s_2}(\mathbf{r}_2)} v(\mathbf{r}_1 - \mathbf{r}_2) \theta_{s_3}(\mathbf{r}_1) \, \theta_{s_4}(\mathbf{r}_2)$$

$$= \frac{1}{L_x L_y} \sum_{\mathbf{q}} v(\mathbf{q}) I_{1,3}(\mathbf{q}) I_{2,4}(-\mathbf{q})$$

The integral I is independent of the potential, and is now evaluated:

$$I_{s,s'}(\mathbf{q}) = \int_\omega d\mathbf{r} \, \overline{\theta_s(\mathbf{r})} \theta_{s'}(\mathbf{r}) \exp(i\mathbf{q} \cdot \mathbf{r}) = e^{-\frac{1}{4}|\mathbf{q}|^2 \ell^2 + iq_x \frac{\pi \ell^2}{L_y}(s+s')} \delta'_{s - s' + n_y, 0}$$

where δ' means *equality modulo* N_s.

Proof. The integral in y is straightforward:

$$I_{s,s'}(\mathbf{q}) = \sum_{mm'} \delta_{s-s'+(m-m')N_s+n_y,0} \int_0^{L_x} \frac{dx}{\ell\sqrt{\pi}} e^{-\frac{1}{2}\left[\frac{x-mL_x}{\ell}-\frac{2\pi\ell}{L_y}s\right]^2 - \frac{1}{2}\left[\frac{x-m'L_x}{\ell}-\frac{2\pi\ell}{L_y}s'\right]^2 + iq_x x}$$

$$= e^{-\frac{1}{4}|\mathbf{q}|^2\ell^2 + iq_x\frac{\pi\ell^2}{L_y}(s+s')} \sum_{mm'} \delta_{s-s'+(m-m')N_s+n_y,0} \int_0^{L_x} \frac{dx}{\ell\sqrt{\pi}} e^{-\left[\frac{x-\frac{1}{2}(m+m')L_x}{\ell}-\frac{\pi\ell}{L_y}(s+s')-\frac{i}{2}q_x\ell\right]^2}$$

The double sum involves $m + m' = \mu$ and $m - m' = \nu$, and $\sum_{m,m'} f(m+m', m-m') = \sum_{\mu,\nu} f(2\mu, 2\nu) + f(2\mu+1, 2\nu+1)$. Therefore:

$$I_{s,s'}(\mathbf{q}) = e^{-\frac{1}{4}|\mathbf{q}|^2\ell^2 + iq_x\frac{\pi\ell^2}{L_y}(s+s')} \sum_{\mu,\nu} \left[\delta_{s-s'+2\nu N_s+n_y,0} \int_0^{L_x} \frac{dx}{\ell\sqrt{\pi}} e^{-\left[\frac{x-\mu L_x}{\ell}-\frac{\pi\ell}{L_y}(s+s')-\frac{i}{2}q_x\ell\right]^2} \right.$$

$$\left. + \delta_{s-s'+(2\nu+1)N_s+n_y,0} \int_0^{L_x} \frac{dx}{\ell\sqrt{\pi}} e^{-\left[\frac{x-\mu L_x}{\ell}-\frac{L_x}{2\ell}-\frac{\pi\ell}{L_y}(s+s')-\frac{i}{2}q_x\ell\right]^2} \right]$$

The sum on ν produces a Gaussian integral on $\mathbb{R}$. The two integrals have the same value. The final result is obtained. $\square$

The matrix element is:

$$\langle s_1, s_2 | v | s_3, s_4 \rangle = \frac{1}{L_x L_y} \sum_{\mathbf{q}} \frac{2\pi e^2}{|\mathbf{q}|} e^{-\frac{1}{2}|\mathbf{q}|^2\ell^2 + iq_x\frac{\pi\ell^2}{L_y}(s_1+s_3-s_2-s_4)} \delta'_{s_1-s_3+n_y,0}\delta'_{s_2-s_4-n_y,0}$$

The two constraints imply momentum conservation: $s_1 + s_2 = s_3 + s_4$. Eq. (2.9) in Yoshioka's paper [147] is obtained:

$$\langle s_1, s_2 | v | s_3, s_4 \rangle = \frac{\delta_{s_1+s_2,s_3+s_4}}{L_x L_y} \sum_{\mathbf{q}} \frac{2\pi e^2}{|\mathbf{q}|} e^{-\frac{\ell^2}{2}q^2 + iq_x\frac{2\pi\ell^2}{L_y}(s_3-s_2)} \delta'_{s_3-s_1, q_y L_y/2\pi} \tag{7.6}$$

It is an exact formula.

From Yoshioka's formula (7.6), the one by Tao-Thouless [17] is now obtained. First use the constraint δ' to sum on q_y:

$$\langle s_1, s_2 | v | s_3, s_4 \rangle$$

$$= 2\pi e^2 \frac{\delta_{s_1+s_2,s_3+s_4}}{L_x L_y} \sum_{q_x} e^{-\frac{\ell^2}{2}q_x^2 + iq_x\frac{2\pi\ell^2}{L_y}(s_3-s_2)} \sum_{m=-\infty}^{\infty} \frac{e^{-\frac{\ell^2}{2}\frac{4\pi^2}{L_y^2}(s_3-s_1+mN_s)^2}}{\sqrt{q_x^2 + \frac{4\pi^2}{L_y^2}(s_3-s_1+mN_s)^2}}$$

Approximate the sum on q_x by an integral ($\sum_{q_x} \approx \frac{L_x}{2\pi} \int dq_x$):

$$= e^2 \frac{\delta_{s_1+s_2,s_3+s_4}}{L_y} \int_{-\infty}^{\infty} dq\, e^{-\frac{\ell^2}{2}q^2 + iq\frac{2\pi\ell^2}{L_y}(s_3-s_2)} \sum_{m=-\infty}^{\infty} \frac{e^{-\frac{2\pi^2\ell^2}{L_y^2}(s_3-s_1+mN_s)^2}}{\sqrt{q^2 + \frac{4\pi^2}{L_y^2}(s_3-s_1+mN_s)^2}}$$

Neglect terms $m \neq 0$ because of the exp factor. Eq.(3) in Tao and Thouless, [17] is obtained:

$$V = \langle s_1, s_2 | v | s_3, s_4 \rangle = \frac{e^2}{L_y} \delta_{s_1+s_2,s_3+s_4} e^{-\frac{2\pi^2\ell^2}{L_y^2}(s_3-s_1)^2} \int_{-\infty}^{\infty} dq\, \frac{e^{-\frac{\ell^2}{2}q^2 + iq\frac{2\pi\ell^2}{L_y}(s_3-s_2)}}{\sqrt{q^2 + \frac{4\pi^2}{L_y^2}(s_3-s_1)^2}}$$

We notice that the Tao-Thouless formula is indipendent from $s_2 - s_3$ in the thin torus limit $L_x/\ell \ll 1$. However, because of this special limit is safer to analyze the exact Yoshioka formula (7.6).

$$\langle s_1, s_2 | v | s_3, s_4 \rangle = \frac{e^2}{L_y} \sum_{m, n_x} e^{-\frac{\ell^2}{2} \frac{4\pi^2}{L_x^2} n_x^2 + i \frac{2\pi n_x}{L_x} \frac{2\pi \ell^2}{L_y} s_{23}} \frac{e^{-\frac{\ell^2}{2} \frac{4\pi^2}{L_y^2}(s_{13} + mN_s)^2}}{\sqrt{n_x^2 + \frac{L_x^2}{L_y^2}(s_{13} + mN_s)^2}}$$

$$= \frac{2e^2}{L_y} \int_0^\infty \frac{du}{\sqrt{\pi}} \sum_{m=-\infty}^\infty e^{-(\frac{2\pi^2 \ell^2}{L_y^2} + u^2 \frac{L_x^2}{L_y^2})(s_{13} + mN_s)^2} \sum_{n=-\infty}^\infty e^{-(u^2 + \frac{2\pi \ell^2}{L_x^2})n^2 + i2\pi nb}$$

$$= \frac{2e^2}{L_y} \int_0^\infty \frac{du}{\sqrt{\pi}} \sum_{m=-\infty}^\infty e^{-(u^2 + \frac{\pi^2}{N})\frac{N^2}{\pi^2}(a+m)^2} \vartheta_3(\pi b, e^{-u^2 - \frac{\pi^2}{N}}),$$

where $N = L_x^2/2\ell^2$, $a = s_{13}/N_s$ and $b = s_{23}/N_s$. Here we use eq. 20.13.4 of NIST:

$$\sum_m e^{-(m + \frac{z}{\pi})^2 \pi \beta} = \frac{1}{\sqrt{\beta}} \vartheta_3(z, e^{-\frac{\pi}{\beta}})$$

$$\langle s_1 s_2 | v | s_3 s_4 \rangle = \frac{2e^2}{L_x N_s} \int_0^\infty \frac{du}{\sqrt{u^2 + \frac{\pi^2}{N}}} \vartheta_3(\pi a, e^{-\frac{\pi^4}{N^2} \frac{1}{u^2 + \frac{\pi^2}{N}}}) \vartheta_3(\pi b, e^{-u^2 - \frac{\pi^2}{N}})$$

This is an exact expression of the Yoshioka integral, where:

$$\vartheta_3(z, q) = \sum_{n=-\infty}^\infty q^{n^2} e^{i2nz} = 1 + 2 \sum_{n>1} q^{n^2} \cos(2nz)$$

The change $u = \frac{\pi}{\sqrt{N}} t$ gives:

$$\langle s_1 s_2 | v | s_3 s_4 \rangle = \frac{2e^2}{L_x N_s} \int_0^\infty \frac{dt}{\sqrt{t^2 + 1}} \vartheta_3(\pi a, e^{-\frac{\pi^2}{N} \frac{1}{t^2 + 1}}) \vartheta_3(\pi b, e^{-\frac{\pi^2}{N}(t^2 + 1)}) \qquad (7.7)$$

We change variable $t^2 + 1 \to 1/t$ and introduce the notation $q = \exp(i\pi\tau)$, $\vartheta_3(z, q) = \vartheta_3(z|\tau)$.

$$\langle s_1 s_2 | v | s_3 s_4 \rangle = \frac{e^2}{L_y} \frac{\pi}{N} \int_0^1 \frac{dt}{t\sqrt{1-t}} \vartheta_3(\pi a | i \frac{\pi}{N} t) \vartheta_3(\pi b | i \frac{\pi}{N} \frac{1}{t}) \qquad (7.8)$$

1)One checks that if $N \ll 1$ (our thin torus limit) then the matrix elements $0 < b < 1$ collapse to that with $b = 0$.

2) the matrix element is periodic in $a \in [0, 1]$ with minimum at $a = 0.5$.

The function with $b = 0$ is periodic in $a \in [1/2, -1/2]$:

$$\langle s', s | v | s, s' \rangle = \sum_{k \in \mathbb{Z}} e^{i2\pi ka} F(k)$$

$$F(k) = \frac{e^2}{L_y} \frac{\pi}{N} \int_0^1 dt \, \frac{1}{t\sqrt{1-t}} \vartheta_3 \left(0 \Big| i\frac{\pi}{N}\frac{1}{t}\right) \int_{1/2}^{1/2} da \, \vartheta_3 \left(\pi a \Big| i\frac{\pi}{N}t\right) \cos(2\pi ka)$$

$$= \frac{e^2}{L_y} \frac{\pi}{N} \int_0^1 dt \, \frac{1}{t\sqrt{1-t}} \vartheta_3 \left(0, e^{-\frac{\pi^2}{N}\frac{1}{t}}\right) e^{-\frac{\pi^2}{N}k^2 t}$$

In the thin torus limit $N \ll 1$ it is numerically checked that $\vartheta_3(0, e^{-\frac{\pi^2}{N}\frac{1}{t}}) \approx \sqrt{x\pi/N}$. Then

$$F(k) \approx \frac{e^2}{L_y} \frac{\pi^{3/2}}{N^{3/2}} \int_0^1 dt \, \frac{1}{\sqrt{t(1-t)}} e^{-(\pi^2/N)k^2 t}$$

$$= \frac{e^2}{L_y} \frac{\pi^{3/2}}{N^{3/2}} 2 \int_0^{\pi/2} d\theta \, e^{-(\pi^2/N)k^2 \cos^2\theta}$$

$$= \frac{e^2}{L_y} \frac{\pi^{3/2}}{N^{3/2}} 2 \int_0^{\pi/2} d\theta \, e^{-\frac{\pi^2 k^2}{2N}(1+\cos 2\theta)} = \frac{e^2}{L_y} \frac{\pi^{3/2}}{N^{3/2}} e^{-\frac{\pi^2 k^2}{2N}} \int_0^{\pi} d\theta \, e^{-\frac{\pi^2 k^2}{2N}\cos\theta}$$

$$= \frac{e^2}{L_y} \frac{\pi^{3/2}}{N^{3/2}} e^{-\frac{\pi^2 k^2}{2N}} \pi I_0\left(\frac{\pi^2 k^2}{2N}\right)$$

This function goes to zero as long as $k \to \infty$ and moreover is convex. Thus fulfills the requirements of the one dimensional repulsive lattice gas of the previous chapter.

7.1.2 Incompressibility of the ground states in the thin torus limit and phase diagram

By plugging this result into the Coulomb Hamiltonian we obtain

$$H_c = \frac{e^2}{\ell} \sum_{s_1, s_2, s} W_s \, a^\dagger_{s_1+s} a^\dagger_{s_2-s} a_{s_2} a_{s_1} . \tag{7.9}$$

In the grand-canonical ensemble, the total Hamiltonian is the sum of the Coulomb term, the constant kinetic term and a term with chemical potential $\tilde{\mu}$:

$$H_{LLL} = -\mu(B) \sum_{s=1}^{N_s} n_s + \frac{e^2}{\ell} \sum_{s_1, s_2, s} W_s a^\dagger_{s_1+s} a^\dagger_{s_2-s} a_{s_2} a_{s_1} , \tag{7.10}$$

where the definition $\mu(B) = (\tilde{\mu} - \omega_c)$ highlights the dependence of the effective chemical potential on the magnetic field. Electrons in the lowest LL form a one dimensional lattice (that in the following we will call *target space*). Importantly, they interact through a translational invariant interaction (in the target space). The Hamiltonian is diagonalized in the Fourier basis, where the creation operator for the mode k is $c^\dagger_k = 1/\sqrt{N_s} \sum_{s=1}^{N_s} e^{-\frac{2\pi i k s}{N_s}} a^\dagger_s$. We obtain the following diagonal Hamiltonian with periodic boundary conditions:

$$H_{LLL} = -\mu(B) \sum_{k=1}^{N_s} n_k + \frac{e^2}{\ell} \sum_{k_1 \neq k_2} \tilde{W}(|k_1 - k_2|) n_{k_1} n_{k_2} , \tag{7.11}$$

with $n_k = c^\dagger_k c_k$ and $\tilde{W}(k) = \sum_{s=1}^{N_s} e^{\frac{2\pi i k s}{N_s}} W(s)$ a repulsive potential. The explicit form of $\tilde{W}(k)$ is given in written in the previous section; it decays as $L_x/(\ell k)$ for large k.

This form of the Hamiltonian realises a mapping (in the thin torus limit $L_x/\ell \ll 1$) of the FQHE on a one-dimensional lattice gas with repulsive interactions, whose degrees of freedom are the Fourier modes of the target space. As noted above, in these models the density as a function of the chemical potential exhibits a complete devil's staircase structure. Inspection of the Hamiltonian (7.11) shows that the role of the density is played by the filling fraction ν, whereas the chemical potential can be tuned by the magnetic field B.

Schematically, the investigation of this class of models follows two steps: i) The ground state of the system is sought at fixed $\nu = p/q$ (p and q coprime); this problem was solved by Hubbard [23]. ii) The stability region $\Delta\mu$ (under single particle/hole exchange) of each ground state is determined; this was done by Bak and Bruinsma [12], and by Burkov and Sinai [24]. Both steps are subject to the technical condition that the potential be convex; we make this hypothesis, and reproduce this two-step construction in the following.

Intuitively, the ground state of a repulsive lattice gas at fixed filling fraction $\nu = p/q$ is a configuration where particles are placed as far as possible from each other. The underlying lattice structure introduces the possibility of frustration, exhibited by deviations from the continuum equilibrium positions. The pattern of displacements can be obtained through the continued-fraction expansion of $\nu = p/q$:

$$\frac{p}{q} = \cfrac{1}{n_0 + \cfrac{1}{n_1 + \cfrac{1}{\ddots + \cfrac{1}{n_\lambda}}}} \tag{7.12}$$

Each level in the expansion realises a better approximation of ν; for rational ν the number of levels $\lambda + 1$ is finite. At $\lambda = 0$ (i.e. $p = 1$), the ground state is a periodic crystal with inter-particle distance $n_0 = q$, corresponding to Laughlin-type states. At $\lambda = 1$ the inter-particle distances can not be all equal, and a "defect" appears: the periodic ground state is formed by $(n_1 - 1)$ Laughlin-type blocks of density $1/n_0$ and one block with density $1/(n_0 + 1)$; these correspond to Jain-type states (a concise representation is $(n_0)^{n_1-1}(n_0 + 1)$). This construction can be generalized iteratively to the level λ (see Fig. 7.1 for three examples, and the SM): the general rule uses the ground states at one level as building blocks to construct the ground states at the next level. The position of the j-th particle in the $\nu = p/q$ ground state can be expressed compactly as $\lfloor q/pj \rfloor$, where $\lfloor \cdot \rfloor$ denotes the integer part. (We notice *en passant* the connection with the sequences of characters known as *Sturmian words*.)

Due to the periodic boundary conditions, the ground state at filling factor $\nu = p/q$ has a q-fold degeneracy, corresponding to the possible translations in the reciprocal target space. This plays an important role when quantum effects are taken into account (see below). Summing up the foregoing observations, a compact form of our wave functions

ν	C_ν	Configuration
$\frac{1}{3}$	(3)	● ○ ○ ● ○ ○ ● ○ ○ ● ○ ○ ● ⋯
$\frac{3}{7}$	(322)	● ○ ○ ● ○ ● ○ ● ○ ○ ● ○ ● ⋯
$\frac{5}{13}$	$(32)^2(3)$	● ○ ○ ● ○ ● ○ ○ ● ○ ● ○ ○ ⋯

Figure 7.1: Hubbard ground states for different filling fractions ν and their explicit periodic structure. The first two from the top belong respectively to Laughlin ($\nu = 1/3$) and Jain ($\nu = 3/7$) series. Each periodic configuration may be expressed in a compact way through the sequence C_ν of its interparticle distances. (The general algorithm to construct Hubbard ground states is extensively reviewed in Chapter 5.)

is the following:

$$|\nu = p/q\rangle_r = \prod_{j=1}^{\lfloor pN_s/q \rfloor} c_{\lfloor qj/p \rfloor + r}^\dagger |0\rangle \quad r = 0, \cdots, q - 1. \tag{7.13}$$

Once the ground states at general ν have been determined, their stability under single particle/hole exchange can be established. The stability interval in the effective chemical potential is given by [24]

$$\Delta\mu(p/q) = 2q \sum_{k=1}^{\infty} k \left(\tilde{W}(qk + 1) + \tilde{W}(qk - 1) - 2\tilde{W}(qk) \right). \tag{7.14}$$

As $\Delta\mu(\nu) > 0$ for all rational filling fractions, this construction yields a phase diagram where each rational ν appears as the stable density for a finite interval of μ (hence of B), thus realizing a complete devil's staircase. It is worth remarking that the precise form of the potential does not affect qualitatively this structure. However, filling fractions with even denominators are not seen in the experiments. This important issue can be elucidated in our microscopic framework by symmetry considerations. It is well known that the quantum Hall system enjoys a peculiar symmetry: the *magnetic* translational group [148]. Its explicit form in the Landau gauge is $T_M(X, Y) = e^{iXy/\ell^2} e^{iXp_x + iYp_y}$. Seidel showed recently [145] that periodic one dimensional patterns are strongly constrained by this symmetry. In particular if the representation of the magnetic group is fermionic, only gapped odd denominators survive. The argument depends on an assumption about the modular invariance of the representation of the quantum group on the ground states.

The results reported above allow to plot a snapshot of the relation between magnetic field and inverse filling fraction, by using the stability formula (7.14) and discarding all even denominators (under the assumption that the admissible even-denominator ground states are gapless). The potential $\tilde{W}$ has a non trivial dependence on the magnetic length ℓ. As noted above, it decays algebraically as $1/(\ell k)$. To obtain a large distance ℓ-independent behaviour, the chemical potential needs to be rescaled as $\mu \to \mu\ell^2$, which is equivalent to a rescaling of the entire Hamiltonian, $H \to H\ell^2$. Operatively, we
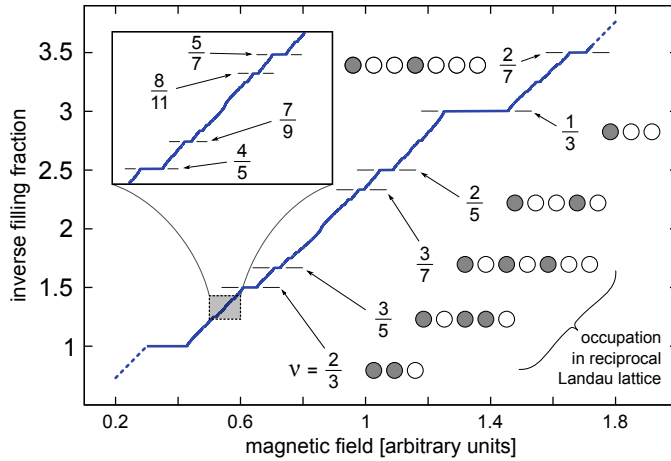
Figure 7.2: Inverse filling fraction $1/\nu$ plotted against the magnetic field B (in arbitrary units). The most visible plateaux are highlighted with their corresponding occupational periodic pattern in the reciprocal target space. This snapshot shows a qualitative agreement with the experimental measures of Hall resistivity, both for the relative widths of the plateaux and for the quasi linear trend of the landscape as a function of B. In the inset, a portion of the staircase is magnified and some experimentally-observed plateaux (some of them only in the longitudinal resistance [119]) are pointed out.

set a cutoff q_{max} on the possible denominators, we list (in increasing order) all filling fractions p/q such that q is odd, $q \leq q_{max}$, and $p = 1, \ldots, q$, and we compute $\Delta\mu$ for each one of them. Doing this by increasing order allows to obtain iteratively the two stability boundaries μ_- and μ_+ for each plateau; the corresponding values of the magnetic field B_- and B_+ can then be calculated from the relation $\mu = -\tilde{\mu}/(eB) - 1/m$. The resulting landscape, presented in Fig. 7.2, is qualitatively in accord with the well-known behavior obtained in experiments. Notice that Eq. (7.14) implies that the width (in μ) of a plateau only depends on the denominator. However, the non linear dependence of B on μ "deforms" the staircase; this has the effect of enhancing the stability of low density plateaux. The most evident example can be recognized in the asymmetry between the filling fractions $\nu = 1/3$ and $\nu = 2/3$. Moreover, our microscopic approach captures the quasi linear trend of the FQHE landscape.

In statistical mechanics systems with slowly decaying potentials are rather pathological: their free energy is not extensive as a function of the particle number. In our map, this has the effect to push the devil's staircase toward infinity as the cutoff q_{max} is increased. This issue may be overcome by regularizing the Coulomb potential. The thin torus analysis is largely independent from the precise form of the potential.

The continued-fraction expansion that we employ to construct the ground states naturally provides a definition of "fractality" of a given filling fraction, via its level λ. We remark that this construction has a natural interpretation in terms of quasi particles [149], that we do not further pursue here.

Inspired by these results in the thin torus limit, we investigate, in the following sec-

tion, the connection between the Laughlin wavefunction and the Tao-Thouless states. In order to understand this relationship, we need to know the coefficients of the Slater decomposition of the Laughlin functions. Despite the numerous symmetries of this expansion, this was considered an intractable problem until a few years ago. However recently, Bernevig and Regnault discovered a remarkable recurrence relation for these coefficients, using known mathematical results for Jack polynomials (these results are summarized in the previous chapter).

Inspired by this breakthrough, we propose a consistent second quantization picture of the Laughlin state. We anticipate the result: Laughlin wavefunction is a *squeezed* Tao-Thouless state. This statement will be more transparent at the end of the next section.

7.2   Second quantization picture of fractional quantum Hall states

Let us briefly summarize the important properties of the Jacks describing fractional quantum Hall states:

1. the Jacks of N variables are labelled by a rational parameter $\alpha = -(k+1)/(r-1)$ and by a partition $\lambda = (\lambda_1, \cdots, \lambda_N)$;

2. the Jacks describing bosonic FQH states are labelled by the special partition $n(\lambda) = (k, 0^{r-1}, k, 0^{r-1}, \cdots)$;

3. polarized fermionic states are Jacks times a Vandermonde determinant and their reference partition is obtained from the bosonic one through the formula: $\lambda_i^F = \lambda_i^B + N - 1$;

4. all the permanents (Slater determinants) in the expansion of bosonic (fermionic) states are *squeezed* inward from the reference partition (see Figure (7.3));

5. a recurrence relation for the coefficients in the permanent (Slater) expansion exists for bosonic (fermionic) states.

Our goal is the following: starting from these properties, we would like to find an explicit formula for FQH states in second quantization. We will consider fermionic wavefunctions, but our proof can be straightforwardly generalized to the bosonic ones.

Our strategy is the following:

1. we propose an ansatz for the generic FQH state in the Fock space and we verify that the coefficients of the expansion in Slater determinants fulfill the recurrence relations discovered by Bernevig and Regnault;

2. we prove that the Slaters in our trial state are the same produced by the repeated single squeezing protocol described in the previous Chapter. This procedure exaustively find out all the possible contributions to a FQH state;

3. we check numerically for $N = 3, 4, 5$ that our state has the same coefficients of Laughlin wavefunction with $\nu = 1/3$.
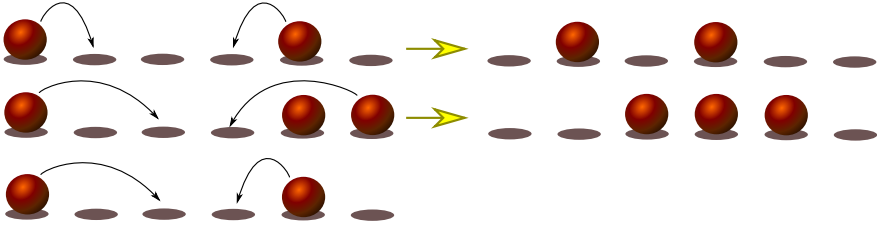
Figure 7.3: Pictorial representation of a squeezing operator. The first two on the top are allowed in the expansion because they are inward squeezing and they conserve total angular momentum. In particular the second one (if the state is fermionic) gets an overall minus sign because of the particle swap. The last squeeze, although is inward, it does not conserve angular momentum, and therefore it is not allowed in the Jacks expansion.

In the derivation we focus on Laughlin wavefunction, but our proof is valid in general for all FQH states in the form Jack times a Vandermonde.

Our approach is based on the following idea (inspired by the properties of the Jacks): we can obtain the Laughlin wavefunction in the Slater basis applying a particular operator to the maximally uniform state (the reference state) in the lowest Landau level. Such a state has the form $|\{1, 0, 0, 1, 0, 0, 1, \cdots\}\rangle$ for $\nu = 1/3$ and more in general for the general Laughlin at $\nu = 1/(2m + 1)$ is the corresponding Tao-Thouless state. This is a free particle state, namely it is a tensor product of eigenstates of the free Hamiltonian in the symmetric gauge:

$$H = \frac{1}{2}\left[\left(-i\frac{\partial}{\partial x} - \frac{y}{2}\right)^2 + \left(-i\frac{\partial}{\partial y} - \frac{x}{2}\right)^2\right].\tag{7.15}$$

If we have N non-interacting particles, each of them is in a state $|m_i\rangle$, so we can represent the full system state as

$$|m_1, m_2, \ldots, m_N\rangle$$

i.e. writing the angular momentum of each particle (in decreasing order). Or we can write (for instance)

$$|0, 0, 1, 0, 0, 1, 0, 1, \ldots\rangle$$

where each number is an angular momentum orbital (or, for brevity, a site), and it is 1 if it is full, 0 otherwise (to fulfill Pauli principle).

Now, let us define the *squeezing operator* as follows:

$$U = \sum_{s=0}^{\infty}\sum_{t=1}^{\infty}\sum_{u=t}^{\infty}(u - t)\, a_{s+t}^{\dagger}\, a_{s+u}^{\dagger}\, a_{s+t+u}\, a_s \,.\tag{7.16}$$

where $a_x^{\dagger}$ and a_x are creator and destructor of a particle in the site x. Its name is immediately justified: except for the weight $u - t$, the operatorial part destroy two particles in sites s and $s + t + u$ and create two particles in sites $s + t$ and $s + u$, i.e. the destructed
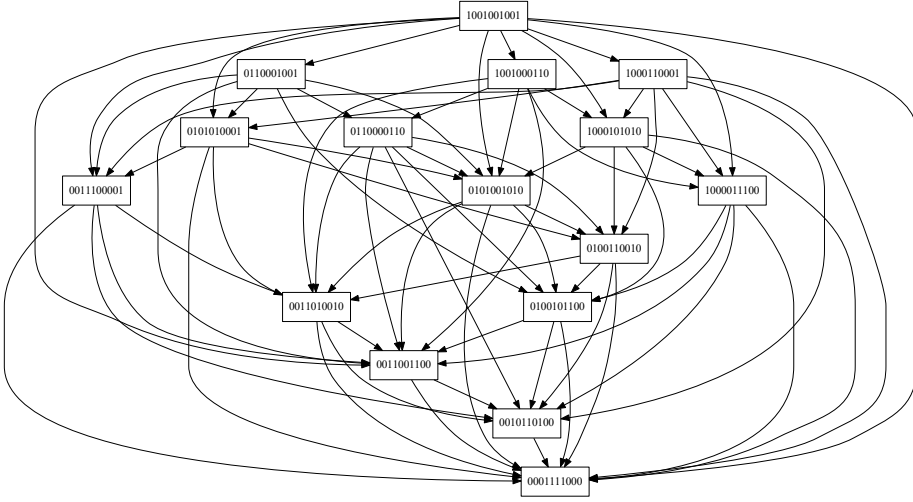
Figure 7.4: Fermionic graph for the Laughlin wavefunction for $N = 4$ and $\nu = 1/3$ and explicit action of our squeezing operator on the reference Tao-Thouless state. This graph should be compared with the one obtained by Bernevig and coworkers (see Chapter 6). Differently from them, we consider *all* the possible squeezing and not only the single ones. Therefore our graph contains much more directed arrows. Also the definition of level is slightly different: for us the level of a partition is the maximum number of squeezing in order to obtain that partition.

particles are re-created shifted toward each other of t sites (see also Figure (7.4)). An example is:

$$U|1, 0, 0, 0, 0, 1\rangle = 3|0, 1, 0, 0, 1, 0\rangle + |0, 0, 1, 1, 0, 0\rangle .$$

There is an obvious but important property of the operator (7.16) that we stress: it preserves the total angular momentum of the state on which it acts. Now, let us define the state:

$$|\psi\rangle = (\mathbb{I} - QU)^{-1}|\lambda\rangle = \left(\mathbb{I} + QU + (QU)^2 + \cdots\right)|\lambda\rangle , \qquad (7.17)$$

where $|\lambda\rangle$ is a maximally uniform state and Q is an operator defined by

$$Q = \frac{2(1/\alpha - 1)}{\rho_\lambda^F - \widetilde{Q}} , \qquad (7.18)$$

with

$$\widetilde{Q} = \sum_s \left[s \left(s - \sum_{t<s} 2(1/\alpha - 1)a_t^\dagger a_t \right) \right] a_s^\dagger a_s \qquad (7.19)$$

and ρ_ν^F is the eigenvalue of $\widetilde{Q}$ relative to the eigenstate $|\{\nu\}\rangle$. So

$$Q|\{\mu\}\rangle = \frac{k}{\rho_\lambda^F - \rho_\mu^F}|\{\mu\}\rangle .$$

Before proceeding it is useful to introduce a partial order relation (slightly different from the one introduced in the previous chapter) between the states: let the state

$$\big| 1, \overbrace{0,\dots,0}^{2m+1\ times}, \cdots, 1 \big\rangle \tag{7.20}$$

$$\underbrace{}_{N-1\ times}$$

be the maximally uniform state at N fermions, with filling factor $\nu = 1/(2m+1)$. The *level* of a state $|s\rangle$ is the *maximum* number of squeeze we can do to obtain $|s\rangle$ from the reference (or root) state (7.20). The root partition is the only state at level zero and the bunch state, in which all fermions are close to each other, is the only one at the maximum level.

Now we are finally ready to prove the recurrence relation between the coefficients of the Laughlin state expansion in the Slater basis. We recall it from the previous chapter

$$b_\mu = \frac{k}{\rho_\lambda^F - \rho_\mu^F} \sum_{\theta;\mu>\theta\geq\lambda} (\mu_i - \mu_j) b_\theta (-1)^{N_{sw}}\ . \tag{7.21}$$

Here the sum is extended over each state $|\{\theta\}\rangle$ whose level is lower than the one of the state $|\{\mu\}\rangle$. Moreover $b_\lambda = 1$.

The generic state in Fock space can be written down as

$$|\psi\rangle = \sum_\mu b_\mu |\{\mu\}\rangle$$

and so, multiplying for $\langle\{\nu\}|$ and using $\langle\{\nu\}|\{\mu\}\rangle = \delta_{\nu\mu}$, we find for our trial state:

$$b_\nu = \langle\{\nu\}|(\mathbb{I} - QU)^{-1}|\lambda\rangle\ . \tag{7.22}$$

Now there are two possibilities: if $\{\nu\} = \{\lambda\}$, we obtain $b_\lambda = 1$. If $\{\nu\} \neq \{\lambda\}$, $\langle\{\nu\}|\{\lambda\}\rangle = 0$ and so:

$$b_\nu = \langle\{\nu\}|QU\,(\mathbb{I} + QU + (QU)^2 + \cdots)|\lambda\rangle = \langle\{\nu\}|QU|\psi\rangle \tag{7.23}$$

We can calculate it applying the operator QU at the left hand side of the expression in (7.23) and using that:

$$\langle\{\nu\}|QU = \big[(QU)^\dagger|\{\nu\}\rangle\big]^\dagger = \big[q(\nu)U^\dagger|\{\nu\}\rangle\big]^\dagger$$

where q(ν) is the eigenvalue of Q applied to the state $|\nu\rangle$.

Now we need to calculate $U^\dagger|\{\nu\}\rangle$. $U^\dagger$ is the inverse operator of U, namely the "*un–squeezing*" operator:

$$U^\dagger = \sum_s \sum_{t=1}^\infty \sum_{u=t}^\infty (t-u)\, a_{s+t+u}^\dagger\, a_s^\dagger\, a_{s+t}\, a_{s+u}\ .$$

Applying that to $|\{\nu\}\rangle$ we obtain non-zero terms only when $s + u = \nu_j$ and $s + t = \nu_i$, with $\nu_i > \nu_j$ and ν_i and ν_j any two filled sites of $|\nu\rangle$. We can then write the result as:

$$U^\dagger|\{\nu\}\rangle = \sum_{\theta;\nu>\theta} (\nu_i - \nu_j) b_\theta^\lambda (-1)^{N_{sw}}|\theta\rangle\ , \tag{7.24}$$

where the sum over the partition θ is another way to write the sum over index i and j (namely, i and j are biunivocally linked to the partition θ that we get after the un–squeezing process).

The factor $(-1)^{N_{sw}}$ is, in our formalism, perfectly justified. In fact, let us write the generic N–particle state $|\{\mu\}\rangle$ as $|\mu_1, \mu_2, \ldots, \mu_N\rangle$, with $\mu_1 < \mu_2 < \cdots < \mu_N$. With this notation, we can write the sums over the new indices $\mu_i = s + u$ and $\mu_j = s + t$:

$$U^\dagger |\mu_1, \mu_2, \ldots, \mu_N\rangle = \sum_u \sum_{\mu_i, \mu_j} (-1)^{i+j} (\mu_i - \mu_j) a^\dagger_{\mu_i + u} a^\dagger_{\mu_j - u} \cdot$$
$$\cdot |\mu_1, \ldots, \mu_{i-1}, \cancel{\mu_i}, \mu_{i+1}, \ldots, \cancel{\mu_j}, \ldots, \mu_N\rangle . \tag{7.25}$$

Now, when the creation operators act on the state, we have to put the created particles with angular momenta $\mu_j - u$ and $\mu_i + u$ in their position to re–write this state in the form $|\widetilde{\mu}\rangle$. So we get exactly $N_{sw} + i + j - 2$ times the factor -1 and then we obtain $(-1)^{N_{sw}}$.[1]

Using now the adjoint of equation (7.24) in the equation (7.23), we obtain:

$$b_\nu = q(\nu) \sum_{\theta; \nu > \theta} (\nu_i - \nu_j)(-1)^{N_{sw}} \langle \theta | \psi \rangle$$

and then, noting that $\langle \theta | \psi \rangle = b_\theta$, we get the recurrence relation (7.21).

At this stage, we have just shown that the recurrence relation between coefficients of the decomposition into Slater basis are the same in our formalism and in the literature [121]. Now we have to show that our candidate state includes all but only the admissible squeezed states.

First of all, we note that if the state (7.17) has the correct terms, it also has the correct coefficients, because they are univocally obtained from the recurrence relation (7.21) and the fact that $b^\lambda_\lambda = 1$.

There are two ways to proceed: we can prove that the operator (7.16) creates exactly the same terms that Bernevig et al. have, or we can prove directly that our terms are all the ones found in the Laughlin state expansion.

In the first case, the only thing we have to show is that each squeeze in which the fermions are shifted toward each other of more than one unit in angular momentum can be obtained composing more than one squeeze in which the fermions are shifted toward each other of one unit in angular momentum. Indeed, Bernevig and coworkers consider only the first type of squeeze to obtain all the terms in the expansion, then calculate the coefficient considering also the second type of squeezing.

In the second case, we should prove that the Laughlin state has only terms with subsequent squeezing of the maximally uniform state. We choose the first route.

A one-unit squeeze is obtained as the action of the operator:

$$A_{s,u} = a^\dagger_{s+1} a^\dagger_{s+u} a_{s+u+1} a_s .$$

A t-unit squeeze is, in contrast, the result of the action of the operator

$$A^t_{s,u} = a^\dagger_{s+t} a^\dagger_{s+u} a_{s+u+t} a_s ,$$

---

[1] actually the system state can only be a complete antisymmetrization of $|\mu_1, \ldots, \mu_N\rangle$; however, this not change in any way the argument used here, because $\mathcal{A}|a, b\rangle = -\mathcal{A}|b, a\rangle$.

with $t > 1$. We want to prove that we can always obtain $A_{s,u}^t$ with subsequent action of $A_{s,u}$. However, there is a better notation for a squeezing operator for our purpose. Let $A_{a,b}^l$ be the squeezing operator which squeezes the fermions in sites a and b, shifting them of l steps toward each other. Let also

$$|s\rangle = |\mu_1, \ldots, \mu_n, [\cdots], \nu_1, \ldots, \nu_m\rangle$$

be the (part of a) state we are considering, with $N = n + m$ fermions of angular momenta $\mu_1, \ldots, \nu_m$. We want to show that the action of operator A_{μ_1, ν_m}^l can be achieved as subsequent actions of operators $A_{a,b}$, with $\mu_1 + l > \mu_n$ and $\nu_m - l < \nu_1$. Note that before μ_1 and after ν_m, as between $\mu_1 + l$ and $\nu_m - l$, we can have anything: this can not change in any way the proof we are going to give. Let us consider only the two more internal fermions, i.e. the state $|\mu_n, [\cdots], \nu_1\rangle$. Now, without any loss in generality, we suppose that $(\mu_1 - l) - \mu_n < \nu_1 - (\nu_m - l)$. So, if we apply the operator A_{μ_n, ν_1}, we get:

$$A_{\mu_n, \nu_1} |\mu_n, [\cdots], \nu_1\rangle = |\mu_n + 1, [\cdots], \nu_1 - 1\rangle .$$

We can now apply the operator A_{μ_n+1, ν_1-1} and continue doing so, until we reach the state $|\mu_n + l', [\cdots], \nu_1 - l'\rangle$, with $\nu_1 - l' = \nu_m - l$, and so $l' = \nu_1 - (\nu_m - l)$. Doing this, we have put the fermion that was in ν_1, in the position where, applying A_{μ_1, ν_m}^l to the state $|s\rangle$ would have jumped the fermion that was in ν_m. So this is the trick: we want to shift each fermion in the state $|s\rangle$ to the position of the following, while μ_n and ν_1 take the position (respectively) $\mu_n + l$ and $\nu_1 - l$. Now we have to manage the state

$$|s'\rangle = |\mu_1, \ldots, \mu_n + l', [\cdots], \nu_2, \ldots, \nu_m\rangle$$

exactly like the state $|s\rangle$: we consider only the more internal part, $|\mu_n + l', [\cdots], \nu_2\rangle$, and move the fermions with light squeezes, until one of them reaches his final position (i.e., in this case, $\mu_n + l$ and ν_1). We can iterate this process until we get the state (again, we can suppose that in the previous step we used μ_1 and not ν_m, without any loss in generality):

$$|s^{(n)}\rangle = |\mu_1 + a, [\cdots], \nu_m\rangle .$$

Now we can do a one-unit squeeze until one of the two fermions reaches his final position: the other will always do the same, because of the angular momentum conservation. In fact, the state $A_{\mu_1, \nu_m}^l |s\rangle$ and $|s\rangle$ have the same total angular momentum, like every state we can reach starting from $|s\rangle$ and doing one-unit squeezes. So the final state too must have the same angular momentum, and so if it has $N - 1$ fermions in the same position as $A^l |s\rangle$, the N–th is fixed by the angular momentum conservation law.

This concludes our proof. Moreover for Laughlin state with $\nu = 1/3$ we also checked numerically the coefficients of the Slater expansion of our state up to $N = 5$. We notice that in our derivation the particular form of the reference state never enters explicitly. Thus we proved the following theorem:

Theorem 7.2.1. *Given the general fermionic FQH state in the form of a Jack polynomial times a Vandermonde determinant:*

$$J_\lambda^\alpha(z_1, \cdots, z_N) \times \prod_{i<j} (z_i - z_j),$$

its representation in the Fock space is given by the state:

$$|\psi_\lambda^\alpha\rangle = (\mathbb{I} - QU)^{-1}|\lambda\rangle = \left(\mathbb{I} + QU + (QU)^2 + \cdots\right)|\lambda\rangle \,,$$

where $|\lambda\rangle$ is the reference state state, U is an universal squezing operator given by:

$$U = \sum_{s=0}^{\infty}\sum_{t=1}^{\infty}\sum_{u=t}^{\infty}(u-t)\,a_{s+t}^\dagger\,a_{s+u}^\dagger\,a_{s+t+u}\,a_s \,,$$

and Q is an operator defined by

$$Q = \frac{2(1/\alpha - 1)}{\rho_\lambda^F - \widetilde{Q}} \,,$$

with

$$\widetilde{Q} = \sum_s\left[s\left(s - \sum_{t<s}2(1/\alpha - 1)a_t^\dagger a_t\right)\right]a_s^\dagger a_s \,,$$

and ρ_ν^F is the eigenvalue of $\widetilde{Q}$ relative to the eigenstate $|\{\nu\}\rangle$, so that

$$Q|\{\mu\}\rangle = \frac{k}{\rho_\lambda^F - \rho_\mu^F}|\{\mu\}\rangle \,.$$

An analogous theorem can be proved easily for bosonic FQH states:

Theorem 7.2.2. *Given the general bosonic FQH state in the form of a Jack polynomial:*

$$J_\lambda^\alpha(z_1, \cdots, z_N) \,,$$

its representation in the Fock space is given by the state:

$$|\psi_\lambda^\alpha\rangle = (\mathbb{I} - Q_B U_B)^{-1}|\lambda\rangle = \left(\mathbb{I} + Q_B U_B + (Q_B U_B)^2 + \cdots\right)|\lambda\rangle \,,$$

where $|\lambda\rangle$ is the reference state, U_B is an universal squezing operator given by:

$$U_B = \sum_{s=0}^{\infty}\sum_{t=1}^{\infty}\sum_{u=t}^{\infty}(u+t)\,a_{s+t}^\dagger\,a_{s+u}^\dagger\,a_{s+t+u}\,a_s \,,$$

and Q_B is an operator defined by

$$Q_B = \frac{2/\alpha}{\rho_\lambda^B - \widetilde{Q}_B} \,,$$

with

$$\widetilde{Q}_B = \sum_s\left[s\left(s - 1 + 2/\alpha - \sum_{t<s}2/\alpha a_t^\dagger a_t\right)\right]a_s^\dagger a_s \,,$$

and ρ_ν^B is the eigenvalue of $\widetilde{Q}_B$ relative to the eigenstate $|\{\nu\}\rangle$, so that

$$Q_B|\{\mu\}\rangle = \frac{k}{\rho_\lambda^B - \rho_\mu^B}|\{\mu\}\rangle \,.$$

7.3   Conclusions and future directions

In this chapter we considered, in the beginning, a thin torus limit of the FQHE. Our thin torus is related to the one considered by Bergholtz and coworkers by an S-duality [145], mapping the Hamiltonian on the original lattice on its dual (via Fourier transform) and $L_x \to L_y$. We estabilished on rigorous grounds the connection with repulsive lattice gases showing explicitly the one to one correspondence between the chemical potential (in Bak Hamiltonian) and the magnetic field in the quantum Hall problem. This mapping suggests a way to plot a devil's staircase phase diagram for the FQHE in this limit. The staircase is deformed because of a simple scaling deformation due to the magnetic length.

In the second part of the chapter we focused on the connection between Laughlin wavefunction and the Tao-Thouless state. By using the recurrence relation by Bernevig and Regnault, we were able to show that the Laughlin state is a squeezed Tao-Thouless state. More in general all Jack polynomials FQH states can be written as a quasi-universal Jastrow operator acting on a reference state.

We suggest some possible future directions of this work:

- the Jastrow factor acting on the reference state is not universal: it depends both on the reference state λ and on α, that label the Jack. We suspect that a more elegant and universal form may exists for this operator, which is indipendent of the FQH state.

- the Fock representation that we obtained may be of mathematical relevance. To our knowledge, indeed, such a representation is not known by mathematicians and could be useful to prove properties (perhaps new) of the Jacks.

- The Hall Hamiltonian in the lowest LL is a one dimensional quantum lattice gas with long range repulsive interactions, built up from squeezing and un-squeezing operators. Recently a proposal for observing FQH states in the thin torus limit in alkaline-earth fermionic gases has been put forward [150]. In our opinion it would be interesting to understand if it is possible to go beyond the thin torus limit and proposing a quantum simulator for an Hall Hamiltonian whose ground state is, for instance, the Laughlin state.

Bibliography

[1] P. Hauke, F. M. Cucchietti, L. Tagliacozzo, I. Deutsch, and M. Lewenstein. *Reports on Progress in Physics*, 75(8):082401, 2012.

[2] R. P. Feynman. *International Journal of Theoretical Physics*, 21(6-7):467–488, 1982.

[3] S. Gopalakrishnan, B. L. Lev, and P. Goldbart. *Phys. Rev. Lett.*, 107:277201, 2011.

[4] P. Strack and S. Sachdev. *Phys. Rev. Lett.*, 107:277202, 2011.

[5] K. Hepp and E. Lieb. *Ann. Phys.*, 76:360–404, 1973.

[6] K. Hepp and E. Lieb. *Phys. Rev. A*, 8:2517–2525, 1973.

[7] Y. K. Wang and F. T. Hioe. *Phys. Rev. A*, 7:831–836, 1973.

[8] M. Mezard, G. Parisi, and M. Virasoro. *Spin Glass Theory and beyond*. World Scientific, 1986.

[9] D. J. Amit, H. Gutfreund, and H. Sompolinsky. *Phys. Rev. A*, 32:1007–1018, 1985.

[10] E. Farhi, J. Goldstone, S. Gutmann, J. Lapan, A. Lundgren, and D. Preda. *Science*, 292(5516):472–475, 2001.

[11] P. Schauß, J. Zeiher, T. Fukuhara, S. Hild, M. Cheneau, T. Macrì, T. Pohl, I. Bloch, and C. Gross. *Science*, 347(6229):1455–1458, 2015.

[12] P. Bak and R. Bruinsma. *Phys. Rev. Lett.*, 49(4):249, 1982.

[13] E. Levi, J. Minář, and I. Lesanovsky. *arXiv preprint arXiv:1503.03268*, 2015.

[14] D. Yoshioka. *The Quantum Hall Effect*. Springer Berlin Heidelberg, 2002.

[15] E. J. Bergholtz, T. H. Hansson, M. Hermanns, and A. Karlhede. *Phys. Rev. Lett.*, 99:256803, Dec 2007.

[16] R. B. Laughlin. *Phys. Rev. Lett.*, 50(18):1395, 1983.

[17] R. Tao and D. J. Thouless. *Phys. Rev. B*, 28(2):1142, 1983.

[18] P. Rotondo, E. Tesio, and S. Caracciolo. *Phys. Rev. B*, 91:014415, Jan 2015.

[19] P. Rotondo, M. Cosentino Lagomarsino, and G. Viola. *Phys. Rev. Lett.*, 114(14):143601, 2015.

[20] D. J. Amit, H. Gutfreund, and H. Sompolinsky. *Phys. Rev. Lett.*, 55:1530, 1985.

[21] S. Mertens. *Phys. Rev. Lett.*, 81:4281–4284, 1998.

[22] K. Baumann, C. Guerlin, F. Brenneke, and T. Esslinger. *Nature (London)*, 464:1301, 2010.

[23] J. Hubbard. *Phys. Rev. B*, 17(2):494, 1978.

[24] S. E. Burkov and Y. G. Sinai. *Russian Mathematical Surveys*, 38(4):235–257, 1983.

[25] B. A. Bernevig and F. D. M. Haldane. *Phys. Rev. Lett.*, 100(24):246802, 2008.

[26] K. H. Fischer and J. A. Hertz. *Spin glasses*, volume 1. Cambridge university press, 1993.

[27] S. Cocco, S. Leibler, and R. Monasson. *Proceedings of the National Academy of Sciences*, 106(33):14058–14062, 2009.

[28] S. Cocco and R. Monasson. *Phys. Rev. Lett.*, 83(24):5178, 1999.

[29] S. A. Kauffman. *Journal of theoretical biology*, 22(3):437–467, 1969.

[30] J. P. Bouchaud and M. Mézard. *Physica A: Statistical Mechanics and its Applications*, 282(3):536–545, 2000.

[31] M. Mézard, G. Parisi, and R. Zecchina. *Science*, 297(5582):812–815, 2002.

[32] D. Sherrington and S. Kirkpatrick. *Phys. Rev. Lett.*, 35:1792–1796, 1975.

[33] J. J. Hopfield. *PNAS*, 79:2554–2558, 1982.

[34] V. Dotsenko. *Introduction to the replica theory of disordered statistical systems*. Cambridge University Press, 2005.

[35] G. Parisi. *Phys. Rev. Lett.*, 43:1754–1756, 1979.

[36] G. Parisi. *Phys. Rev. Lett*, 50:1946–1948, 1983.

[37] R. M. Karp. *Reducibility among combinatorial problems*. Springer, 1972.

[38] S. Kirkpatrick, C. D. Gelatt, M. P. Vecchi, et al. *Science*, 220(4598):671–680, 1983.

[39] S. Geman and D. Geman. *Pattern Analysis and Machine Intelligence, IEEE Transactions on*, (6):721–741, 1984.

[40] R. Dicke. *Phys. Rev.*, 93:99–110, Jan 1954.

[41] S. Sachdev. *Quantum phase transitions*. Wiley Online Library, 2007.

[42] D. Braak. *Phys. Rev. Lett.*, 107(10):100401, 2011.

[43] K. Rzazewski, K. Wodkiewicz, and W. Zacowicz. *Phys. Rev. Lett.*, 35:432–434, 1975.

[44] M. Greiner, O. Mandel, T. Esslinger, W. Hansch, and I. Bloch. *Nature*, 415:39–44, 2002.

[45] F. Dimer, B. Estienne, A. S. Parkins, and H. J. Carmichael. *Phys. Rev. A*, 75:013804, 2007.

[46] M. P. Baden, K. J. Arnold, A. L. Grimsmo, S. Parkins, and M. D. Barrett. *Phys. Rev. Lett.*, 113:020408, Jul 2014.

[47] D. Nagy, G. Kónya, G. Szirmai, and P. Domokos. *Phys. Rev. Lett.*, 104:130401, 2010.

[48] H. Ritsch, P. Domokos, F. Brennecke, and T. Esslinger. *Rev. Mod. Phys.*, 85:553–601, Apr 2013.

[49] M. Mezard, G. Parisi, N. Sourlas, G. Toulouse, and M. Virasoro. *Phys. Rev. Lett.*, 52:1156–1159, 1984.

[50] L. Angelani, C. Conti, G. Ruocco, and F. Zamponi. *Phys. Rev. Lett.*, 96:065702, 2006.

[51] L. Angelani, C. Conti, G. Ruocco, and F. Zamponi. *Phys. Rev. B*, 74:104207, 2006.

[52] L. Leuzzi, C. Conti, V. Folli, L. Angelani, and G. Ruocco. *Phys. Rev. Lett*, 102:083901, 2009.

[53] M. Leonetti, C. Conti, and C. Lopez. *Nat. Phot.*, 5:615–617, 2011.

[54] S. Morrison, A. Kantian, A. J. Daley, H. G. Katzgraber, M. Lewenstein, H. P. Büchler, and P. Zoller. *N. J. Phys.*, 10:073032, 2008.

[55] I. Bloch. *Nat. Phys.*, 1:23–30, 2005.

[56] L. Sanchez-Palencia and M. Lewenstein. *Nat. Phys.*, 6:87, 2010.

[57] L. Fallani, J. E. Lye, V. Guarrera, C. Fort, and M. Inguscio. *Phys. Rev. Lett.*, 98:130404, 2007.

[58] J. Billy, V. Josse, Z. Zuo, A. Bernard, B. Hambrecht, P. Lugan, D. Clément, L. Sanchez-Palencia, P. Bouyer, and A. Aspect. *Nature*, 453:891–894, 2008.

[59] A. Niederberger, T. Schulte, J. Wehr, M. Lewenstein, L. Sanchez-Palencia, and K. Sacha. *Phys. Rev. Lett.*, 100:030403, 2008.

[60] C. Emary and T. Brandes. *Phys. Rev. Lett.*, 90:044101, 2003.

[61] A. D. Greentree, C. Tahan, J. H. Cole, and L. C. L. Hollenberg. *Nat. Phys.*, 2:856–861, 2006.

[62] A. L. C. Hayward, A. M. Martin, and A. D. Greentree. *Phys. Rev. Lett.*, 108:223602, 2012.

[63] A. E. Siegman. *Lasers*. University Science Books, 1986.

[64] J. R. L. de Almeida and D. J. Thouless. *J. Phys. A: Math. Gen*, 11:983, 1978.

[65] G. Mussardo. *Statistical Field Theory*. Oxford University press, 2010.

[66] D. Ruelle. *Statistical Mechanics: rigorous results*. World Scientific, 1969.

[67] A. Billoire and E. Marinari. *J. Phys. A*, 33:L265–L272, 2000.

[68] K. Hukushima and K. Nemoto. *J. Phys. Soc. Jap.*, 65:1604–1608, 1996.

[69] M. Palassini and S. Caracciolo. *Phys. Rev. Lett.*, 82:5128–5131, 1999.

[70] T. Schultz, D. Mattis, and E. Lieb. *Rev. Mod. Phys.*, 36:856–871, 1964.

[71] M. A. Nielsen and I. L. Chuang. *Quantum computation and quantum information*. Cambridge university press, 2010.

[72] A. Barenco, C. H. Bennett, R. Cleve, D. P. DiVincenzo, N. Margolus, P. Shor, T. Sleator, J. A. Smolin, and H. Weinfurter. *Phys. Rev. A*, 52:3457–3467, Nov 1995.

[73] G. E. Santoro, R. Martoňák, E. Tosatti, and R. Car. *Science*, 295(5564):2427–2430, 2002.

[74] V. Bapst, L. Foini, F. Krzakala, G. Semerjian, and F. Zamponi. *Phys. Rep.*, 523:127–205, February 2013.

[75] I. Buluta and F. Nori. *Science*, 326(5949):108–111, 2009.

[76] I. M. Georgescu, S. Ashhab, and F. Nori. *Rev. Mod. Phys.*, 86:153–185, Mar 2014.

[77] M. Lewenstein, A. Sanpera, V. Ahufinger, B. Damski, A. Sen, and U. Sen. *Advances in Physics*, 56(2):243–379, 2007.

[78] K. Baumann, R. Mottl, F. Brennecke, and T. Esslinger. *Phys. Rev. Lett.*, 107:140402, Sep 2011.

[79] L.J. Zou, D. Marcos, S. Diehl, S. Putz, J. Schmiedmayer, and P. Rabl. *Phys. Rev. Lett.*, 113:023603, 2014.

[80] Y. Zhang, L. Yu, J.-Q. Liang, G. Chen, S. Jia, and F. Nori. *Scientific Reports*, 4:4083, February 2014.

[81] P. Nataf and C. Ciuti. *Nature Communications*, 1(6):72, 2010.

[82] O. Viehmann, J. von Delft, and F. Marquardt. *Phys. Rev. Lett.*, 107:113602, Sep 2011.

[83] J. A. Mlynek, A. A. Abdumalikov, C. Eichler, and A. Wallraff. *Nature Communications*, 5:5186, November 2014.

[84] A. Mezzacapo, U. Las Heras, J. S. Pedernales, L. DiCarlo, E. Solano, and L. Lamata. *Scientific Reports*, 4:7482, 2014.

[85] L. Chirolli, M. Polini, V. Giovannetti, and A. MacDonald. *Phys. Rev. Lett.*, 109:267404, Dec 2012.

[86] D. Hagenmüller and C. Ciuti. *Phys. Rev. Lett.*, 109:267403, Dec 2012.

[87] F. M. D. Pellegrino, L. Chirolli, R. Fazio, V. Giovannetti, and M. Polini. *Phys. Rev. B*, 89:165406, Apr 2014.

[88] D. Rossini and R. Fazio. *Phys. Rev. Lett.*, 99:186401, Oct 2007.

[89] S. Gopalakrishnan, B. L. Lev, and P. Goldbart. *Nat. Phys.*, 5:845–850, 2009.

[90] S. Gopalakrishnan, B. L. Lev, and P. Goldbart. *Phys. Rev. A*, 82:043612, 2010.

[91] S. Gopalakrishnan, B. L. Lev, and P. Goldbart. *Philosophical Magazine*, 92(1-3):353–361, 2012.

[92] A. Lucas. *Frontiers in Physics*, 2(5), 2014.

[93] C. Aron, M. Kulkarni, and H. E. Türeci. *ArXiv e-prints*, December 2014.

[94] D. O. Hebb. *Archives of Neurology and Psychiatry*, 44:421–438, 1940.

[95] D. O. Hebb. *Brain Mechanism and Learning*, 1961.

[96] J. Larson and M. Lewenstein. *New Journal of Physics*, 11(6):063027, 2009.

[97] A. Wickenbrock, M. Hemmerling, G. R. M. Robb, C. Emary, and F. Renzoni. *Phys. Rev. A*, 87:043817, Apr 2013.

[98] D. J. Egger and F. K. Wilhelm. *Phys. Rev. Lett.*, 111:163601, Oct 2013.

[99] M. Leib and M. J. Hartmann. *Phys. Rev. Lett.*, 112:223603, Jun 2014.

[100] T. H. Kyaw, D. A. Herrera-Martí, E. Solano, G. Romero, and L.-C. Kwek. *Phys. Rev. B*, 91:064503, Feb 2015.

[101] A. J. Kollár, A. T. Papageorge, K. Baumann, M. A. Armen, and B. L. Lev. *ArXiv e-prints*, November 2014.

[102] F. Nogrette, H. Labuhn, S. Ravets, D. Barredo, L. Béguin, A. Vernier, T. Lahaye, and A. Browaeys. *Phys. Rev. X*, 4:021034, May 2014.

[103] Y. Nonomura and H. Nishimori. *eprint arXiv:cond-mat/9512142*, December 1995.

[104] D. Loss and D. P. DiVincenzo. *Phys. Rev. A*, 57:120–126, Jan 1998.

[105] R. Raussendorf, D. Browne, and H. Briegel. *Phys. Rev. A*, 68:022312, Aug 2003.

[106] T. Graß, D. Raventós, B. Juliá-Díaz, C. Gogolin, and M. Lewenstein. *arXiv preprint arXiv:1507.07863*, 2015.

[107] W. Lechner, P. Hauke, and P. Zoller. *Science Advances*, 1(9):e1500838, 2015.

[108] A. Goban, C. L. Hung, S. P. Yu, J. D. Hood, J. A. Muniz, J. H. Lee, M. J. Martin, A. C. McClung, K. S. Choi, and D. E. Chang. *Nature communications*, 5, 2014.

[109] G. Moore and N. Read. *Nuclear Physics B*, 360(2):362–396, 1991.

[110] N. Read and E. Rezayi. *Phys. Rev. B*, 59(12):8084, 1999.

[111] R. P. Stanley. *Advances in Mathematics*, 77(1):76–115, 1989.

[112] B. A. Bernevig and N. Regnault. *Phys. Rev. Lett.*, 103(20):206801, 2009.

[113] E. H. Hall. *American Journal of Mathematics*, 2(3):pp. 287–292, 1879.

[114] D. C. Tsui. *Rev. Mod. Phys.*, 71:891–895, Jul 1999.

[115] K. von Klitzing, G. Dorda, and M. Pepper. *Phys. Rev. Lett.*, 45:494–497, Aug 1980.

[116] D. C. Tsui, H. L. Stormer, and A. C. Gossard. *Phys. Rev. Lett.*, 48:1559–1562, May 1982.

[117] Fritz Herlach and Noboru Miura, editors. *High Magnetic Fields. Science and Technology. Volume 2: Theory and Experiments I.* World Scientific, 2003.

[118] H. Aoki and T. Ando. *Solid State Communications*, 38(11):1079 – 1082, 1981.

[119] W. Pan, J. S. Xia, H. L. Stormer, D. C. Tsui, C. Vicente, E. D. Adams, N. S. Sullivan, L. N. Pfeiffer, K. W. Baldwin, and K. W. West. *Phys. Rev. B*, 77(7):075307, 2008.

[120] J. K. Jain. *Composite fermions*. Cambridge University Press, 2007.

[121] R. Thomale, B. Estienne, N. Regnault, and B. A. Bernevig. *Phys. Rev. B*, 84(4):045127, 2011.

[122] B. I. Halperin. *Phys. Rev. Lett.*, 52(18):1583, 1984.

[123] Jain. K. Jain. *Phys. Rev. Lett.*, 63(2):199, 1989.

[124] C. Nayak, S. H. Simon, A. Stern, M. Freedman, and S. Das Sarma. *Reviews of Modern Physics*, 80(3):1083, 2008.

[125] G. V. Dunne. *International Journal of Modern Physics B*, 7(28):4783–4813, 1993.

[126] P. Di Francesco, M. Gaudin, C. Itzykson, and F. Lesage. *International Journal of Modern Physics A*, 9(24):4257–4351, 1994.

[127] Daniel C Tsui, Horst L Stormer, and Arthur C Gossard. *Phys. Rev. Lett.*, 48(22):1559, 1982.

[128] H. L. Stormer. *Reviews of Modern Physics*, 71(4):875, 1999.

[129] A. Y. Kitaev. *Annals of Physics*, 303(1):2–30, 2003.

[130] A. Stern. *Annals of Physics*, 323(1):204–249, 2008.

[131] F. D. M. Haldane. *Phys. Rev. Lett.*, 51(7):605, 1983.

[132] F. Wilczek. *Phys. Rev. Lett.*, 49(14):957, 1982.

[133] F. D. M. Haldane. *Phys. Rev. Lett.*, 67(8):937, 1991.

[134] Ludwig A. W. W. Bettelheim E., Gruzberg I. A. *Phys. Rev. B*, 86:165324, 2012.

[135] A. C. Balram, A. Wójs, and J. K. Jain. *Phys. Rev. B*, 88(20):205312, 2013.

[136] W. Pan, H. L. Stormer, D. C. Tsui, L. N. Pfeiffer, K. W. Baldwin, and K. W. West. *Phys. Rev. Lett.*, 90(1):016801, 2003.

[137] J. K. Jain. *Indian Journal of Physics*, 88(9):915–929, 2014.

[138] E. Wigner. *Phys. Rev.*, 46:1002–1011, Dec 1934.

[139] D. J. Thouless. *Phys. Rev. B*, 31(12):8305, 1985.

[140] E. J. Bergholtz and A. Karlhede. *Phys. Rev. B*, 77:155308, Apr 2008.

[141] E. J. Bergholtz and A. Karlhede. *Phys. Rev. Lett.*, 94:026802, Jan 2005.

[142] P. Bak. *Reports on Progress in Physics*, 45(6):587–629, 1982.

[143] S. Aubry. *Journal of Physics C: Solid State Physics*, 16(13):2497, 1983.

[144] E. Levi, J. Minář, J. P. Garrahan, and I. Lesanovsky. *arXiv preprint arXiv:1503.03259*, 2015.

[145] A. Seidel. *Phys. Rev. Lett.*, 105:026802, Jul 2010.

[146] D. Yoshioka, B. I. Halperin, and P. A. Lee. *Phys. Rev. Lett.*, 50:1219–1222, Apr 1983.

[147] D. Yoshioka. *Phys. Rev. B*, 29(12):6833, 1984.

[148] J. Zak. *Phys. Rev.*, 134(6A):A1602, 1964.

[149] V. L. Pokrovsky and G. V. Uimin. *Journal of Physics C: Solid State Physics*, 11(16):3535, 1978.

[150] S. Barbarino, L. Taddia, D. Rossini, L. Mazza, and R. Fazio. *Nature Communications*, 6, 09 2015.